

**Analysis and Applications
of Variational Sensitivity Information
in Structural Optimisation**

von der Fakultät Architektur und Bauingenieurwesen
der Technischen Universität Dortmund
zur Verleihung des akademischen Grades
Doktor-Ingenieur (Dr.-Ing.)
genehmigte Dissertation

von
Dipl.-Ing. Nikolai Gerzen

Dortmund, Mai 2014

Kontakt:

Dipl.-Ing. Nikolai Gerzen
Numerische Methoden und Informationsverarbeitung
Fakultät Architektur und Bauingenieurwesen
Technische Universität Dortmund
August-Schmidt-Str. 8, D-44227 Dortmund
Email: *nikolai.gerzen@tu-dortmund.de*
URL: *www.bauwesen.tu-dortmund.de/nmi*

Prüfungskommission:

Vorsitz:	Prof. Dr.-Ing. Tim Ricken
1. Gutachter:	Prof. Dr.-Ing. Franz-Joseph Barthold
2. Gutachter:	Prof. Dr.-Ing. Kai-Uwe Bletzinger

Tag der Einreichung:	02.12.2013
Tag der mündlichen Prüfung:	05.05.2014

Abstract

This thesis is concerned with the analysis of the *internal structure of sensitivities* of engineering structures with respect to modifications in shape. The term *internal structure of sensitivity* is introduced as an abbreviation for the eigenvalues and singular values, the corresponding eigenvalue spectrum and singular value spectrum as well as for the associated eigenvectors and singular vectors of the sensitivity matrix, the pseudo load matrix and the mesh velocity matrix, which build up the central parts of the sensitivity analysis. These matrices are analysed both qualitatively and quantitatively utilising the singular value decomposition (SVD) and techniques which are based on the principle component analysis (PCA).

The impact of the chosen models on the computed optimal designs, especially the influence of the chosen shape parametrisation, is analysed. This knowledge enables the design engineer to understand and improve the models systematically whereas they are usually set up entirely by engineering experience and intuition. The weaknesses of the models are detected and improved design descriptions are proposed. This human controlled process is called *design exploration*. The aim of this thesis is to contribute new substantial capabilities to the corresponding methods.

Moreover, an algorithmic and automatic treatment of SVD based sensitivity information is presented within this thesis for different kinds of application. In context of model reduction, the complete design space is reduced to the most valuable subspace of design modifications in order to demonstrate the information content of the decomposed sensitivities. Illustrative examples show that reasonable optimal designs can be obtained with a small percentage of properly defined design variables. In addition, the area of application for SVD based sensitivity information is extended to the nonlinear buckling analysis. Here, decomposition of the pseudo load matrix is utilised to generate the ‘worst case’ imperfections.

The generic concept is applied to shape optimisation of shell structures. The design of such structures is extremely important for their stability, robustness and load-bearing capacity. The variational design sensitivity analysis for a nonlinear solid shell is performed and especially the pseudo load matrix and the sensitivity matrix are derived. Within the scope of this thesis, only static nonlinear structural analysis and hyper-elastic material behaviour are considered.

Kurzfassung

Die vorliegende Arbeit befasst sich mit der *inneren Struktur der Empfindlichkeiten* von mechanischen Strukturen bezüglich geometrischer Veränderungen. Der Begriff *innere Struktur der Empfindlichkeiten* wird als abkürzende Bezeichnung für die Eigenwerte und Singulärwerte, die entsprechenden Eigenwert- und Singulärwertspektren, sowie die zugehörigen Eigenvektoren und singulären Vektoren der Pseudolast-, Sensitivitäts- und Designgeschwindigkeitsmatrizen eingeführt. Zusammen bilden diese Größen den Kern der Sensitivitätsanalyse und werden sowohl qualitativ als auch quantitativ mit Hilfe der Singulärwertzerlegung (SVD) und Techniken, die aus dem Bereich der Hauptkomponentenanalyse (PCA) bekannt sind, analysiert.

Beschrieben wird der Einfluss der Modellbildung, insbesondere die Wahl der Formparametrisierung auf die Lösung der Optimierungsaufgabe. Dieses Wissen ermöglicht es dem entwerfenden Ingenieur das Modell zu verstehen und es systematisch zu verbessern, was gewöhnlich nur auf seiner Erfahrung und Intuition basiert. Die Schwächen der Modellbildung werden identifiziert und verbesserte Parametrisierungen des Designraumes vorgeschlagen. Ein solches Vorgehen, das unter anderem die Interaktion zwischen Mensch und Maschine erfordert, wird auch als *Designexploration* bezeichnet und stellt den Schwerpunkt der vorliegenden Arbeit dar.

Des Weiteren wird eine algorithmische und automatische Behandlung der auf SVD basierten Sensitivitätsinformationen für verschiedene Anwendungen vorgestellt. Im Zusammenhang mit der Modellreduktion wird der vollständige Designraum auf einen Unterraum mit der größtmöglichen Varianz projiziert, um den Informationsgehalt der Sensitivitätszerlegungen zu demonstrieren. Beispiele werden zeigen, dass nur ein Bruchteil der neu definierten Designvariablen benötigt wird, um brauchbare Optimierungsergebnisse zu erzielen. Das Anwendungsgebiet der SVD basierten Sensitivitätsinformationen wird auf die nichtlineare Beulanalyse ausgeweitet. Hierbei werden die singulären Vektoren der Pseudolastmatrix mit den 'worst case' Imperfektionen in Verbindung gebracht.

Die entwickelten Konzepte werden auf die Formoptimierung von Schalentragwerken angewandt. Das Design solcher Strukturen hat einen großen Einfluss auf ihre Stabilität, Robustheit und ihre Versagenslast. Die variationelle Sensitivitätsanalyse einer nichtlinearen Schale wird durchgeführt. Insbesondere werden die Sensitivitäts- und Pseudolastmatrizen hergeleitet. Es werden nur statische Probleme mit hyperelastischem, auch nichtlinearem, Materialverhalten betrachtet.

Preface

The work presented in this thesis was carried out between 2008 and 2013 being a research assistant at the chair of Numerical Methods and Information Processing at TU Dortmund. The financial support of the German Research Foundation (DFG) under grant number BA 1828/3-1 and BA 1828/5-1 is gratefully acknowledged.

First of all, I would like to express my heartfelt thanks to my academic advisor Prof. Dr.-Ing. Franz-Joseph Barthold for his support and for providing me with inspiring advice through all these years. I also would like to thank my colleagues in Dortmund for their intentions and for stimulating discussions.

Further, I would like to thank Prof. Dr.-Ing. Kai-Uwe Bletzinger for his willingness to act as reviewer of this thesis and interest in my work. I am also very grateful to Prof. Dr.-Ing. Tim Ricken for taking the chairmanship of the examination committee.

Last but not least, I would like to extend my heartfelt thanks to my wife Olga and to my son Arthur for giving me so much moral support and for their love.

Dortmund, May 2014

Nikolai Gerzen

Contents

1	Introduction	1
1.1	Motivation and research objectives	1
1.2	Outline of the thesis	3
2	Preliminaries	5
2.1	Notation	5
2.2	Derivatives and variations	6
2.3	Software environment	7
3	Elements of structural optimisation	9
3.1	Introduction	9
3.1.1	Branches of structural optimisation	10
3.1.2	General procedure of structural optimisation	11
3.2	Parametrisation of shape	12
3.3	Structural analysis	14
3.4	Sensitivity analysis	14
3.5	Mathematical optimisation	15
3.5.1	Classification of optimisation methods	16
3.5.2	Sequential quadratic programming	16
3.6	Summary and concluding remarks	18
4	Morphing based shape parametrisation	19
4.1	Introduction	19
4.1.1	State of the art	19
4.1.2	Special features of the presented research	19
4.2	An introduction to B-splines	20
4.2.1	B-spline basis	20
4.2.2	B-spline curves	21
4.2.3	B-spline tensor products	22
4.3	CAGD controlled FE-mesh	22
4.3.1	Generation of FE-mesh	23
4.3.2	Design velocity field	24
4.4	Morphing controlled FE-mesh	25
4.4.1	The procedure of morphing	25
4.4.2	CAGD as special case of morphing	26
4.4.3	Inverse computation of FE-node positions	27
4.5	Remarks on NURBS	28

4.6	Summary and concluding remarks	29
5	Structural analysis for solid shells	31
5.1	Introduction	31
5.1.1	State of the art	31
5.1.2	Special features of the presented research	32
5.2	Kinematics	32
5.3	Variational relations	33
5.3.1	The variational functional	33
5.3.2	The weak form of equilibrium	34
5.3.3	Linearisation of the weak form of equilibrium	34
5.4	Discretised relations	35
5.4.1	Approximation of kinematic quantities	35
5.4.2	Approximation of the assumed strain and stress fields	37
5.4.3	Energy approximation	38
5.4.4	Approximation of the weak form and of its linearisation	39
5.5	Summary and concluding remarks	40
6	Sensitivity analysis for solid shells	41
6.1	Introduction	41
6.1.1	State of the art	41
6.1.2	Special features of the presented research	42
6.2	Variational relations	42
6.2.1	First total and partial variations of energy	42
6.2.2	Total and total partial variations of any objective functional	43
6.2.3	Total and partial variations of the physical residual	43
6.2.4	Variations of Cauchy stress tensor	44
6.3	Discretised relations	45
6.3.1	Preliminaries	45
6.3.2	Approximation of material residual	48
6.3.3	Sensitivity and pseudo load matrices	48
6.3.4	Sensitivity of Cauchy stress	50
6.4	Example: clamp	50
6.4.1	Compliance minimisation under volume constraint	51
6.4.2	Volume minimisation under stress constraints	52
6.5	Summary and concluding remarks	54
7	Singular value decomposition (SVD)	55
7.1	Introduction	55
7.1.1	State of the art	55
7.1.2	Special features of the presented research	56
7.2	Singular value decomposition	56
7.2.1	Definition and numerical effort of SVD	56
7.2.2	Applications of SVD	56

7.2.3	Analysis of input-output systems	59
7.3	Generalised singular value decomposition	59
7.3.1	Definition of GSVD	59
7.3.2	Inexpensive SVD of sensitivity matrix	60
7.4	Summary and concluding remarks	60
8	Sensitivity based imperfections for nonlinear buckling analysis	61
8.1	Introduction	61
8.1.1	State of the art	62
8.1.2	Special features of the presented research	63
8.2	Stability of equilibrium	63
8.2.1	Variational relations	63
8.2.2	Discretised relations	64
8.3	Sensitivity based imperfections	64
8.3.1	Global imperfections	65
8.3.2	Local imperfections	66
8.4	Example: compressed cylinder	67
8.4.1	Analysis of the perfect structure	67
8.4.2	SVD of pseudo load matrix	68
8.4.3	Analysis of the imperfect structure	69
8.5	Summary and concluding remarks	69
9	Model reduction based on SVD of sensitivity information	71
9.1	Introduction	71
9.1.1	State of the art	71
9.1.2	Special features of the presented research	72
9.2	Inner structure of shape sensitivities	72
9.2.1	Example: uniaxial strained shell	73
9.2.2	SVD of the sensitivity matrix	73
9.2.3	SVD of the pseudo load matrix	75
9.3	Shape optimisation based on SVD	76
9.3.1	Selection of shape (design) modes	76
9.3.2	Modified optimisation procedure	77
9.4	Example: uniaxial strained shell - continued	78
9.5	Summary and concluding remarks	79
10	SVD based design exploration	81
10.1	Introduction	81
10.1.1	State of the art	81
10.1.2	Special features of the presented research	82
10.2	A structural optimisation assistant	83
10.3	FE model exploration	85
10.3.1	Cantilever shell: FE model	85
10.3.2	Inner structure of the sensitivity matrix	86

10.4	Design exploration	88
10.4.1	Cantilever shell: design model	88
10.4.2	Inner structure of the transformed sensitivity matrix	89
10.4.3	Cantilever shell: optimisation results	91
10.5	Correlation between design and FE model	91
10.6	Summary and concluding remarks	94
11	Numerical examples	95
11.1	Introduction	95
11.1.1	Considered objectives and constraints	95
11.1.2	Special features of the presented examples	96
11.2	Compliance and volume minimisation	96
11.2.1	Reservoir bracket	96
11.2.2	3D hook	98
11.3	Generation of worst imperfections	101
11.3.1	PET tube: model problem	101
11.3.2	PET tube: buckling analysis	101
11.4	SVD based model reduction	103
11.4.1	Ceiling surface	103
11.4.2	Spanner	105
11.5	Summary and concluding remarks	108
12	Conclusion	109
12.1	Summary	109
12.2	Future work	110
	References	111
	Curriculum vitae	122

1 Introduction

This introductory chapter presents the motivation and thematic priorities concerning the research objectives of the work in hand. The state of the art is discussed and the structure of this thesis is outlined.

1.1 Motivation and research objectives

Nowadays structural optimisation is a key discipline within the design process of new products. This is mainly due to the everlasting increase of computer power and the enormous research efforts in the scope of numerical methods such as the *finite element method*. Considering practical applications, the objectives and constraints are usually nonlinear with respect to design variables. Despite of the employment of highly efficient gradient based optimisation strategies, solving structural optimisation problems is expensive concerning the iterative nature of most algorithms. In case of nonlinear structural behaviour, additional iterations are performed within structural analysis.

Solving a given structural optimisation problem is almost an automatic process, where the sensitivities are only computed to serve the mathematical optimiser. However, the definition process of a structural optimisation problem is human controlled and is based on experience and knowledge. Decisions within this process have an extraordinary impact on the quality of optimisation results, on the solubility of the problem and on the corresponding computational effort. Design exploration, which is rather known in context of robustness or uncertainty analysis than in context of optimisation, can facilitate the definition of the problem. Such exploration is usually based on parameter studies, which are evaluated using standard statistical methods. Hence, problems with only a small number of design variables can be considered as several computations of structural response are required for each design variable to create so called *response surfaces*.

This thesis outlines an enhanced analysis of the design sensitivities beyond the standard computation of the gradient values. It is based on the analytical derivation and

efficient computation of the Fréchet derivatives of objectives and constraints with respect to the full space of all possible design variables. This overhead of sensitivity information is examined by a singular value decomposition (SVD) and principal component analysis (PCA) in order to detect major and minor influence of model parameters on the structural response, objectives and constraints. Thus, this methodology leads to valuable qualitative and quantitative insight, which is so far unused in standard approaches to structural optimisation. This knowledge enables the design engineer to understand and improve the models systematically. Design of structures with large number of variables can be explored utilising only few visualisations with enormous information content.

In addition to the mentioned exploration techniques, different applications are presented where the discovered SVD based sensitivity information is treated automatically within optimisation algorithms. A model reduction technique for structural optimisation problems is proposed. Here, the singular value decomposition of sensitivity and of pseudo load matrices is utilised to formulate reduced quadratic sub-problems within the *sequential quadratic programming* (SQP) approach. A technique for creation of ‘worst case’ imperfections for nonlinear buckling analysis is outlined. In this context, right singular vectors, which correspond to the largest singular values, are used as imperfection modes.

Shell elements are most commonly used to model thin structures because of their efficiency and accuracy. The design of such structures is extremely important for their stability, robustness and for their load-bearing capacity. The proposed enhanced design sensitivity analysis is applied to shell structures. It provides information which allows the engineer to find the appropriate shape of a shell and to understand the influence of geometry and layout variants on its behaviour. For this reason, variational and discretised sensitivity relations and the corresponding sensitivity and pseudo load matrices for a nonlinear solid shell element are derived. The considered element can be used either in shell or in solid mode within both structural analysis and optimisation. The utilised shape parametrisation is based on morphing concepts and is valid for shell and solid structures.

Within this thesis, techniques from various scientific disciplines are utilised and very different topics are tackled. The overviews and references on these topics are presented in the introductions of the corresponding chapters. At this point, only the applications of singular value decomposition to structural analysis and especially optimisation are reviewed. The power of SVD in conjunction with a special subspace method can be observed in system identification and dynamical behaviour, see [94]. An improved computational approach for linear differential equations, such as Laplace and Helmholtz equations, motivated by SVD analysis is proposed in [115]. In context of model reduction, the number of degrees of freedom for the analysis model is reduced by means of projections into a lower dimensional space to speed up struc-

tural analysis. Here, the SVD-based, the Krylov-based and the SVD-Krylov-based approximation methods are known, see [16]. These methods are often used to analyse large-scale dynamical systems or time dependent models. Overall, SVD analysis enhances the eigenvalue analysis in structural dynamics and structural stability and is both quantitatively and qualitatively well understood. The review article [72] hints to early works on the application of SVD to optimisation of dynamic response and stability behaviour. The optimal design of beam structures is elaborated controlling singular values of static and dynamic stiffness matrices in [56]. Both, the optimisation model and the computational behaviour are improved by incorporating the insight gained by SVD analysis. Optimum laminate design is detected utilising SVD in a recent work [55]. Here, the worst possible load case is formulated as a minimax problem whose solution is shown to be equivalent to a singular value minimisation problem. The advantages of SVD for the optimal design of piezoelectric actuators are discussed in [95] on simple beam structures. A SVD based sub-problem technique for the restriction of the best individuals to a suitable subspace is proposed in [97] and applied to a genetic optimisation approach. A compact proper orthogonal decomposition basis for optimisation-oriented reduced-order models is proposed in [38]. Here, SVD is utilised to decompose the weighted snapshot matrix of state vector sensitivities. Structural and sensitivity reanalysis based on SVD is presented in [139]. For perturbations in design which lead to low rank changes of system matrices the numerical effort of a reanalysis is reduced. The application of SVD to shape sensitivity analysis in context of FE node based shape optimisation was reported by the author and others in [66]. The author has outlined an equivalent enhanced sensitivity analysis for topology optimisation in [63]. In both contributions, linear structural analysis for the 2D case is considered and pure displacement formulations are utilised. In contrast, nonlinear behaviour of 3D structures employing mixed formulations is investigated within the scope of this thesis.

1.2 Outline of the thesis

The present thesis consists of twelve chapters. Utilised notation and frequently used mathematical operations are explained in Chapter 2. In Chapter 3 structural optimisation is introduced and topics which are relevant for this thesis are commented on with references to literature. Morphing based shape parametrisation is outlined in Chapter 4. Mapping functions which are based on tensor products of B-splines are considered. The corresponding design velocity fields are derived. All necessary relations to perform finite element analysis of the nonlinear solid shell are set up in Chapter 5. Variational and discretised sensitivity relations as well as the corresponding pseudo load and sensitivity matrices are derived in Chapter 6. An introduction to singular value decomposition is given in Chapter 7. The power of SVD is demonstrated on its several applications in science. Chapter 8 tackles the SVD based generation of ‘worst case’ imperfections for nonlinear buckling analysis. Here, SVD of the pseudo load matrix is utilised to create imperfections. A model reduction technique

for structural optimisation problems is presented in Chapter 9. Reduced quadratic sub-problems within the SQP approach are formulated to demonstrate the information content of SVD based sensitivity information. The corresponding optimisation algorithm is outlined. Chapter 10 is concerned with the exploration of the FE model and the corresponding design description. Based on singular value decomposition of sensitivity information, interactive tools are derived which facilitate the definition of a structural optimisation problem. The features and capabilities as well as the shortcomings of the proposed techniques are demonstrated on more practical numerical examples in Chapter 11. Finally, Chapter 12 summarises and discusses the present work, and possible future research objectives are outlined.

2 Preliminaries

Within this chapter the utilised notation is explained. Frequently used mathematical operations and different kinds of derivatives are stated. The software environment, in which the proposed analysis tools have been implemented and tested, is introduced.

2.1 Notation

The notation, presented in Table 2.1, is utilised within this thesis to distinguish between scalars, vectors, matrices and tensors of different order. Some examples are given in this table. Similar notation was introduced in [98]. The meaning of the individual symbols is explained at the places where they appear. Some symbols are used for different purposes in several places, for example, to denote loop parameters.

Table 2.1: Utilised notation

quantities	typographic style	examples
scalars	nonbold	A, a, Λ, λ
vectors matrices second-order tensors	bold	$\mathbf{A}, \mathbf{a}, \mathbf{\Lambda}, \mathbf{\lambda}$
third-order tensors fourth-order tensors	blackboard bold	\mathbb{A}, \mathbb{T}

Standard notation is used to denote products between matrices and vectors. All relevant products between physical tensors are specified in Table 2.2.

Table 2.2: Products between physical tensors

description	symbolic notation
scalar product of two vectors	$c = \mathbf{a} \cdot \mathbf{b}$
cross product of two vectors	$\mathbf{c} = \mathbf{a} \times \mathbf{b}$
dyadic product of two vectors	$\mathbf{C} = \mathbf{a} \otimes \mathbf{b}$
contraction of a second-order tensor and a vector	$\mathbf{c} = \mathbf{A}\mathbf{b}$
contraction of two second-order tensors	$\mathbf{C} = \mathbf{A}\mathbf{B}$
scalar product of two second-order tensors	$c = \mathbf{A} : \mathbf{B}$
scalar product of a fourth-order tensor and two second-order tensors	$d = \mathbf{A} : \mathbf{C} : \mathbf{B}$
contraction of a fourth-order tensor and a second-order tensor	$\mathbf{C} = \mathbb{A} : \mathbf{B}$

2.2 Derivatives and variations

Different kinds of derivatives and variations are explained and the corresponding notation is introduced. The utilised notation is similar to that in [98].

Directional derivative

Let $J(\mathbf{v})$ be a possible functional which is nonlinear with respect to the variable $\mathbf{v} \in \mathcal{V}$. It is defined on a Hilbert space \mathcal{V} , i.e. $J : \mathcal{V} \rightarrow \mathbb{R}$. If $J(\cdot)$ is a differentiable functional on \mathcal{V} , the following notation is used for the *Gâteaux derivatives* (i.e. *directional derivatives*)

$$\begin{aligned}
 J'_v(\mathbf{v}; \boldsymbol{\eta}) &:= \lim_{\varepsilon \rightarrow 0} \frac{J(\mathbf{v} + \varepsilon \boldsymbol{\eta}) - J(\mathbf{v})}{\varepsilon} = \left. \frac{d}{d\varepsilon} J(\mathbf{v} + \varepsilon \boldsymbol{\eta}) \right|_{\varepsilon=0}, \\
 J''_{vv}(\mathbf{v}; \boldsymbol{\eta}, \boldsymbol{\mu}) &:= \lim_{\varepsilon \rightarrow 0} \frac{J'_v(\mathbf{v} + \varepsilon \boldsymbol{\mu}, \boldsymbol{\eta}) - J'_v(\mathbf{v}; \boldsymbol{\eta})}{\varepsilon} = \left. \frac{d}{d\varepsilon} J'_v(\mathbf{v} + \varepsilon \boldsymbol{\mu}; \boldsymbol{\eta}) \right|_{\varepsilon=0}.
 \end{aligned} \tag{2.1}$$

The quantity $J'_v(\mathbf{v}; \boldsymbol{\eta})$ is linear with respect to $\boldsymbol{\eta}$ and the term $J''_{vv}(\mathbf{v}; \boldsymbol{\eta}, \boldsymbol{\mu})$ is linear with respect to $\boldsymbol{\eta}$ and $\boldsymbol{\mu}$. Both quantities are nonlinear with respect to \mathbf{v} .

Variation

A *variation* of a functional $J(\cdot)$ is equal to the directional derivative. Usually, the δ symbol is used to denote a variation. For example, the first variation of $J(\cdot)$ with respect to \mathbf{v} is written as $\delta_v J(\mathbf{v}; \delta \mathbf{v})$ or $\delta_v J(\mathbf{v})(\delta \mathbf{v})$ with $\delta \mathbf{v} \in \mathcal{V}$. The relation

$$\delta_v J(\mathbf{v}; \delta \mathbf{v}) = J'_v(\mathbf{v}; \delta \mathbf{v}) \tag{2.2}$$

holds true and both notations are used within this work.

Partial and total variations

The functional $J(\cdot)$ can also depend on a second nonlinear function $\mathbf{s} \in \mathcal{S}$ and is written as $J(\mathbf{v}, \mathbf{s})$. Also \mathcal{S} is a Hilbert space. The *partial variations* with respect to \mathbf{v} and \mathbf{s} are

$$J'_v(\mathbf{v}, \mathbf{s}; \boldsymbol{\eta}) = \left. \frac{d}{d\varepsilon} J(\mathbf{v} + \varepsilon\boldsymbol{\eta}, \mathbf{s}) \right|_{\varepsilon=0} \quad \text{and} \quad J'_s(\mathbf{v}, \mathbf{s}; \boldsymbol{\psi}) = \left. \frac{d}{d\varepsilon} J(\mathbf{v}, \mathbf{s} + \varepsilon\boldsymbol{\psi}) \right|_{\varepsilon=0}. \quad (2.3)$$

The *total variation* is written as

$$J' = J'_v(\mathbf{v}, \mathbf{s}; \boldsymbol{\eta}) + J'_s(\mathbf{v}, \mathbf{s}; \boldsymbol{\psi}) \quad \text{or} \quad \delta J = \delta_v J(\mathbf{v}, \mathbf{s}; \boldsymbol{\eta}) + \delta_s J(\mathbf{v}, \mathbf{s}; \boldsymbol{\psi}). \quad (2.4)$$

Total partial variation

Within the scope of structural optimisation for the most objective functions and constraints the function \mathbf{v} depends directly on \mathbf{s} , i.e. $\mathbf{v} = \mathbf{v}(\mathbf{s})$. The *total partial variation* with respect to \mathbf{s} is defined as

$$D_s J(\mathbf{v}(\mathbf{s}), \mathbf{s}) \cdot \delta \mathbf{s} = \frac{\partial J}{\partial \mathbf{s}} \cdot \delta \mathbf{s} + \frac{\partial J}{\partial \mathbf{v}} \frac{d\mathbf{v}}{d\mathbf{s}} \cdot \delta \mathbf{s}. \quad (2.5)$$

2.3 Software environment

The proposed analysis tools and algorithms are implemented and tested in *MATLAB R2012b* [9]. The corresponding code is called *structural optimisation program* (SOP). *MATLAB* is platform independent, hence the developed program is tested on *LINUX* and *WINDOWS* operating systems. The following toolboxes are employed

- optimisation toolbox,
- parallel computing toolbox,
- symbolic math toolbox,
- *MATLAB* coder,
- *MATLAB* compiler,
- *MATLAB* report generator.

Within this thesis *sequential quadratic programming* (SQP) is utilised to solve non-linear optimisation problems. The function *QUADPROG*, which is part of the optimisation toolbox, is called to solve quadratic subproblems within SQP procedure. System matrices and vectors are assembled using parallel computing toolbox to speed up the computational time. By means of *MATLAB* coder and compiler the developed code is exported to *C++* files and is compiled to obtain so called *mex-files*, which can be called by *MATLAB* instead of original functions. In this manner, the computational time of some functions is reduced to a fraction of its initial value. Analytical derivatives of some functions are verified by symbolic math toolbox. The developed code is documented utilising the *MATLAB* report generator.

Features of SOP

The structural optimisation program (SOP) can be utilised to analyse nonlinear structural behaviour, which include buckling. Arbitrary elastic 3D materials can be considered. The implemented solid shell element can be used either in solid or in shell mode. Hence, 3D structures can be modelled as curved surfaces or as volumes. Analytical sensitivity analysis and structural optimisation are the major purposes of SOP. Here, geometry and morphing based shape parametrisation techniques are available. SOP is also used for teaching purposes at TU Dortmund within introductory seminars on numerical methods in engineering and on structural optimisation.

Efficient singular value decomposition with MATLAB

Singular value decomposition (SVD), *generalised singular value decomposition* (GSVD) and *eigenvalue decomposition* (EVD) are frequently used linear algebra tools within this work, see chapter 7 for more details on this topic. The corresponding *MATLAB* functions are *SVD*, *GSVD* and *EIG*. Functions mentioned above are only valid for full populated matrices and allow the computation of singular values and eigenvalues without the construction of the corresponding vectors.

Within finite element method sparse populated matrices are utilised to save the storage space. *MATLAB* provides the functions *SVDS* and *EIGS* to deal with such matrices. *ARPACK* [3] and *LAPACK* [8] libraries are called by these functions to compute sparse decompositions. In addition, sparse decompositions make it possible to compute only some first or last vectors and values, which is advantageous for the corresponding numerical effort. There is no possibility to compute sparse generalised singular value decomposition in *MATLAB*, but such an algorithm is already developed and is presented in [80].

Fast visualisation with ParaView

ParaView [11] is an open-source, multi-platform data analysis and visualisation application. *ParaView* can quickly build visualisations to analyse large datasets using qualitative and quantitative techniques. Data can be explored interactively or in batch mode. Within this thesis, *MATLAB* data is exported in *VTK* format and is post processed with *ParaView*. Optimisation history including the structural shape can be tracked rapidly considering the complete model or only parts of it. The provided graphical user interface is very intuitive to use.

3 Elements of structural optimisation

Within this chapter, an introduction to structural optimisation is given. Its main aspects are highlighted and a general optimisation procedure is outlined. Topics which are relevant for this thesis are commented on with references to literature.

3.1 Introduction

Structural optimisation is a field of research which deals with fundamentals, methods and applications of mathematical optimisation for computer aided optimal design of structural components, constructions and general mechanical systems. In this context, mathematical optimisation means the detection of the best choice of all possible alternatives within a decision process employing mathematical and numerical algorithms. Structural optimisation delivers solutions, which are optimal in the proper sense. That means, that determined design parameters minimise or maximise the objective function and satisfy the constraints. Typical objectives in structural optimisation are, for example, the stiffness of structures, natural frequencies, used mass or quantity of material, maximum Von Mises stress and costs of constructions. Typical constraints are stress constraints, manufacturing constraints, volume or mass constraints and damage criteria. Quantities, which have influence on the mentioned objectives and constraints are called design parameters or variables. Such quantities are, for example, thickness or cross-section of structural parts, material distribution and shape parameters like coordinates of control points or radii of circles. In this context, optimisation means an automatic process of design generation in contrast to improvement or even trying out of different designs. There is a lot of literature, books and papers dealing with basic topics of structural optimisation or discussing details on numerical algorithms and their implementation, for example [45, 75, 43, 44, 27, 123, 21, 88, 40].

Within this thesis only shape optimisation is considered, but all developed techniques are also valid for other types of structural optimisation, see for example [63]. These types are briefly introduced and summarised in the next section.

3.1.1 Branches of structural optimisation

Talking about mechanics or mechanical problems four types of structural optimisation can be distinguished

- sizing optimisation,
- shape optimisation,
- topology optimisation,
- material optimisation.

Each of them has its own right to exist. Depending on the task, also mixed applications are possible. Therefore, an individual introduction to each type is necessary.

Sizing optimisation. The most obvious and one of the simplest kinds of structural optimisation is to make use of some simple size parameters like cross-section values or thickness of structural members as design variables. These parameters have no influence on topology and shape of the structure, so they can not be changed. An example for sizing optimisation is the detection of optimal cross-sectional areas of truss members to minimise the volume of the structure under stress constraints. The reader is referred to [45, 75] to be introduced in sizing. Recent articles on this topic are, for example [58, 144, 133].

Shape optimisation. Minimising or maximising an objective function by modifying the geometrical boundary of the structure is called *shape optimisation*. This type of optimisation is not able to change the topological properties of a structure. That means, that no holes or inclusions can be removed or created. To set up the initial model, the design engineer is demanded to have a lot of experience. As the structural analysis is usually performed by *finite element method* (FEM), changes in shape cause distortions of finite element mesh, which must be taken into account within the optimisation process. The advantages of shape optimisation are the smooth shapes with relatively coarse meshes, simple definition of manufacturing constraints and uncomplicated or automatic generation of *computer aided geometric design* (CAGD) model of optimised structure. In addition to standard literature on structural optimisation, see [27, 123, 75], the reader is referred to [77] to be introduced in shape optimisation.

Topology optimisation. Distribution of material in a prescribed space minimising or maximising of a given objective function is called *topology optimisation*. The shape of the structure and its topological properties can be optimised simultaneously. That means that optimal connectivity of material regions and the optimal number, shape and positions of holes and inclusions can be detected. Topology optimisation allows to generate mechanical structures fully automatically. Standard literature on topology optimisation is [29, 27, 28]. Unfortunately, numerical instabilities appear in most formulations. These are, for example, checkerboard patterns, mesh-dependencies and

local minima. A number of techniques were developed to overcome such problems, see [126, 34, 127]. Producibility of optimised structures, automatic extraction of geometrical description (CAGD-model) and the need of fine meshes for smooth details mark the limits of the application area of this type of structural optimisation.

Material optimisation. As already explained, topology optimisation deals with spatial distribution of material. A local optimisation of material properties is called *material optimisation*, see [27]. Here, the local optimal choice of micro structure, which can be different from point to point, is detected. An example for this type of structural optimisation is maximising the stiffness of a structure, which consists of composite material computing optimal layer orientations on discrete points. Such applications have gained an ever increasing popularity especially in aircraft industry, because the corresponding structures exhibit superior mechanical properties and lead to low weight. Recent articles concerned with this topic are [76, 149, 62].

3.1.2 General procedure of structural optimisation

All introduced types of structural optimisation follow the same flowchart, which is pictured in Figure 3.1 and will be explained in this section. Within this thesis, only gradient based methods are considered.

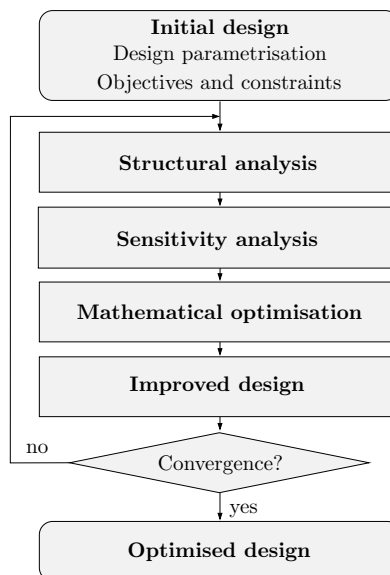


Figure 3.1: General procedure of structural optimisation

Before starting the optimisation process, the mathematical problem is described ex-

actly. Objective function and constraints are defined and the model is parametrised. This includes the definition of design variables. The mechanical problem with the corresponding boundary conditions and material properties is formulated.

Within the optimisation loop, the first task is to perform structural analysis. That means, that the equilibrium state is determined and all necessary quantities like stresses, natural frequencies, buckling loads, energy, etc. are calculated.

Based on this information sensitivity analysis is carried out. The total derivatives of all objectives and constraints with respect to design variables are computed at this stage. The task is to answer the question: ‘How do the objective function and constraints react, if design variables are changed?’.

Values of objective functions and constraints and also their derivatives are passed to the so called *mathematical optimiser*. This is a toolbox, which uses mathematical-numerical algorithms to minimise or maximise the value of objective function taking into account the constraints and delivers an update of design variables.

Then, the mechanical model is updated and quantities of interest are compared with some predefined truncation criteria. All mentioned steps are repeated until convergence is reached. The converged solution is delivered to design engineer as a possible draft and must be interpreted and judged. We note, that optimised structures usually represent local minima of objective functions and are especially not unique. Different initial parameters usually lead to different results.

All steps of the flowchart pictured in Figure 3.1 represent their own scientific disciplines. This is the reason for highly complex stand alone software solutions for structural optimisation. The mentioned disciplines are commented on with references to literature within the next sections of this chapter. Details which are relevant for this thesis are highlighted.

3.2 Parametrisation of shape

To optimise the shape of a given structure a number of parameters, which control the boundary geometry must be chosen as design variables. The three different existing strategies are

- CAGD based shape optimisation,
- parameter-free or FE-node based shape optimisation,
- morphing based shape optimisation.

These parametrisation techniques are explained within this section. We note that only morphing based shape parametrisation is utilised within this work.

CAGD based shape optimisation. *Computer-Aided Geometric Design* (CAGD) is the mathematical description of geometrical objects like lines, areas and volumes, see for example [57], which is suitable for visualisation on computers. Based on CAGD-model, FE-mesh is created to perform structural analysis. Changes in CAGD parameters lead to modified positions of FE-nodes, which define the approximated shape of the structure. Such parameters are, for example, coordinates of control points, radii of circles and lengths of lines. Some of them are chosen as design variables for shape optimisation, see [45, 43, 44, 123]. Gradients of objectives and constraints are then computed with respect to these parameters. Here, the chain rule is applied and firstly, the derivatives with respect to coordinates of FE-nodes are computed and secondly, the derivatives of FE-node coordinates with respect to CAGD parameters are determined. Last mentioned derivatives are called *design velocity fields*. The main advantages of the method are: optimised structures are automatically described by corresponding CAGD-model and can be manufactured immediately; the number of design variables is low. Unfortunately, the effort to be done to define the optimisation model and the corresponding geometrical constraints is enormous for practical applications. To have advantage of analytically derived sensitivities, CAGD software must be extended with sensitivity routines and a bidirectional interface for *Computer-Aided-Engineering* (CAE) software must be implemented. These facts make the parametrisation strategies below more attractive.

Parameter-free shape optimisation. A special approach to shape optimisation is choosing the coordinates of FE-nodes as design variables. No CAGD model is needed, standard CAE preprocessing tools can be used to formulate an optimisation problem and maximal degree of freedom for shape changes is reached. For a long time FE-node based shape optimisation was not considered to be effective as quoted in [73, 35]. The reasons are the large number of FE mesh resolution dependent design variables and the problems with jagged boundaries and disturbed FE-meshes, which causes non-physical optimisation results. The latter drawbacks of parameter-free approach seem to be a matter of the past. The recent works in this area, see [32, 119, 93, 66] and the references therein, report about successful applications of nodal based shape optimisation to real world problems. The jagged boundaries and convergence problems are eliminated either by using a fictitious energy approach [119] or by applying filter techniques [32, 93, 66]. Despite all deficiencies, the absence of CAGD based geometry model and its high modelling effort makes nodal based shape optimisation exceedingly attractive but optimised structures must be post processed manually to obtain CAGD description for manufacturing.

Morphing based shape optimisation. A smooth transformation of an object into another one is called *morphing*. This technique comes from image processing and is widespread in film industry to create video and audio special effects. In context of shape optimisation, morphing is used to parametrise the shape of some parts of a structure. Here, a simple map, which is valid for a part of structural domain (*mor-*

phing box) is defined and controls positions of FE-nodes located in this part. Such a map requires the inverse computation of local coordinates of FE-nodes before optimisation. Mapping function parameters are then used as design variables. Morphing based shape optimisation combines the advantages of parameter-free and CAGD based approaches. The number of design variables does not depend on the finite element mesh and corresponding problems with jagged boundaries are not present. The modelling and implementation effort is low compared with CAGD based approach but is higher compared with parameter-free techniques. As only finite element nodes are involved in mapping process, arbitrary finite elements can be used once morphing is implemented. Further details on morphing and the corresponding literature overview are provided in chapter 4.

3.3 Structural analysis

Mathematical description of mechanical problems usually leads to a system of partial differential equations (PDE), which are to be solved to predict the behaviour of structures. Analytical solutions for such PDEs are only available for some special cases. In general, they are solved numerically and solutions are only approximated, but the quality of such approximations is adjustable. It is beyond the scope of this work to give an overview on this topic. A first-class up-to-date representations of all major computer-oriented numerical methods for solving PDEs in mechanical context is presented in [14]. The most common discretisation methods are

- finite element method (FEM),
- boundary element method (BEM),
- finite differences method (FDM),
- finite volumes method (FVM).

Within this thesis, the finite element method is utilised to perform structural and sensitivity analysis. Standard literature on this topic is, for example, [152, 25].

3.4 Sensitivity analysis

An overview of structural sensitivity analysis is given in standard literature, see for example [43, 44]. Recommended review articles are [142, 136] and [72]. Four different approaches to sensitivity analysis can be distinguished

- global finite differentiation,
- discrete sensitivity analysis,
- semi-analytical sensitivity analysis,
- variational sensitivity analysis.

The variational approach to sensitivity analysis is utilised within this thesis.

Global finite differentiation. This approach consists of repeated evaluation of quantities of interest for perturbed design variables and the use of finite differentiation formulae. Forward, backward and central differences are the most popular techniques. Implementation of global finite differentiation is simple, but the required number of structural analyses directly depends on the number of design variables. This method is too expensive for most practical applications, but it is usually used to verify analytically derived sensitivity relations on academical examples. The quality of derivatives provided by finite differentiation strongly depends on magnitude of perturbation. Truncation errors appear with large step sizes, but computational errors appear when the step size is too small. More details on this topic can be found in [111, 142, 136].

Discrete sensitivity analysis. The governing continuum equations are discretised and subsequently differentiated with respect to the design variables, see [142, 136]. This approach provides analytical derivatives of quantities of interest, but the corresponding implementation of derived formulas leads to convoluted and slow source code. We note that structural analysis is performed only once for each iteration within this approach. Compared with global finite differentiation, the numerical effort is drastically reduced.

Semi-analytical sensitivity analysis. The most popular approach to sensitivity analysis is the semi-analytical one. It is computationally efficient and easy to implement. Within semi-analytical sensitivity analysis, global quantities are derived analytically and local finite differentiation is applied to finite element matrices. Such an approximation causes errors in some cases. But this drawback seems to be a matter of the past as different methods were developed to eliminate the mentioned errors, see [81, 31, 48, 96] for more details.

Variational sensitivity analysis. The variational approach to sensitivity analysis is the most challenging but advantageous one, see [23, 24, 78]. Here, the sensitivity information is first derived on the continuous level and then discretised to yield the analytical expressions on the computational level. The notation of *sensitivity matrix* and *pseudo load matrix* was introduced in [24, 98, 99] and is especially suitable for shape design problems.

3.5 Mathematical optimisation

Within this thesis, general nonlinear constrained optimisation problems are considered and solved. A great number of methods for solving such problems was developed in the last decades. A possible classification of optimisation methods is given in this chapter, but only the *sequential quadratic programming* (SQP) method, see the review articles [71, 33], is described with more details, because it is used within this thesis. Standard literature on this topic is, for example [105].

3.5.1 Classification of optimisation methods

Three groups of optimisation methods can be distinguished

- zero order optimisation methods,
- first order optimisation methods,
- second order optimisation methods.

They are briefly described in this section.

Zero order optimisation methods. These methods are based only on evaluation of objective functions and constraints. Typical strategies are, for example, the *grid search*, *Powell's method*, *simplex method* and *evolutionary algorithms*. Unfortunately, a large number of iterations is needed and efficiency suffers. Review articles on this topic are [19, 104, 151] and [67].

First order optimisation methods. In addition to function evaluations their gradients are computed and used within first order strategies. Typical methods of this kind are the *steepest descent method*, *conjugate gradients method* and *quasi-Newton methods*, see [105]. The combination of SQP method and BFGS [68, 36, 124, 59] approximation of the second derivative also belongs to this category. Additional information evaluating gradients of functions leads to a speed up of optimisation process and to higher convergence rates. These methods require continuously differentiable objectives and constraints. Gradients cause higher implementation effort, but the numerical effort is moderate.

Second order optimisation methods. Functions evaluations, their gradients and especially Hessian matrices are involved in optimisation process within second order techniques. Most famous method of this group is *Newton's method* [105]. These methods lead to the highest convergence rates, but demand functions to be twice continuously differentiable. The implementation effort and storage space requirements are also the highest ones. Only a few iterations are needed to obtain convergence if the starting point is close enough to the solution.

3.5.2 Sequential quadratic programming

Within this thesis, the *sequential quadratic programming* method (SQP) is used to solve optimisation problems. This method is derived from Newton's method taking constraints into account. It generates steps by solving quadratic sub problems. It is appropriate for small or large problems and is one of the most effective methods for nonlinear constrained optimisation. In this section the most important components of the SQP method are summarised. More details on this topic can be found in

standard literature, see for example [105]. Recommended review articles are [71, 33]. We consider a general nonlinear constrained optimisation problem

$$\begin{aligned}
 J(\mathbf{s}) &\longrightarrow \min_{\mathbf{s} \in \mathbb{R}^n} && \text{subject to} \\
 h_j(\mathbf{s}) &= 0 && \text{with } j \in \{1, \dots, m_h\}, \\
 g_p(\mathbf{s}) &\leq 0 && \text{with } p \in \{1, \dots, m_g\}, \\
 s_i^l &\leq s_i \leq s_i^u && \text{with } i \in \{1, \dots, n\}.
 \end{aligned} \tag{3.1}$$

The appearing quantities are

$$\begin{aligned}
 J : \mathbb{R}^n &\longrightarrow \mathbb{R} && \text{objective function,} \\
 \mathbf{s} &= [s_1, \dots, s_n]^T && \text{design variables,} \\
 h_j : \mathbb{R}^n &\longrightarrow \mathbb{R}, \quad j \in \{1, \dots, m_h\} && \text{equality constraints,} \\
 g_p : \mathbb{R}^n &\longrightarrow \mathbb{R}, \quad p \in \{1, \dots, m_g\} && \text{inequality constraints,} \\
 s_i^l, \quad s_i^u, \quad i &\in \{1, \dots, n\} && \text{lower and upper bounds of design variables.}
 \end{aligned}$$

Introducing the following notation

$$\mathbf{h}(\mathbf{s}) = \begin{bmatrix} h_1(\mathbf{s}) \\ \vdots \\ h_{m_h}(\mathbf{s}) \end{bmatrix}, \quad \mathbf{g}(\mathbf{s}) = \begin{bmatrix} g_1(\mathbf{s}) \\ \vdots \\ g_{m_g}(\mathbf{s}) \end{bmatrix}, \quad \mathbf{s}^l = \begin{bmatrix} s_1^l \\ \vdots \\ s_n^l \end{bmatrix} \quad \text{and} \quad \mathbf{s}^u = \begin{bmatrix} s_1^u \\ \vdots \\ s_n^u \end{bmatrix} \tag{3.2}$$

the problem (3.1) can also be described by

$$\begin{aligned}
 J(\mathbf{s}) &\longrightarrow \min_{\mathbf{s} \in \mathbb{R}^n} && \text{subject to} \\
 \mathbf{h}(\mathbf{s}) &= \mathbf{0}, \\
 \mathbf{g}(\mathbf{s}) &\leq \mathbf{0}, \\
 \mathbf{s}^l &\leq \mathbf{s} \leq \mathbf{s}^u.
 \end{aligned} \tag{3.3}$$

The problem is quadratically approximated in every iteration k for current design \mathbf{s}_k . We receive the following sub problem

$$\begin{aligned}
 \nabla_s J(\mathbf{s}_k)^T \Delta \mathbf{s} + \frac{1}{2} \Delta \mathbf{s}^T \nabla_{ss}^2 L(\mathbf{s}_k, \boldsymbol{\lambda}_k, \boldsymbol{\mu}_k, \mathbf{c}_k) \Delta \mathbf{s} &\longrightarrow \min_{\Delta \mathbf{s} \in \mathbb{R}^n} && \text{subject to} \\
 D_s \mathbf{h}(\mathbf{s}_k) \Delta \mathbf{s} + \mathbf{h}(\mathbf{s}_k) &= \mathbf{0}, \\
 D_s \mathbf{g}(\mathbf{s}_k) \Delta \mathbf{s} + \mathbf{g}(\mathbf{s}_k) &\leq \mathbf{0}, \\
 \mathbf{s}^l - \mathbf{s}_k &\leq \Delta \mathbf{s} \leq \mathbf{s}^u - \mathbf{s}_k.
 \end{aligned} \tag{3.4}$$

The first relation is quadratic in $\Delta \mathbf{s}$. The constraints are approximated linearly. The term $\nabla_{ss}^2 L(\mathbf{s}_k, \boldsymbol{\lambda}_k, \boldsymbol{\mu}_k, \mathbf{c}_k)$ is the second derivative of the Lagrangian function

$$L(\mathbf{s}_k, \boldsymbol{\lambda}_k, \boldsymbol{\mu}_k, \mathbf{c}_k) = J(\mathbf{s}_k) + \sum_{j=1}^{m_h} \lambda_{k,j} h_j(\mathbf{s}_k) + \sum_{p=1}^{m_g} \mu_{k,p} (h_p(\mathbf{s}_k) + c_{k,p}^2), \tag{3.5}$$

with Lagrange multipliers $\boldsymbol{\lambda}_k$, $\boldsymbol{\mu}_k$ and sloop variables \boldsymbol{c}_k . The approximated optimisation problem (3.4) can be solved efficiently with one of the standard methods from quadratic programming, see [105] for more details. Within this thesis, the quadratic subproblems are solved utilising the *QUADPROG* function of the *MATLAB optimisation toolbox*. Thus, we obtain increments of the design variables $\Delta \boldsymbol{s}_k$, Lagrangian multipliers $\boldsymbol{\lambda}_{k+1}$, $\boldsymbol{\mu}_{k+1}$ and sloop variables \boldsymbol{c}_{k+1} for the next iteration. Herewith, the design variables set can be ameliorated with the following update formula

$$\boldsymbol{s}_{k+1} = \boldsymbol{s}_k + \Delta \boldsymbol{s}_k \quad (3.6)$$

in the sense of the optimisation problem. The truncation criterion is fulfilled if

$$\|\Delta \boldsymbol{s}_k\| \leq \textit{tol} \quad (3.7)$$

applies. The norm of the difference vector of variables is denoted $\|\Delta \boldsymbol{s}_k\|$ and the tolerance *tol* is predefined by the user.

The computation of the second derivative of Lagrangian function $\nabla_{\boldsymbol{s}\boldsymbol{s}}^2 L(\boldsymbol{s}_k, \boldsymbol{\lambda}_k, \boldsymbol{\mu}_k, \boldsymbol{c}_k)$ causes high numerical effort and enormous memory requirements. This matrix is usually approximated utilising the Broyden-Fletcher-Goldfarb-Shanno (BFGS) update formula, see [68, 36, 124, 59], which is based on the first derivative of Lagrangian function and some iteration history. BFGS is also utilised in this thesis.

3.6 Summary and concluding remarks

The main aspects and possible settings of structural optimisation environment are discussed in this chapter. Theoretical approaches and numerical techniques which are utilised within this thesis are highlighted. In following, they are summarised. Shape optimisation problems with morphing based parametrisation are considered. Nonlinear finite element analysis is employed for structural analysis. Variational approach to sensitivity analysis is utilised. Sequential quadratic programming method which is based on gradients of objectives and constraints is used to solve general nonlinear constrained optimisation problems. *QUADPROG* function of the *MATLAB optimisation toolbox* is utilised to solve the corresponding quadratic subproblems.

4 Morphing based shape parametrisation

Within this chapter, morphing based shape parametrisation is introduced. Mapping functions, which are based on tensor products of B-splines with arbitrary number of control points and of arbitrary degree, are considered. Especially, analytical design velocity fields are derived.

4.1 Introduction

The term morphing is used in computer graphics for a technique which produces a smooth and continuous transition from a source object into a target object. It is derived from metamorphosis which means the change of shape in biology or geology.

4.1.1 State of the art

The idea of morphing was first applied to 2D images. A review of different approaches is given in [146]. The techniques were extended to 3D geometry models, see [130] and [147] for an overview. Image morphing has been developed to a powerful tool for visual effects in entertainment industry, medical imaging or scientific visualization.

Many iterations with multiple changes of the geometry are often involved in shape optimisation. For rapid updating the FE-mesh to the modified geometry the morphing techniques have been adopted to avoid costly remeshing, see [110]. Different researches advance the functionality of these methods, some approaches are compared in [108] and [131]. Based on [108] and [131] further studies improve the quality of mesh-morphing, [125]. Morphing based optimisation is used in commercial software like ANSA [1], *HYPERMORPH* [7] and *OPTISLANG* [10].

4.1.2 Special features of the presented research

Within this thesis, morphing boxes are described by general *B-spline* tensor products with arbitrary number of control points and arbitrary degree of basis splines.

Hence, the most possible freedom is given to the design engineer during the problem definition. The corresponding implementation in *MATLAB* leads to a toolbox where requirements on the smoothness and differentiability of shape functions can be taken into account. A technique is proposed, which allows the reverse computation of local coordinates of finite element nodes, considering morphing boxes with complex initial shape. In addition, the geometry based shape parametrisation is considered as a special case of morphing of FE-mesh. Advantages of morphing like the usage of arbitrary finite element types, simple parametrisation of the optimisation model and its uncomplicated implementation are discussed.

Furthermore, sensitivity of FE-node positions with respect to changes of control point positions is derived analytically and implemented in the above mentioned toolbox. Hence, analytically derived *design velocity fields matrices* are available, which complement variational design sensitivity analysis of shell structures, see chapter 6, and are hardly to find in literature.

4.2 An introduction to B-splines

The expression B-spline is a short form for basis spline, see [49, 57] and [112]. Here a basis to a given degree, smoothness and domain partition is calculated and linear combination of its components is used to create curves. The parameters (scale factors) of such linear combination are called *control points*. Utilising tensor products of B-splines areas and volumes can be created. Local changes of control points cause only local shape changes of such geometrical objects. This is the main advantage in contrast to *Bézier based geometries*, for example.

4.2.1 B-spline basis

Basis for a B-spline curve $\mathbf{L}_k^n(r)$ or short $\mathbf{L}(r)$ of order k through $n + 1$ control points consists of $n + 1$ blending functions $N_{i,k}$ with $i = 0, \dots, n$. These functions are of degree $k - 1$ and can be calculated recursively

$$N_{i,1} = \begin{cases} 1 & \text{for } r_i \leq r \leq r_{i+1} \\ 0 & \text{otherwise} \end{cases}, \quad (4.1)$$

$$N_{i,m} = \frac{(r - r_i)N_{i,m-1}(r)}{r_{i+m-1} - r_i} + \frac{(r_{i+m} - r)N_{i+1,m-1}(r)}{r_{i+m} - r_{i+1}} \quad \text{with } m = 2, 3, \dots, k.$$

The node vector $\mathbf{r} = [r_0, \dots, r_{n+k}]^T$ consists of components r_j with $j = 0, \dots, n + k$ and can be created utilising the following scheme

$$r_j = \begin{cases} 0 & \text{for } j < k \\ j - k + 1 & \text{for } k \leq j \leq n \\ n - k + 2 & \text{for } j > n \end{cases}. \quad (4.2)$$

The first k node vector values and the last k ones are each equal. Inner nodes are different but are ordered equidistant. Basis functions defined in equation (4.1) are set to zero in cases where their numerator and denominator are equal zero. Basis functions for $m = 1$ are piecewise constant and jump at interval bounds. They are equal to one within the interval and to zero outside. For $m = 2$ these functions are first degree polynomials and so on. Main properties of basis functions are

- $N_{i,m} \neq 0$ only within the interval $[r_i, r_{i+m}]$,
- $N_{i,m}$ is a polynomial of degree $m - 1$,
- transitions of $N_{i,m}$ are continuous till the $m - 2$ th derivative.

Utilising the scheme in equation (4.2), the curve parameter r is in interval $[0, n-k+2]$. It is more convenient to work with normalised curve parameter \hat{r} which is in interval $[0,1]$. In this case the value of \hat{r} can be mapped to r as follows

$$r = \hat{r}(n - k + 2). \tag{4.3}$$

4.2.2 B-spline curves

A B-spline curve is defined as

$$\mathbf{L} : \mathbb{R} \longrightarrow \mathbb{R}^3 \quad \text{with} \quad \mathbf{L}(r) = \sum_{i=0}^n \mathbf{C}_i N_{i,k}(r), \tag{4.4}$$

where coordinates of control point i are stored in vector $\mathbf{C}_i \in \mathbb{R}^3$. The 3D case is considered within this thesis. B-spline curves which are defined by eight control points are pictured in Figure 4.1 for different values of k .

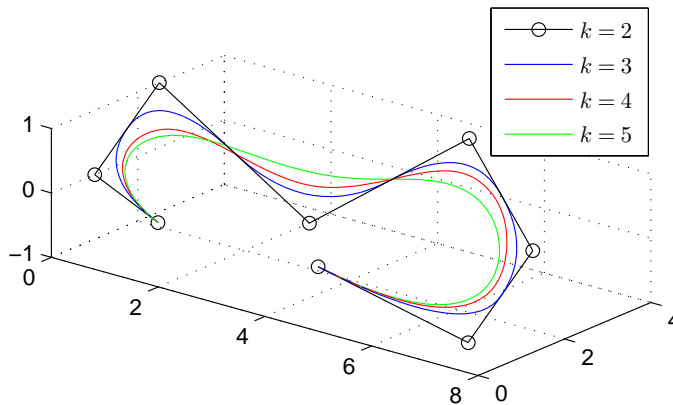


Figure 4.1: B-spline curves for different values of k

For $k = 2$ the curve corresponds to the control polygon. For values $k > 2$ all curves interpolate the first and the last control points. Tangents at these points are defined by the second and penultimate nodes. For curve order $k = 3$ quadratic splines are used as basis functions. In this case the middle points of internal lines of the control polygon are also interpolated. B-spline curves of order $k = 3$ are used within this thesis because the last mentioned property is convenient for defining bounds of design variables. B-spline curves of order 4 are based on cubic basis functions and are most widespread in CAGD and CAE because of their smoothness.

4.2.3 B-spline tensor products

Applying tensor products to bases of different B-splines areas and volumes can be created, see [57]. B-spline area is defined as

$$\mathbf{A} : \mathbb{R}^2 \longrightarrow \mathbb{R}^3 \quad \text{with} \quad \mathbf{A}(r, s) = \sum_{i=0}^n \sum_{j=0}^p \mathbf{C}_{i,j} N_{i,k}(r) N_{j,l}(s). \quad (4.5)$$

Control points $\mathbf{C}_{i,j} \in \mathbb{R}^3$ define a two dimensional grid. Number of control points and degree of basis functions can be different in each direction. Only control points in the corners are interpolated. All these properties are also valid for B-spline volumes which are defined as follows

$$\mathbf{V} : \mathbb{R}^3 \longrightarrow \mathbb{R}^3 \quad \text{with} \quad \mathbf{V}(r, s, t) = \sum_{i=0}^n \sum_{j=0}^p \sum_{h=0}^u \mathbf{C}_{i,j,h} N_{i,k}(r) N_{j,l}(s) N_{h,v}(t), \quad (4.6)$$

and where $\mathbf{C}_{i,j,h}$ represent a three dimensional grid. In context of morphing, the mapping function $\mathbf{V}(r, s, t)$ is used within this thesis. Normalising its parameters we obtain a more convenient map for shape optimisation which reads

$$\begin{aligned} \hat{\mathbf{V}} : [0, 1] \times [0, 1] \times [0, 1] &\longrightarrow \mathbb{R}^3 \quad \text{with} \\ \hat{\mathbf{V}}(\hat{r}, \hat{s}, \hat{t}) &= \sum_{i=0}^n \sum_{j=0}^p \sum_{h=0}^u \mathbf{C}_{i,j,h} N_{i,k}(r(\hat{r})) N_{j,l}(s(\hat{s})) N_{h,v}(t(\hat{t})) \quad \text{and} \\ r(\hat{r}) &= \hat{r}(n - k + 2), \\ s(\hat{s}) &= \hat{s}(p - l + 2), \\ t(\hat{t}) &= \hat{t}(u - v + 2). \end{aligned} \quad (4.7)$$

4.3 CAGD controlled FE-mesh

In CAGD based shape optimisation the geometry of the structure is completely described by CAGD objects. Such objects are then processed successively and are subdivided into simple geometric forms, see [57, 51, 60]. The finite element mesh is

generated which is an approximation of the physical geometry. CAGD parameters are changed and FE-node positions are recalculated to modify the approximated shape of the structure. In this thesis, only B-spline volumes are considered as CAGD objects.

4.3.1 Generation of FE-mesh

Creation of finite element mesh based on CAGD model is briefly described in this section as it exhibits several commonalities with morphing procedure. This process is based on the following three steps:

- construction of FE-mesh in local coordinates,
- mapping of FE-nodes to global coordinates,
- controlling the quality of FE-elements in global coordinates.

For each B-spline volume a grid is constructed in local coordinates $\hat{r}, \hat{s}, \hat{t} \in [0, 1]$, see for example Figure 4.2a. The topology and density of this grid, i.e. number of nodes in each direction and element connectivity, correspond to desired FE-mesh but the coordinates of nodes must be mapped to global coordinate system (CS). This step is done utilising the map in equation (4.7). The final FE-mesh and the corresponding control polygon of considered example are pictured in Figure 4.2b. The approximated shape of the structure is mainly described by control points which are defined in CAGD model.

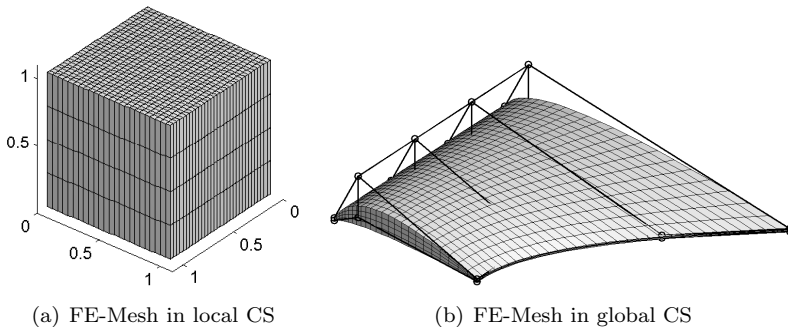


Figure 4.2: FE-mesh generation for a part of a wing

Changes in positions of control points cause changes in coordinates of FE-nodes. Therefore, coordinates of control points are used as design variables to control the shape of the structure. During optimisation process coordinates of control points are modified by mathematical optimiser. Then, global positions of all nodes are recalculated. Local coordinates of FE-nodes are considered to be fixed. To demonstrate this process, the upper control point in Figure 4.2b is moved upward. The updated CAGD model and the corresponding FE-mesh are pictured in Figure 4.3.

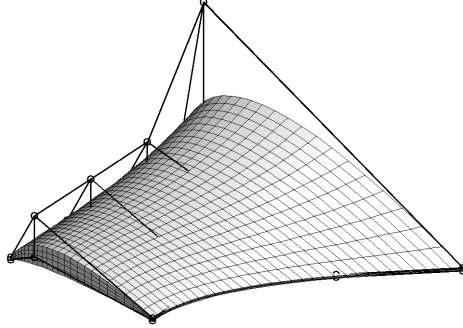


Figure 4.3: CAGD based geometry modification for a part of a wing

The disadvantage of this type of shape parametrisation consist in the usage of parameters provided by CAGD model as design variables. Course CAGD models restrict the design space. The definition of bounds and constraints for design variables cause a high modelling effort for realistic models.

Considering multiple B-spline volumes it is sometimes important to ensure continuity and smoothness of body transitions during shape optimisation. For continuity control points of different bodies at interfaces must be either at the same places or they must be commonly used by these bodies. To ensure smoothness of lines interface control points must be on a straight with next interior control points on the lines. This transitional condition can be simply extended to surfaces.

4.3.2 Design velocity field

To perform sensitivity analysis of objectives and constraints with respect to design variables, total derivatives of coordinates of FE-nodes with respect to coordinates of control points are required. These derivatives are called *design velocity fields* and are derived in this section. We consider equation (4.7) and suggest global coordinates to be x, y and z . Therefore, components of vectors are denoted as $\hat{\mathbf{V}} = [\hat{V}^x \ \hat{V}^y \ \hat{V}^z]^T$ and $\mathbf{C} = [C^x \ C^y \ C^z]^T$. With indices $\alpha, \beta \in \{x, y, z\}$ we obtain the first derivative of a 3D point in global coordinates with respect to coordinates of control points

$$\frac{d\hat{\mathbf{V}}^\alpha(\hat{r}, \hat{s}, \hat{t})}{dC_{i,j,h}^\beta} = \delta_{\alpha\beta} N_{i,k}(r(\hat{r})) N_{j,l}(s(\hat{s})) N_{h,v}(t(\hat{t})) \quad \text{with} \quad (4.8)$$

$$\delta_{\alpha\beta} = \begin{cases} 1 & \text{for } \alpha = \beta \\ 0 & \text{for } \alpha \neq \beta \end{cases}.$$

This equation must be evaluated for each FE-node $\hat{\mathbf{X}}_m(\hat{r}_m, \hat{s}_m, \hat{t}_m)$ for all possible values of α and β . The calculated derivatives are stored in the so called *design velocity*

fields matrix Ψ . The column j of this matrix is the variation of FE-node coordinates with respect to a variation of the design variable j . The row i represents gradient of FE-node coordinate i . All components of all FE-nodes are summarised in the vector $\hat{\mathbf{X}}$ and that of control points in the vector $\hat{\mathbf{C}}$. The desired sensitivity relation reads

$$d\hat{\mathbf{X}} = \Psi d\hat{\mathbf{C}}. \quad (4.9)$$

We note, that this sensitivity relation is also true in context of morphing as it is explained in the next section.

4.4 Morphing controlled FE-mesh

In context of morphing the geometry of the structure is given in form of FE-mesh. Only global coordinates of nodes and connectivity of elements are provided. Regions of structure whose shape is to be changed during optimisation process are marked by the so called *morphing boxes*. These boxes are simple CAGD objects and they do not have to describe the geometric boundary of the structure. They may cross structural surfaces and can lie within or outside the structure. Within this thesis, general B-spline volumes are utilised as morphing boxes.

4.4.1 The procedure of morphing

Steps of the flow chart pictured in Figure 4.4 are performed to morph a given mesh.

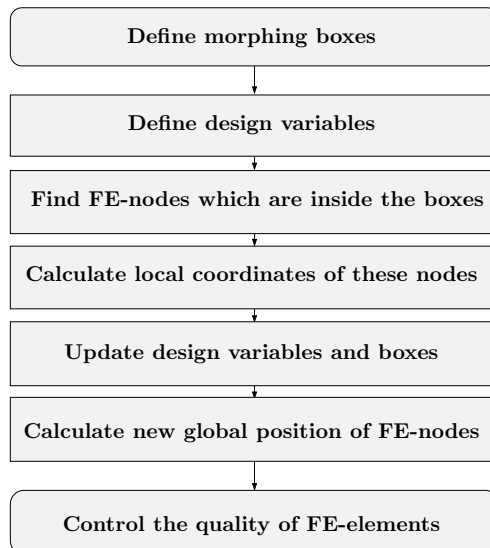


Figure 4.4: Flow chart of morphing

After the definition of morphing boxes, design variables are chosen. In case of B-spline volumes as morphing boxes, these are the positions of some control points. FE-nodes are scanned to find out which of them must be considered during morphing. The corresponding nodes are called *active nodes*. At the same time local coordinates of nodes which are in the boxes are calculated. Details on this topic are explained in the section 4.4.3. These steps are performed before the optimisation process starts. During the optimisation procedure positions of control points are updated and global coordinates of active nodes are calculated similar to CAGD based shape optimisation, utilising the mapping function (4.7). The computation of design velocity fields matrix is in accordance with section 4.3.2 as it is done for CAGD based FE-mesh control.

To demonstrate this technique, FE-mesh pictured in Figure 4.2b is considered. A morphing box is defined to modify the right part of the wing, see Figure 4.5a. This box crosses the wing in about its middle. Active nodes are marked by a star. Positions of some control points are changed. The corresponding control polygon and the modified FE-mesh are pictured in Figure 4.5b.

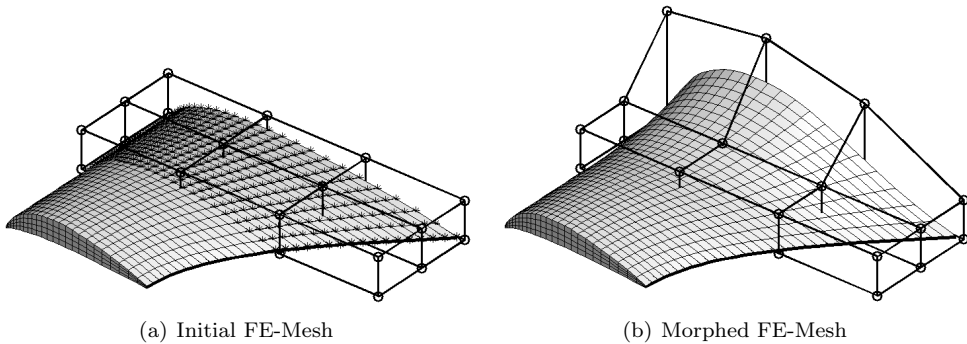


Figure 4.5: FE-mesh morphing for a part of a wing

The transition continuity of the left and the right parts of the wing is ensured since the control points which define the interface are not moved. The smoothness of the transition is maintained because control points near the interface surface are not moved. As one can recognise, experience of CAGD-based shape optimisation is also advantageous within morphing techniques.

4.4.2 CAGD as special case of morphing

In the special case where morphing boxes describe the geometric boundary of the structure, the shape parametrisation is in accordance with CAGD-based model. That means, that exactly the same shape changes as pictured in Figure 4.3 can be reached by morphing of FE-mesh introduced in Figure 4.2b. For this reason the initial mesh

is marked utilising the morphing box pictured in Figure 4.6a. The positions of control points are updated, as shown in Figure 4.6b and FE-nodes are recalculated.

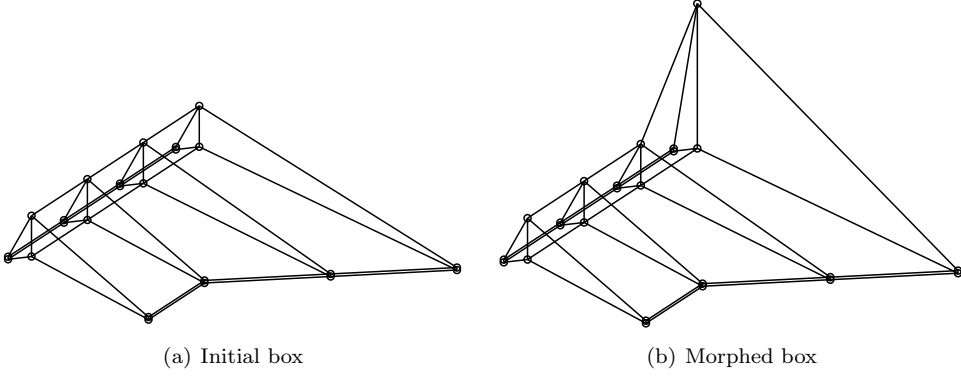


Figure 4.6: Morphing box based on CAGD description

The mentioned property is also valid if only some surfaces of the structure and of the morphing boxes are considered. This fact makes it possible to obtain directly a CAGD-based geometry description of optimised parts of a structure. Faces and edges of the considered morphing boxes are, for example, B-spline areas and lines which control points are directly delivered by the boxes.

4.4.3 Inverse computation of FE-node positions

Usually, global coordinates of FE-nodes are given. Local coordinates of these nodes are required to perform morphing based on the mapping function $\hat{\mathbf{V}}(\hat{r}, \hat{s}, \hat{t})$ which is given in equation (4.7). Therefore, for a given three dimensional point $\bar{\mathbf{X}} = [\bar{x} \ \bar{y} \ \bar{z}]^T$ its local coordinates \bar{r} , \bar{s} and \bar{t} must be calculated. Derivation of the corresponding inverse function is complicated and its implementation is expensive. To avoid this circumstance, the following system of nonlinear equations is considered

$$\bar{\mathbf{X}} - \hat{\mathbf{V}}(\hat{r}, \hat{s}, \hat{t}) = \mathbf{0}. \quad (4.10)$$

The desired local coordinates are obtained by solving this system of equations. For this reason, Newton's method is utilised. The first derivative of the map $\hat{\mathbf{V}}(\hat{r}, \hat{s}, \hat{t})$

with respect to parameters \hat{r} , \hat{s} and \hat{t} must be calculated in each iteration and reads

$$\begin{aligned}
 \frac{\partial \hat{V}(\hat{r}, \hat{s}, \hat{t})}{\partial \hat{r}} &= \sum_{i=0}^n \sum_{j=0}^p \sum_{h=0}^u C_{i,j,h} \frac{\partial}{\partial r} N_{i,k}(r(\hat{r})) (n-k+2) N_{j,l}(s(\hat{s})) N_{h,v}(t(\hat{t})), \\
 \frac{\partial \hat{V}(\hat{r}, \hat{s}, \hat{t})}{\partial \hat{s}} &= \sum_{i=0}^n \sum_{j=0}^p \sum_{h=0}^u C_{i,j,h} N_{i,k}(r(\hat{r})) \frac{\partial}{\partial s} N_{j,l}(s(\hat{s})) (p-l+2) N_{h,v}(t(\hat{t})), \\
 \frac{\partial \hat{V}(\hat{r}, \hat{s}, \hat{t})}{\partial \hat{t}} &= \sum_{i=0}^n \sum_{j=0}^p \sum_{h=0}^u C_{i,j,h} N_{i,k}(r(\hat{r})) N_{j,l}(s(\hat{s})) \frac{\partial}{\partial t} N_{h,v}(t(\hat{t})) (u-v+2).
 \end{aligned} \tag{4.11}$$

To evaluate these equations, derivatives of B-spline bases given in equation (4.1) with respect to their parameter are necessary and are given in general form

$$\frac{\partial}{\partial r} N_{i,m} = \frac{(m-1)N_{i,m-1}(r)}{r_{i+m-1} - r_i} + \frac{(m-1)N_{i+1,m-1}(r)}{r_{i+m} - r_{i+1}} \quad \text{with } m = 3, \dots, k. \tag{4.12}$$

The mentioned Newton's method is applied to every FE-node. Usually less than ten iterations are needed to obtain convergence. In case of convergence the corresponding node is marked as active (node is in the box) and its local coordinates are stored. Otherwise, this node is excluded from morphing. The numerical effort for the described operation is relatively low as the considered system of equations consists of only three unknowns. For large scale problems calculation of local coordinates can be done in parallel. The nodes can also be preprocessed or presorted comparing their locations with coarse box positions to save computational time.

4.5 Remarks on NURBS

B-spline curves, surfaces and volumes are now introduced. All these objects are based on the B-spline bases where each component has an equal influence on the resulting geometric properties. It is also possible to weight components of the B-spline base with some scale factors. The corresponding curves, surfaces and volumes are then called *NURBS* (*non-uniform rational B-spline*). NURBS control points, which correspond to larger scale factors exhibit more impact on the resulting curve or surface. Such scale factors could also be used as design variables. Unfortunately, such variables introduce additional non uniqueness to the optimisation problem. It is, for example, possible to describe a given curve with different NURBS representations. As an alternative, either coordinates of control points or their scale factors should be used as design variables. Because of the mentioned NURBS properties, B-splines are used in context of morphing within this thesis.

4.6 Summary and concluding remarks

Morphing based shape parametrisation is introduced. B-spline tensor products are utilised to describe morphing boxes. Number of control points in each direction and the degree of B-splines can be chosen by the user. Hence, requests with respect to smoothness and differentiability of design changes can be considered.

For morphing purposes local positions of finite element nodes, which are usually given in global coordinates, must be computed. Commonly, morphing boxes are defined as ashlar to simplify this task. In contrast, a reverse computation of local coordinates of FE-nodes is presented within this chapter. Hence, morphing boxes which have complex initial shape, can be treated utilising the presented techniques.

The sensitivity of finite element node positions is derived analytically considering the coordinates of control points as design variables. The corresponding *design velocity fields matrices* can be utilised to transform variationally derived gradients of objectives and constraints. The implementation of the analytical derivatives allows a fast computation of sensitivity relations.

Next, advantages of morphing based shape parametrisation are highlighted:

- Computation is based on FE-mesh. Geometry model is not required.
- FE-meshes with arbitrary element types and shapes can be morphed.
- Only relevant parts of the structure are captured by morphing boxes.
- Boundary of boxes do not need to match geometry boundary.
- The number of design variables does not depend on FE or CAGD models.
- CAGD controlled mesh can be considered as a special case of morphing.
- Experience in the scope of CAGD is also applicable in context of morphing.
- The corresponding implementation consists of only few functions.

Usually, an automatic CAGD description of the optimised shape is not possible and human controlled postprocessing is necessary. This is the only drawback of the method which also exists in context of the FE-node based shape optimisation and does not appear in CAGD based shape parametrisation.

The most time consuming operations within the described morphing concept are the inverse computation of local node coordinates and the mapping of local to global coordinates. The corresponding functions are precompiled in SOP utilising the *MATLAB* coder toolbox, and mex-routines are called instead of the original ones.

5 Structural analysis for solid shells

The present chapter deals with the finite element analysis of a nonlinear solid shell. All variational relations are summarised and discretised to provide the physical residual and the consistent tangent stiffness matrix for Newton's method. In particular, a notation which suits variational sensitivity analysis is introduced.

5.1 Introduction

Shell elements are most commonly used to model thin structures because of their efficiency and accuracy. Wide range of possible applications increases the popularity of shell elements in science and industry.

5.1.1 State of the art

In past years a number of shell elements have been developed, an overview is given in [30]. Classical shell formulations model a reference surface, solid shell formulations differ by modelling top and bottom surface of the shell structure. Shell elements including 3D material laws avoid the necessity to condensate the constitutive relations corresponding to the special plane stress state. This is advantageous to take complex nonlinear constitutive relations into account, because solid shell elements can use the same material libraries as brick elements. Also classical shell formulations, based on rotational degrees of freedom, using 3D constitutive relations exist, see [90].

A robust nonlinear solid shell element based on a mixed variational formulation was proposed in [89]. Here, the Hu-Washizu functional, which includes a displacement field, an assumed strain field and an assumed stress field, is employed. In this context robust means that larger load steps are possible without losing convergence. In contrast to [89], the independent stress and the enhanced assumed strain interpolations are assumed to be orthogonal in the approach proposed in [91]. The element in the

latter work is utilised in this thesis. At this point, I would like to thank Prof. Dr.-Ing. Werner Wagner from *Karlsruhe Institute of Technology (KIT)* and Prof. Dr.-Ing. Sven Klinkel from *RWTH Aachen University* for providing me with *FORTTRAN* code of the mentioned element and for their support.

5.1.2 Special features of the presented research

An important feature of this chapter is, that the notation of the original publications is advanced in order to suit sensitivity analysis which is performed in the next chapter. This notation was introduced in [65]. In addition, true stresses, which are given by the Cauchy stress tensor, are considered.

5.2 Kinematics

The present section represents a brief summary of fundamental relations of the underlying geometrically exact kinematic framework.

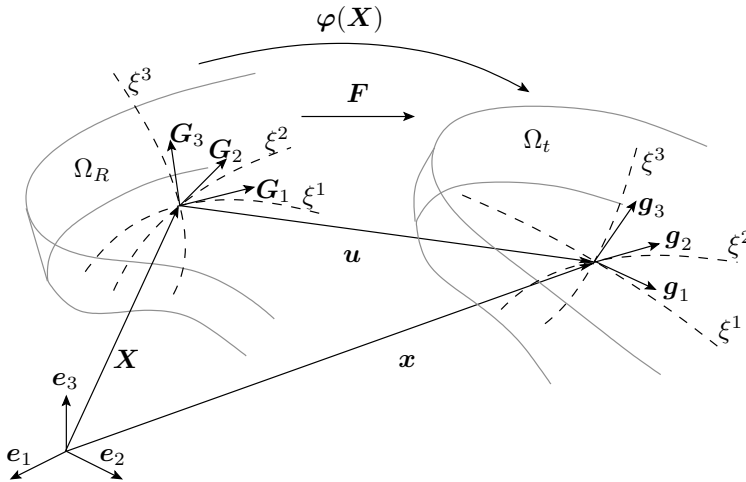


Figure 5.1: Deformation, reference and current configuration

Convective curvilinear coordinates are used in this work. For the considered shell formulation, the thickness coordinate ξ^3 and the in-plane coordinates ξ^1, ξ^2 are used, see Figure 5.1. The position vectors of the reference configuration Ω_R and the current configuration Ω_t are denoted by \mathbf{X} and $\mathbf{x} = \mathbf{X} + \mathbf{u}$, respectively. Here, \mathbf{u} denotes the displacement vector of a point in the shell domain. The covariant tangent vectors are

$$\mathbf{G}_i = \frac{\partial \mathbf{X}}{\partial \xi^i}, \quad \mathbf{g}_i = \frac{\partial \mathbf{x}}{\partial \xi^i}, \quad i = 1, 2, 3. \quad (5.1)$$

The standard definition of the contravariant basis is used $\mathbf{G}_i \cdot \mathbf{G}^j = \delta_i^j$ and $\mathbf{g}_i \cdot \mathbf{g}^j = \delta_i^j$. The metric coefficients of the reference configuration are $G_{ij} = \mathbf{G}_i \cdot \mathbf{G}_j$ and of the current configuration $g_{ij} = \mathbf{g}_i \cdot \mathbf{g}_j$. As only time independent problems are considered, the deformation of the material body from Ω_R into a deformed configuration Ω_t is given by the nonlinear mapping

$$\varphi : \begin{cases} \Omega_R \longrightarrow \Omega_t \\ \mathbf{X} \longrightarrow \mathbf{x} = \varphi(\mathbf{X}) \end{cases}. \quad (5.2)$$

The deformation gradient \mathbf{F} , i.e. the tangent map of φ as well as the displacement gradient \mathbf{H} are given by

$$\mathbf{F} := \text{Grad } \varphi = \nabla_{\mathbf{x}} \varphi = \mathbf{g}_i \otimes \mathbf{G}^i = \mathbf{I} + \mathbf{H}, \quad \mathbf{H} := \text{Grad } \mathbf{u} = \nabla_{\mathbf{x}} \mathbf{u}. \quad (5.3)$$

The Green-Lagrangean strain tensor is defined as

$$\mathbf{E} := E_{ij} \mathbf{G}^i \otimes \mathbf{G}^j \quad \text{with} \quad E_{ij} = \frac{1}{2}(\mathbf{g}_{ij} - G_{ij}). \quad (5.4)$$

Alternatively, this tensor can be expressed in terms of the deformation gradient \mathbf{F} or by means of the displacement gradient \mathbf{H} as follows

$$\mathbf{E} = \frac{1}{2}(\mathbf{F}^T \mathbf{F} - \mathbf{I}), \quad \mathbf{E} = \frac{1}{2}(\mathbf{H} + \mathbf{H}^T + \mathbf{H}^T \mathbf{H}). \quad (5.5)$$

5.3 Variational relations

A generalized state function $\mathbf{v} = (\mathbf{u}, \hat{\mathbf{S}}, \bar{\mathbf{E}})$ is introduced in an abstract sense to simplify the following expressions. The assumed stress $\hat{\mathbf{S}}$ and the assumed strain $\bar{\mathbf{E}}$ are work conjugate quantities. The true stress, which is given by the Cauchy stress tensor $\boldsymbol{\sigma}$ can be determined by the following transformation

$$\boldsymbol{\sigma} = \frac{1}{|\mathbf{F}|} \mathbf{F} \hat{\mathbf{S}} \mathbf{F}^T. \quad (5.6)$$

5.3.1 The variational functional

The variational Hu-Washizu three-field functional reads

$$\Pi(\mathbf{v}, \mathbf{X}) = \Pi(\mathbf{u}, \hat{\mathbf{S}}, \bar{\mathbf{E}}, \mathbf{X}) = \int_{\Omega_R} \left(W_R(\bar{\mathbf{E}}) + \hat{\mathbf{S}} : (\mathbf{E} - \bar{\mathbf{E}}) - \mathbf{u} \cdot \mathbf{b} \right) d\Omega - \int_{\Gamma_N} \mathbf{u} \cdot \mathbf{t} d\Gamma. \quad (5.7)$$

It depends on the state \mathbf{v} and on the design \mathbf{X} . Here, Ω_R and Γ_N denote the reference configuration and the Neumann boundary, respectively.

5.3.2 The weak form of equilibrium

The first variation with respect to the state \mathbf{v} provides the physical residual

$$\begin{aligned}
 R(\mathbf{v}, \mathbf{X}; \delta \mathbf{v}) &= \delta_v \Pi(\mathbf{v}, \mathbf{X})(\delta \mathbf{v}) = \int_{\Omega_R} \left(\delta_u \mathbf{E} : \hat{\mathbf{S}} - \delta \mathbf{u} \cdot \mathbf{b} \right) d\Omega - \int_{\Gamma_N} \delta \mathbf{u} \cdot \mathbf{t} d\Gamma \\
 &\quad + \int_{\Omega_R} \delta \hat{\mathbf{S}} : (\mathbf{E} - \bar{\mathbf{E}}) d\Omega + \int_{\Omega_R} \delta \bar{\mathbf{E}} : \left(\frac{\partial W_R}{\partial \bar{\mathbf{E}}} - \hat{\mathbf{S}} \right) d\Omega = 0,
 \end{aligned} \tag{5.8}$$

which is also known as the weak form of equilibrium. Here, the variation of the state $\delta \mathbf{v} = (\delta \mathbf{u}, \delta \hat{\mathbf{S}}, \delta \bar{\mathbf{E}})$ is introduced to shorten the corresponding terms. The relation in equation (5.8) can also be expressed as a system of equations

$$\begin{aligned}
 R_u(\mathbf{v}, \mathbf{X}; \delta \mathbf{u}) &= \delta_u \Pi(\mathbf{v}, \mathbf{X})(\delta \mathbf{u}) = \int_{\Omega_R} \left(\delta_u \mathbf{E} : \hat{\mathbf{S}} - \delta \mathbf{u} \cdot \mathbf{b} \right) d\Omega - \int_{\Gamma_N} \delta \mathbf{u} \cdot \mathbf{t} d\Gamma = 0, \\
 R_{\hat{\mathbf{S}}}(\mathbf{v}, \mathbf{X}; \delta \hat{\mathbf{S}}) &= \delta_{\hat{\mathbf{S}}} \Pi(\mathbf{v}, \mathbf{X})(\delta \hat{\mathbf{S}}) = \int_{\Omega_R} \delta \hat{\mathbf{S}} : (\mathbf{E} - \bar{\mathbf{E}}) d\Omega = 0, \\
 R_{\bar{\mathbf{E}}}(\mathbf{v}, \mathbf{X}; \delta \bar{\mathbf{E}}) &= \delta_{\bar{\mathbf{E}}} \Pi(\mathbf{v}, \mathbf{X})(\delta \bar{\mathbf{E}}) = \int_{\Omega_R} \delta \bar{\mathbf{E}} : \left(\frac{\partial W_R}{\partial \bar{\mathbf{E}}} - \hat{\mathbf{S}} \right) d\Omega = 0.
 \end{aligned} \tag{5.9}$$

This notation is more convenient for sensitivity analysis, which is presented in the next chapter, because partial variations with respect to different fields are considered separately. The variation of the Green-Lagrangean strains can be expressed in convective curvilinear coordinates as $\delta_u \mathbf{E} = \frac{1}{2}(\delta_u \mathbf{g}_i \cdot \mathbf{g}_j + \mathbf{g}_j \cdot \delta_u \mathbf{g}_i) \mathbf{G}^i \otimes \mathbf{G}^j$.

5.3.3 Linearisation of the weak form of equilibrium

The linearisation of the weak form of equilibrium results in

$$\begin{aligned}
 L(R(\mathbf{v}, \mathbf{X}; \delta \mathbf{v}))(\Delta \mathbf{v}) &= \int_{\Omega_R} \left(\Delta_u \delta_u \mathbf{E} : \hat{\mathbf{S}} + \delta \mathbf{E} : \Delta \hat{\mathbf{S}} \right) d\Omega \\
 &\quad + \int_{\Omega_R} \left(\delta \hat{\mathbf{S}} : \Delta \mathbf{E} - \delta \hat{\mathbf{S}} : \Delta \bar{\mathbf{E}} \right) d\Omega \\
 &\quad + \int_{\Omega_R} \left(\delta \bar{\mathbf{E}} : \frac{\partial \partial W_R}{\partial \bar{\mathbf{E}} \partial \bar{\mathbf{E}}} : \Delta \bar{\mathbf{E}} - \delta \bar{\mathbf{E}} : \Delta \hat{\mathbf{S}} \right) d\Omega.
 \end{aligned} \tag{5.10}$$

The linearised virtual Green-Lagrangean strain tensor reads $\Delta_u \delta_u \mathbf{E} = \frac{1}{2}(\delta_u \mathbf{g}_i \cdot \Delta_u \mathbf{g}_j + \Delta_u \mathbf{g}_j \cdot \delta_u \mathbf{g}_i) \mathbf{G}^i \otimes \mathbf{G}^j$.

5.4 Discretised relations

An eight node solid shell element is considered. Isoparametric concept is used. The superscript h indicates the finite element approximation and the index e denotes quantities on element level.

5.4.1 Approximation of kinematic quantities

The geometry and the displacements are given by

$$\mathbf{X}^h = \mathbf{N} \hat{\mathbf{X}}_e \quad \text{and} \quad \mathbf{u}^h = \mathbf{N} \hat{\mathbf{u}}_e. \quad (5.11)$$

The vectors $\hat{\mathbf{X}}_e \in \mathbb{R}^{24 \times 1}$ and $\hat{\mathbf{u}}_e \in \mathbb{R}^{24 \times 1}$ contain the nodal coordinates and the nodal displacements, respectively. The shape functions per node $I = 1, 2, \dots, 8$

$$N_I = \frac{1}{8} (1 + \xi_I^1 \xi^1) (1 + \xi_I^2 \xi^2) (1 + \xi_I^3 \xi^3) \quad \text{with} \quad -1 \leq \xi^i \leq +1 \quad (5.12)$$

are arranged in the matrix $\mathbf{N} = [\mathbf{N}_1, \dots, \mathbf{N}_8]$ with $\mathbf{N}_I = \text{diag}[N_I, N_I, N_I]$. The interpolation of the virtual displacement vector $\delta \mathbf{u}^h$ is the same as for the displacement vector. The Cartesian coefficients of the Green-Lagrangean strains \mathbf{E} are ordered in a vector $\mathbf{E} = [E_{11}, E_{22}, E_{33}, 2E_{12}, 2E_{13}, 2E_{23}]^T$. Corresponding to the convective description the approximations of the covariant basis vectors are given as

$$\mathbf{G}_i^h = \mathbf{N}_{,i} \hat{\mathbf{X}}_e, \quad \mathbf{g}_i^h = \mathbf{N}_{,i} (\hat{\mathbf{X}}_e + \hat{\mathbf{u}}_e), \quad (5.13)$$

where \mathbf{N} is differentiated with respect to ξ^i . Approximations of the displacement and of the deformation gradients are denoted with \mathbf{H}^h and \mathbf{F}^h . Their computation requires first derivatives of shape functions with respect to global coordinates. These derivatives are given by the following relation

$$\frac{\partial N_I}{\partial \mathbf{X}} = [\mathbf{G}_1 \mathbf{G}_2 \mathbf{G}_3]^{-T} \frac{\partial N_I}{\partial \boldsymbol{\xi}}. \quad (5.14)$$

Further details are omitted here.

Transformation to Cartesian coordinates. The Green-Lagrangean strain components in equation (5.4) are transformed to Cartesian coordinates by the matrix \mathbf{T}_S^{-T} . Utilising the matrix

$$\mathbf{T} = \begin{bmatrix} (J_{11})^2 & (J_{12})^2 & (J_{13})^2 & aJ_{11}J_{12} & aJ_{11}J_{13} & aJ_{12}J_{13} \\ (J_{21})^2 & (J_{22})^2 & (J_{23})^2 & aJ_{21}J_{22} & aJ_{21}J_{23} & aJ_{22}J_{23} \\ (J_{31})^2 & (J_{32})^2 & (J_{33})^2 & aJ_{31}J_{32} & aJ_{31}J_{33} & aJ_{32}J_{33} \\ bJ_{11}J_{21} & bJ_{12}J_{22} & bJ_{13}J_{23} & J_{11}J_{22} + J_{12}J_{21} & J_{11}J_{23} + J_{13}J_{21} & J_{12}J_{23} + J_{13}J_{22} \\ bJ_{11}J_{31} & bJ_{12}J_{32} & bJ_{13}J_{33} & J_{11}J_{32} + J_{12}J_{31} & J_{11}J_{33} + J_{13}J_{31} & J_{12}J_{33} + J_{13}J_{32} \\ bJ_{21}J_{31} & bJ_{22}J_{32} & bJ_{23}J_{33} & J_{21}J_{32} + J_{22}J_{31} & J_{21}J_{33} + J_{23}J_{31} & J_{22}J_{33} + J_{23}J_{32} \end{bmatrix} \quad (5.15)$$

the matrix $\mathbf{T}_S = \mathbf{T}(a = 2, b = 1)$ is obtained. With orthonormal basis vectors \mathbf{e}_i in Cartesian coordinate space the quantities $J_{ik} = \mathbf{e}_i \cdot \mathbf{G}_k^h$ are computed.

Collocation points for assumed natural strain (ANS) interpolation. Values evaluated at the collocation points $i = (-1, -1, 0)$, $ii = (1, -1, 0)$, $iii = (1, 1, 0)$ and $iv = (-1, 1, 0)$ are denoted with superscript $L = i, ii, iii, iv$. The collocation points are defined in convective coordinates ξ^i . Values evaluated at the collocation points $A = (-1, 0, 0)$, $B = (0, -1, 0)$, $C = (1, 0, 0)$ and $D = (0, 1, 0)$ are denoted with superscript A, B, C and D .

Approximation of strains and their variations. The approximation of the Cartesian strain components is given by

$$\mathbf{E}^h = \mathbf{T}_S^{-T} \mathbf{E}_L^h \quad \text{with} \quad \mathbf{E}_L^h = \begin{bmatrix} \frac{1}{2}(g_{11}^h - G_{11}^h) \\ \frac{1}{2}(g_{22}^h - G_{22}^h) \\ \sum_{L=i}^{iv} \frac{1}{4}(1 + \xi_L^1 \xi^1)(1 + \xi_L^2 \xi^2) \frac{1}{2}(g_{33}^L - G_{33}^L) \\ (g_{12}^h - G_{12}^h) \\ \frac{1}{2}((1 - \xi^2)(g_{13}^B - G_{13}^B) + (1 + \xi^2)(g_{13}^D - G_{13}^D)) \\ \frac{1}{2}((1 - \xi^1)(g_{23}^A - G_{23}^A) + (1 + \xi^1)(g_{23}^C - G_{23}^C)) \end{bmatrix}. \quad (5.16)$$

The approximation of the virtual Green-Lagrangean strains on element level reads

$$\delta \mathbf{E}^h = \mathbf{B} \delta \hat{\mathbf{u}}_e \quad \text{with} \quad \mathbf{B} = \mathbf{T}_S^{-T} \mathbf{B}_L \quad \text{and} \quad \mathbf{B}_L = [\mathbf{B}_{L1}, \dots, \mathbf{B}_{L8}]. \quad (5.17)$$

The matrix \mathbf{B}_{LI} at node I is specified by

$$\mathbf{B}_{LI} = \begin{bmatrix} N_{I,1}(\mathbf{g}_1^h)^T \\ N_{I,2}(\mathbf{g}_2^h)^T \\ \sum_{L=i}^{iv} \frac{1}{4}(1 + \xi_L^1 \xi^1)(1 + \xi_L^2 \xi^2) N_{I,3}^L(\mathbf{g}_3^L)^T \\ N_{I,1}(\mathbf{g}_2^h)^T + N_{I,2}(\mathbf{g}_1^h)^T \\ \frac{1}{2}((1 - \xi^2)(N_{I,1}^B(\mathbf{g}_3^B)^T + N_{I,3}^B(\mathbf{g}_1^B)^T) + (1 + \xi^2)(N_{I,1}^D(\mathbf{g}_3^D)^T + N_{I,3}^D(\mathbf{g}_1^D)^T)) \\ \frac{1}{2}((1 - \xi^1)(N_{I,2}^A(\mathbf{g}_3^A)^T + N_{I,3}^A(\mathbf{g}_2^A)^T) + (1 + \xi^1)(N_{I,2}^C(\mathbf{g}_3^C)^T + N_{I,3}^C(\mathbf{g}_2^C)^T)) \end{bmatrix}. \quad (5.18)$$

The incremental Green-Lagrangean strains are approximated by $\Delta \mathbf{E}^h = \mathbf{B} \Delta \hat{\mathbf{u}}_e$. In the linearised weak form of equilibrium in equation (5.10) the quantity $\Delta \delta \mathbf{E} : \hat{\mathbf{S}}$ appears. Its approximation is

$$(\Delta \delta \mathbf{E} : \hat{\mathbf{S}})^h = \delta \hat{\mathbf{u}}_e^T \mathbf{G} \Delta \hat{\mathbf{u}}_e \quad \text{with} \quad \mathbf{G} = \begin{bmatrix} \mathbf{G}_{11} & \cdots & \mathbf{G}_{18} \\ \vdots & \ddots & \vdots \\ \mathbf{G}_{81} & \cdots & \mathbf{G}_{88} \end{bmatrix}, \quad (5.19)$$

where \mathbf{G}_{IJ} is defined for a node combination I and J as $\mathbf{G}_{IJ} = \text{diag}[G_{IJ}, G_{IJ}, G_{IJ}]$. The scalar G_{IJ} is obtained as

$$G_{IJ} = \left(\hat{\mathbf{S}}^h \right)^T \mathbf{T}_S^{-T} \begin{bmatrix} N_{I,1}N_{J,1} \\ N_{I,2}N_{J,2} \\ \sum_{L=i}^{iv} \frac{1}{4}(1 + \xi_L^1 \xi^1)(1 + \xi_L^2 \xi^2)N_{I,3}^L N_{J,3}^L \\ N_{I,1}N_{J,2} + N_{I,2}N_{J,1} \\ \frac{1}{2}((1 - \xi^2)(N_{I,1}^B N_{J,3}^B + N_{I,3}^B N_{J,1}^B) + (1 + \xi^2)(N_{I,1}^D N_{J,3}^D + N_{I,3}^D N_{J,1}^D)) \\ \frac{1}{2}((1 - \xi^1)(N_{I,2}^A N_{J,3}^A + N_{I,3}^A N_{J,2}^A) + (1 + \xi^1)(N_{I,2}^C N_{J,3}^C + N_{I,3}^C N_{J,2}^C)) \end{bmatrix} \quad (5.20)$$

where $\hat{\mathbf{S}}^h$ is the approximation of the stress field $\hat{\mathbf{S}}$, which components are organized in vector notation as $\hat{\mathbf{S}}^h = [\hat{S}_{11}, \hat{S}_{22}, \hat{S}_{33}, \hat{S}_{12}, \hat{S}_{13}, \hat{S}_{23}]^T$.

5.4.2 Approximation of the assumed strain and stress fields

The strain tensor $\bar{\mathbf{E}}$ is additively decomposed in $\hat{E}^{ij} \mathbf{G}_i \otimes \mathbf{G}_j$ and $\tilde{E}_{ij} \mathbf{G}^i \otimes \mathbf{G}^j$ with

$$\bar{\mathbf{E}} = \hat{\mathbf{E}} + \tilde{\mathbf{E}}. \quad (5.21)$$

Considering vector notation the contravariant components of the strain field $\hat{\mathbf{E}}$ are interpolated and transformed to Cartesian space. Cartesian components are obtained with the transformation matrix \mathbf{T}_E . According to equation (5.15) \mathbf{T}_E is defined as $\mathbf{T}_E = \mathbf{T}(a = 1, b = 2)$. The approximation of the strain field is defined as

$$\hat{\mathbf{E}}^h = \mathbf{N}_E \boldsymbol{\alpha}_e^1, \quad \boldsymbol{\alpha}_e^1 \in \mathbb{R}^{18}, \quad \mathbf{N}_E = \mathbf{T}_E^0 \mathbf{N}_L \quad \text{with} \quad \mathbf{N}_L = [\mathbf{I} \quad \hat{\mathbf{N}} \quad \hat{\hat{\mathbf{N}}}] \quad (5.22)$$

The superscript 0 indicates, that the quantity is evaluated at the center of the element and $\mathbf{I} \in \mathbb{R}^{6 \times 6}$ denotes the identity matrix. The interpolation matrices $\hat{\mathbf{N}}$ and $\hat{\hat{\mathbf{N}}}$ are

$$\hat{\mathbf{N}} = \begin{bmatrix} \xi^3 & \xi^2 \xi^3 & 0 & 0 & 0 \\ 0 & 0 & \xi^3 & \xi^1 \xi^3 & 0 \\ 0 & 0 & 0 & 0 & 0 \\ 0 & 0 & 0 & 0 & \xi^3 \\ 0 & 0 & 0 & 0 & 0 \\ 0 & 0 & 0 & 0 & 0 \end{bmatrix}, \quad \hat{\hat{\mathbf{N}}} = \begin{bmatrix} \xi^2 & 0 & 0 & 0 & 0 & 0 & 0 \\ 0 & \xi^1 & 0 & 0 & 0 & 0 & 0 \\ 0 & 0 & \xi^1 & \xi^2 & \xi^1 \xi^2 & 0 & 0 \\ 0 & 0 & 0 & 0 & 0 & 0 & 0 \\ 0 & 0 & 0 & 0 & 0 & \xi^2 & 0 \\ 0 & 0 & 0 & 0 & 0 & 0 & \xi^1 \end{bmatrix}. \quad (5.23)$$

For the enhanced assumed strain field $\tilde{\mathbf{E}}^h$ the covariant components are interpolated and transformed to Cartesian space. These operations lead to

$$\tilde{\mathbf{E}}^h = \mathbf{M}_E \boldsymbol{\alpha}_e^2, \quad \boldsymbol{\alpha}_e^2 \in \mathbb{R}^7 \quad \text{with} \quad \mathbf{M}_E = \mathbf{T}_M \mathbf{M} \quad \text{and} \quad \mathbf{T}_M = \frac{\det \mathbf{J}^0}{\det \mathbf{J}} (\mathbf{T}_S^0)^{-T}. \quad (5.24)$$

Here, $\mathbf{J} = [\mathbf{G}_1^h, \mathbf{G}_2^h, \mathbf{G}_3^h]^T$ is the Jacobian matrix. The interpolation matrix \mathbf{M} reads

$$\mathbf{M} = \begin{bmatrix} \xi^1 & \xi^1 \xi^2 & 0 & 0 & 0 & 0 & 0 \\ 0 & 0 & \xi^2 & \xi^1 \xi^2 & 0 & 0 & 0 \\ 0 & 0 & 0 & 0 & \xi^3 & \xi^1 \xi^3 & \xi^2 \xi^3 \\ 0 & 0 & 0 & 0 & 0 & 0 & 0 \\ 0 & 0 & 0 & 0 & 0 & 0 & 0 \\ 0 & 0 & 0 & 0 & 0 & 0 & 0 \end{bmatrix}. \quad (5.25)$$

The interpolation of the total strain is summarised as

$$\bar{\mathbf{E}}^h = \mathbf{N}_E \boldsymbol{\alpha}_e^1 + \mathbf{M}_E \boldsymbol{\alpha}_e^2. \quad (5.26)$$

This interpolation is also applied for the virtual strains $\delta \bar{\mathbf{E}}^h$ and the incremental strains $\Delta \bar{\mathbf{E}}^h$. The approximation of the stress field reads

$$\hat{\mathbf{S}}^h = \mathbf{N}_S \boldsymbol{\beta}_e, \quad \boldsymbol{\beta}_e \in \mathbb{R}^{18} \quad \text{with} \quad \mathbf{N}_S = \mathbf{T}_S^0 \mathbf{N}_L. \quad (5.27)$$

For the approximation of the virtual stress $\delta \hat{\mathbf{S}}^h$ and the incremental stress $\Delta \hat{\mathbf{S}}^h$ the same interpolation is applied. The true stress, which is given by the Cauchy stress tensor $\boldsymbol{\sigma}$ is approximated as follows

$$\boldsymbol{\sigma}^h = \frac{1}{|\mathbf{F}^h|} \mathbf{F}^h \hat{\mathbf{S}}_m^h (\mathbf{F}^h)^T \quad \text{with} \quad \hat{\mathbf{S}}_m^h = \begin{bmatrix} \hat{S}_1^h & \hat{S}_4^h & \hat{S}_5^h \\ \hat{S}_4^h & \hat{S}_2^h & \hat{S}_6^h \\ \hat{S}_5^h & \hat{S}_6^h & \hat{S}_3^h \end{bmatrix}. \quad (5.28)$$

5.4.3 Energy approximation

The approximation of the energy given in equation (5.7) reads

$$\begin{aligned} \Pi_e &= \Pi_e^{\text{int}} - \Pi_e^{\text{ext}} \quad \text{with} \\ \Pi_e^{\text{int}} &= \int_{\Omega_{Re}} \left(W_{Re} + (\hat{\mathbf{S}}^h)^T \mathbf{E}^h - (\hat{\mathbf{S}}^h)^T \hat{\mathbf{E}}^h \right) d\Omega_e \quad \text{and} \\ \Pi_e^{\text{ext}} &= \int_{\Omega_{Re}} (\mathbf{N} \hat{\mathbf{u}}_e)^T \mathbf{b} d\Omega_e + \int_{\Gamma_{Ne}} (\mathbf{N} \hat{\mathbf{u}}_e)^T \mathbf{t} d\Gamma_e. \end{aligned} \quad (5.29)$$

The method of finite differentiation is utilised within this theses to verify the derived analytical relations. Discretised structural energy is perturbed with respect to the state to check the weak form of equilibrium and its linearisation. Perturbations with respect to design are performed to verify the material residual vector and the pseudo load. Structural energy is also used to define the compliance of the structure $C = -\Pi$ which is an important objective function in structural optimisation.

5.4.4 Approximation of the weak form and of its linearisation

The quantities $\bar{\mathbf{S}}^h$ and $\bar{\mathbf{C}}^h$ are introduced with

$$\bar{\mathbf{S}}^h = \frac{\partial W_{Re}}{\partial \bar{\mathbf{E}}^h}, \quad \bar{\mathbf{C}}^h = \frac{\partial^2 W_{Re}}{\partial \bar{\mathbf{E}}^h \partial \bar{\mathbf{E}}^h} \quad (5.30)$$

to reduce the amount of writing. Considering the above introduced interpolations in equation (5.8) and (5.10) the element matrices

$$\begin{aligned} \mathbf{K}_e &= \int_{\Omega_{Re}} \mathbf{G} d\Omega_e, & \mathbf{L}_e &= \int_{\Omega_{Re}} \mathbf{N}_S^T \mathbf{B} d\Omega_e, & \mathbf{C}_e &= \int_{\Omega_{Re}} \mathbf{N}_S^T \mathbf{N}_E d\Omega_e, \\ \mathbf{A}_e^{11} &= \int_{\Omega_{Re}} \mathbf{N}_E^T \bar{\mathbf{C}}^h \mathbf{N}_E d\Omega_e, & \mathbf{A}_e^{12} &= \int_{\Omega_{Re}} \mathbf{N}_E^T \bar{\mathbf{C}}^h \mathbf{M}_E d\Omega_e, \\ \mathbf{A}_e^{21} &= \int_{\Omega_{Re}} \mathbf{M}_E^T \bar{\mathbf{C}}^h \mathbf{N}_E d\Omega_e, & \mathbf{A}_e^{22} &= \int_{\Omega_{Re}} \mathbf{M}_E^T \bar{\mathbf{C}}^h \mathbf{M}_E d\Omega_e \end{aligned} \quad (5.31)$$

and the element vectors

$$\begin{aligned} \mathbf{f}_e^{\text{int}} &= \int_{\Omega_{Re}} \mathbf{B}^T \hat{\mathbf{S}}^h d\Omega_e, & \mathbf{f}_e^{\text{ext}} &= \int_{\Omega_{Re}} \mathbf{N}^T \mathbf{b} d\Omega_e + \int_{\Gamma_N^e} \mathbf{N}^T \mathbf{t} d\Gamma_e, \\ \mathbf{a}_e^1 &= \int_{\Omega_{Re}} \mathbf{N}_E^T (\bar{\mathbf{S}}^h - \hat{\mathbf{S}}^h) d\Omega_e, & \mathbf{a}_e^2 &= \int_{\Omega_{Re}} \mathbf{M}_E^T \bar{\mathbf{S}}^h d\Omega_e, \\ \mathbf{b}_e &= \int_{\Omega_{Re}} \mathbf{N}_S^T (\mathbf{E}^h - \hat{\mathbf{E}}^h) d\Omega_e, \end{aligned} \quad (5.32)$$

are defined. Here, the integrals are calculated by employing Gaussian integration scheme with eight integration points. To solve equation (5.8) iteratively with Newton's method, the following approximation, after assembly over all elements is necessary

$$A_{e=1}^{nelm} \begin{bmatrix} \mathbf{K}_e & \mathbf{0} & \mathbf{0} & \mathbf{L}_e^T \\ \mathbf{0} & \mathbf{A}_e^{11} & \mathbf{A}_e^{12} & -\mathbf{C}_e \\ \mathbf{0} & \mathbf{A}_e^{21} & \mathbf{A}_e^{22} & \mathbf{0} \\ \mathbf{L}_e & -\mathbf{C}_e & \mathbf{0} & \mathbf{0} \end{bmatrix} A_{e=1}^{nelm} \begin{bmatrix} \Delta \hat{\mathbf{u}}_e \\ \Delta \boldsymbol{\alpha}_e^1 \\ \Delta \boldsymbol{\alpha}_e^2 \\ \Delta \boldsymbol{\beta}_e \end{bmatrix} = -A_{e=1}^{nelm} \begin{bmatrix} \mathbf{f}_e^{\text{int}} - \mathbf{f}_e^{\text{ext}} \\ \mathbf{a}_e^1 \\ \mathbf{a}_e^2 \\ \mathbf{b}_e \end{bmatrix}. \quad (5.33)$$

Taking into account, that the finite element interpolations for the strain field $\bar{\mathbf{E}}$ and the stress field $\hat{\mathbf{S}}$ are discontinuous across the element boundaries, a static condensation on element level yields the element stiffness matrix and the right hand side

$$\begin{aligned} \mathbf{K}_{T_e} &= \mathbf{K}_e + \mathbf{L}_e^T \mathbf{C}_e^{-T} \mathbf{A}_e \mathbf{C}_e^{-1} \mathbf{L}_e, \\ \mathbf{f}_e &= -\mathbf{f}_e^{\text{ext}} + \mathbf{f}_e^{\text{int}} + \mathbf{L}_e^T \mathbf{C}_e^{-T} \mathbf{A}_e \mathbf{C}_e^{-1} \mathbf{b}_e + \mathbf{L}_e^T \mathbf{C}_e^{-1} \mathbf{a}_e \end{aligned} \quad (5.34)$$

with $\mathbf{A}_e = \mathbf{A}_e^{11} - \mathbf{A}_e^{12} (\mathbf{A}_e^{22})^{-1} \mathbf{A}_e^{21}$ and $\mathbf{a}_e = \mathbf{a}_e^1 - \mathbf{A}_e^{12} (\mathbf{A}_e^{22})^{-1} \mathbf{a}_e^2$. After assembly over all elements $\mathbf{K}_T = \mathbf{A}_{e=1}^{\text{nelm}} \mathbf{K}_{T_e}$, $\Delta \hat{\mathbf{U}} = \mathbf{A}_{e=1}^{\text{nelm}} \Delta \hat{\mathbf{u}}_e$ and $\mathbf{R} = \mathbf{A}_{e=1}^{\text{nelm}} \mathbf{f}_e$ one obtains a pure displacement problem

$$\mathbf{K}_T \Delta \hat{\mathbf{U}} = -\mathbf{R} \quad (5.35)$$

with the unknown incremental nodal displacements. The stresses and strains are updated with the increments

$$\begin{aligned} \Delta \alpha_e^1 &= \mathbf{C}_e^{-1} (\mathbf{L}_e \Delta \hat{\mathbf{u}}_e + \mathbf{b}_e), \\ \Delta \alpha_e^2 &= -(\mathbf{A}_e^{22})^{-1} (\mathbf{a}_e^2 + \mathbf{A}_e^{21} \Delta \alpha_e^1), \\ \Delta \beta_e &= \mathbf{C}_e^{-T} (\mathbf{A}_e \Delta \alpha_e^1 + \mathbf{a}_e). \end{aligned} \quad (5.36)$$

5.5 Summary and concluding remarks

Structural analysis of a solid shell element is presented. All necessary variational and discretised relations are summarised using notation, which suits subsequent sensitivity analysis. Furthermore, the true stress, which is given by the Cauchy stress tensor is considered. This is an important quantity in structural optimisation and many practical optimisation problems are restricted by stress constraints.

Solid shell elements can be combined easily with 1D, 2D and 3D continuum elements. The definition of boundary conditions and structural optimisation problems is simplified through the absence of rotational degrees of freedom. The nodal coordinates of solid shell elements define its shape as well as its thickness. They can be used excellently as design variables. Using solid shell elements optimisation problems can be modelled intuitively with low effort. In comparison to classical shell formulations sensitivity analysis of solid shells benefits from extensive researches in sensitivity analysis of continuum problems.

All element routines are precompiled in SOP utilising the *MATLAB* coder toolbox to speed up the computation of element contributions. System matrices and vectors are assembled using parallel computing toolbox to exhaust computer resources. Concepts of sparse matrix computation are used to save up computer memory.

6 Sensitivity analysis for solid shells

This chapter is concerned with the variational design sensitivity analysis for a nonlinear solid shell element. Fundamental sensitivity relations are stated and especially the pseudo load and the sensitivity matrices are derived. Sensitivities of energy and stresses are considered.

6.1 Introduction

To model thin-walled structures most commonly shell elements are used because of their efficiency and accuracy. For such structures the design is extremely important regarding their stability, robustness and load-bearing capacity. Design sensitivity analysis provides information, which gives the engineer the possibility to find a suitable shape of a shell and to understand the influence of geometry and layout changes on its behaviour. Furthermore, sensitivity information is an essential prerequisite for gradient based optimisation procedures.

6.1.1 State of the art

Recent publications deal with analytical derivation of sensitivity information of shell structures. In [39] design sensitivity analysis, which is based on the continuous problem of a linear elastic non-shallow shell is introduced. Shape and topology design sensitivity analysis of a double curved (Hughes-Liu) shell is shown in [42]. The material derivative concept of continuum mechanics together with the adjoint variable method are used to derive the shape and topology design sensitivity expressions in the domain integral form. For laminated plate and shell structures design sensitivity analysis considering nonlinear response is presented in [102]. Therein, the design variables are fiber orientation angles and distances from middle surface to upper surface of each layer. Design sensitivity analysis regarding size, shape and configuration design variables is presented in [87] for a mesh-free shell structure.

6.1.2 Special features of the presented research

The notation of *sensitivity matrix* and *pseudo load matrix* was introduced in [24, 98, 99] and is especially suitable for shape design problems. So far these matrices were derived mainly for continuum elements using the displacement formulation. A few more sophisticated formulations exist, see e.g. [145] for the sensitivity analysis of mixed finite elements. The challenge of this contribution is to derive sensitivity and pseudo load matrices for a shell element considering a mixed formulation. The content of this chapter is also presented in [65]. In addition, sensitivity relations of stresses are derived in this chapter. The capabilities of the presented analysis are demonstrated on an example with stress constraints.

6.2 Variational relations

Variational sensitivity relations are derived in this section. The starting point of the consideration is the Hu-Washizu three-field functional.

6.2.1 First total and partial variations of energy

The first total variation of the Hu-Washizu three-field functional (5.7) reads

$$\begin{aligned} \Pi'(\mathbf{v}, \mathbf{X}; \delta\mathbf{v}, \delta\mathbf{X}) &= \Pi'_v(\mathbf{v}, \mathbf{X}; \delta\mathbf{v}) + \Pi'_X(\mathbf{v}, \mathbf{X}; \delta\mathbf{X}) \quad \text{with} \\ \Pi'_v(\mathbf{v}, \mathbf{X}; \delta\mathbf{v}) &= R(\mathbf{v}, \mathbf{X}; \delta\mathbf{v}) \quad \text{and} \\ \Pi'_X(\mathbf{v}, \mathbf{X}; \delta\mathbf{X}) &= V(\mathbf{v}, \mathbf{X}; \delta\mathbf{X}). \end{aligned} \quad (6.1)$$

Here, R and V denote the physical and material residuals, respectively. The quantity R_v is given in equation (5.8) and the term V reads

$$\begin{aligned} V(\mathbf{v}, \mathbf{X}; \delta\mathbf{X}) &= \int_{\Omega_R} \left(W_R(\bar{\mathbf{E}}) + \hat{\mathbf{S}} : (\mathbf{E} - \bar{\mathbf{E}}) - \mathbf{u} \cdot \mathbf{b} \right) \text{Div} \delta\mathbf{X} \, d\Omega \\ &\quad + \int_{\Omega_R} \left(W_R(\bar{\mathbf{E}}) + \hat{\mathbf{S}} : (\mathbf{E} - \bar{\mathbf{E}}) - \mathbf{u} \cdot \mathbf{b} \right)'_X \, d\Omega \end{aligned} \quad (6.2)$$

with $\text{Div}(\bullet) = \nabla_X \cdot (\bullet)$ and the assumption, that the term $\int_{\Gamma_N} \mathbf{u} \cdot \mathbf{t} \, d\Gamma$ is design independent. The integrand of the last term in equation (6.2) reads

$$\begin{aligned} \left(W_R(\bar{\mathbf{E}}) + \hat{\mathbf{S}} : (\mathbf{E} - \bar{\mathbf{E}}) - \mathbf{u} \cdot \mathbf{b} \right)'_X &= \frac{\partial W_R(\bar{\mathbf{E}})}{\partial \bar{\mathbf{E}}} : \delta_x \bar{\mathbf{E}} + \delta_x \hat{\mathbf{S}} : (\mathbf{E} - \bar{\mathbf{E}}) \\ &\quad + \hat{\mathbf{S}} : \delta_x \mathbf{E} - \hat{\mathbf{S}} : \delta_x \bar{\mathbf{E}}. \end{aligned} \quad (6.3)$$

For a given solution $\mathbf{v} \in \mathcal{V}$ the equilibrium condition $R(\mathbf{v}, \mathbf{X}; \delta\mathbf{v}) = 0$ holds true. With this, the first part of the first variation of the Hu-Washizu functional vanishes and remains only the material residual, which is

$$\Pi'(\mathbf{v}, \mathbf{X}; \delta\mathbf{v}, \delta\mathbf{X}) = \Pi'_X(\mathbf{v}, \mathbf{X}; \delta\mathbf{X}) = V(\mathbf{v}, \mathbf{X}; \delta\mathbf{X}). \quad (6.4)$$

6.2.2 Total and total partial variations of any objective functional

An arbitrary objective functional $J(\mathbf{v}(\mathbf{X}), \mathbf{X})$ is considered. Its total partial variation with respect to \mathbf{X} reads

$$D_X J(\mathbf{v}(\mathbf{X}), \mathbf{X}) \cdot \delta\mathbf{X} = \frac{\partial J}{\partial \mathbf{X}} \cdot \delta\mathbf{X} + \frac{\partial J}{\partial \mathbf{v}} \frac{d\mathbf{v}}{d\mathbf{X}} \cdot \delta\mathbf{X} \quad (6.5)$$

and its total variation is given by

$$J'(\mathbf{v}, \mathbf{X}; \delta\mathbf{v}, \delta\mathbf{X}) = J'_v(\mathbf{v}, \mathbf{X}; \delta\mathbf{v}) + J'_X(\mathbf{v}, \mathbf{X}; \delta\mathbf{X}). \quad (6.6)$$

In both cases the variation of the state $\delta\mathbf{v} = \frac{d\mathbf{v}}{d\mathbf{X}} \cdot \delta\mathbf{X}$ is unknown. This quantity is derived in the next section.

6.2.3 Total and partial variations of the physical residual

For a given solution \mathbf{v} and \mathbf{X} the weak form $R(\mathbf{v}, \mathbf{X}; \delta\mathbf{v}) = 0$ must be invariant with respect to variations $\delta\bar{\mathbf{v}}$ and $\delta\mathbf{X}$. Its total variation reads

$$R'(\mathbf{v}, \mathbf{X}; \delta\mathbf{v}, \delta\bar{\mathbf{v}}, \delta\mathbf{X}) = R'_v(\mathbf{v}, \mathbf{X}; \delta\mathbf{v}, \delta\bar{\mathbf{v}}) + R'_X(\mathbf{v}, \mathbf{X}; \delta\mathbf{v}, \delta\mathbf{X}) = 0. \quad (6.7)$$

For the variations of the physical residual R the following operators are introduced

$$\begin{aligned} k(\mathbf{v}, \mathbf{X}; \delta\mathbf{v}, \delta\bar{\mathbf{v}}) &:= R'_v(\mathbf{v}, \mathbf{X}; \delta\mathbf{v}, \delta\bar{\mathbf{v}}), \\ p(\mathbf{v}, \mathbf{X}; \delta\mathbf{v}, \delta\mathbf{X}) &:= R'_X(\mathbf{v}, \mathbf{X}; \delta\mathbf{v}, \delta\mathbf{X}), \end{aligned} \quad (6.8)$$

where $k(\mathbf{v}, \mathbf{X}; \cdot, \cdot)$ is the well-known *tangent physical stiffness operator* and the quantity $p(\mathbf{v}, \mathbf{X}; \cdot, \cdot)$ is called the *tangent pseudo load operator* for the physical problem. Considering the equation (6.7) and the above definitions, one obtains a variational equation for the sensitivity of the state due to changes in the design as follows

$$k(\mathbf{v}, \mathbf{X}; \delta\mathbf{v}, \delta\bar{\mathbf{v}}) = -p(\mathbf{v}, \mathbf{X}; \delta\mathbf{v}, \delta\bar{\mathbf{X}}) \quad (6.9)$$

with a fixed design variation $\delta\bar{\mathbf{X}}$. For a given variation in the design $\delta\bar{\mathbf{X}}$, the variation in the state $\delta\bar{\mathbf{v}}$ can be calculated. Considering equation (5.10) the following relation

$$k(\mathbf{v}, \mathbf{X}; \cdot, \cdot) = L(R(\mathbf{v}, \mathbf{X}; \cdot))(\cdot) \quad (6.10)$$

holds true. The tangent pseudo load operator p is derived as follows

$$p = R'_X = (R_u)'_X + (R_{\hat{s}})'_X + (R_{\bar{E}})'_X = p_u + p_{\hat{s}} + p_{\bar{E}} \quad (6.11)$$

with the partial derivatives

$$\begin{aligned} p_u(\mathbf{v}, \mathbf{X}; \delta \mathbf{u}, \delta \mathbf{X}) &= \int_{\Omega_R} \left(\delta_u \mathbf{E} : \hat{\mathbf{S}} - \delta \mathbf{u} \cdot \mathbf{b} \right) \text{Div} \delta \mathbf{X} \, d\Omega \\ &\quad + \int_{\Omega_R} \left(\delta_x (\delta_u \mathbf{E}) : \hat{\mathbf{S}} + \delta_u \mathbf{E} : \delta_x \hat{\mathbf{S}} \right) \, d\Omega, \\ p_{\hat{s}}(\mathbf{v}, \mathbf{X}; \delta \hat{\mathbf{S}}, \delta \mathbf{X}) &= \int_{\Omega_R} \delta \hat{\mathbf{S}} : (\mathbf{E} - \bar{\mathbf{E}}) \text{Div} \delta \mathbf{X} \, d\Omega \\ &\quad + \int_{\Omega_R} \delta_x \left(\delta \hat{\mathbf{S}} : (\mathbf{E} - \bar{\mathbf{E}}) \right) \, d\Omega, \\ p_{\bar{E}}(\mathbf{v}, \mathbf{X}; \delta \bar{\mathbf{E}}, \delta \mathbf{X}) &= \int_{\Omega_R} \delta \bar{\mathbf{E}} : \left(\frac{\partial W_R}{\partial \bar{\mathbf{E}}} - \hat{\mathbf{S}} \right) \text{Div} \delta \mathbf{X} \, d\Omega \\ &\quad + \int_{\Omega_R} \delta_x \left(\delta \bar{\mathbf{E}} : \left(\frac{\partial W_R}{\partial \bar{\mathbf{E}}} - \hat{\mathbf{S}} \right) \right) \, d\Omega. \end{aligned} \quad (6.12)$$

6.2.4 Variations of Cauchy stress tensor

Stresses are often used to constrain the optimisation problem or are utilised as objectives. In such cases, total partial variation of the Cauchy stress tensor is required to perform sensitivity analysis. We consider the total variation of the Cauchy stress

$$\delta \boldsymbol{\sigma} = \delta_x \boldsymbol{\sigma} + \delta_u \boldsymbol{\sigma} + \delta_{\hat{s}} \boldsymbol{\sigma}. \quad (6.13)$$

We note that Cauchy stress does not depend on the assumed strain. In terms of assumed stress, see equation (5.6), the total variation reads

$$\begin{aligned} \delta \boldsymbol{\sigma} &= - \frac{1}{|\mathbf{F}|^2} \delta_x |\mathbf{F}| \mathbf{F} \hat{\mathbf{S}} \mathbf{F}^T + \frac{1}{|\mathbf{F}|} \delta_x \mathbf{F} \hat{\mathbf{S}} \mathbf{F}^T + \frac{1}{|\mathbf{F}|} \mathbf{F} \hat{\mathbf{S}} \delta_x \mathbf{F}^T + \frac{1}{|\mathbf{F}|} \mathbf{F} \delta_x \hat{\mathbf{S}} \mathbf{F}^T \\ &\quad - \frac{1}{|\mathbf{F}|^2} \delta_u |\mathbf{F}| \mathbf{F} \hat{\mathbf{S}} \mathbf{F}^T + \frac{1}{|\mathbf{F}|} \delta_u \mathbf{F} \hat{\mathbf{S}} \mathbf{F}^T + \frac{1}{|\mathbf{F}|} \mathbf{F} \hat{\mathbf{S}} \delta_u \mathbf{F}^T \\ &\quad + \frac{1}{|\mathbf{F}|} \mathbf{F} \delta_{\hat{s}} \hat{\mathbf{S}} \mathbf{F}^T. \end{aligned} \quad (6.14)$$

The deformation gradient does not depend on the assumed stress. Its variations with respect to design and displacement fields, see [98], are given by

$$\delta_x \mathbf{F} = \mathbf{F}'_X = -\mathbf{H} \text{Grad} \delta \mathbf{X}, \quad \delta_u \mathbf{F} = \mathbf{F}'_u = \text{Grad} \delta \mathbf{u}. \quad (6.15)$$

Variations of the deformation gradient determinant are given by

$$\begin{aligned}\delta_x |\mathbf{F}| &= \frac{\partial |\mathbf{F}|}{\partial \mathbf{F}} : \delta_x \mathbf{F} = |\mathbf{F}| \mathbf{F}^{-T} : \delta_x \mathbf{F}, \\ \delta_u |\mathbf{F}| &= \frac{\partial |\mathbf{F}|}{\partial \mathbf{F}} : \delta_u \mathbf{F} = |\mathbf{F}| \mathbf{F}^{-T} : \delta_u \mathbf{F}.\end{aligned}\tag{6.16}$$

The total partial variation of Cauchy stress tensor with respect to design is obtained replacing partial variations with respect to displacement and assumed stress in equation (6.14) with

$$\delta_u(\cdot) = \frac{\partial(\cdot)}{\partial \mathbf{u}} \delta_x \mathbf{u}, \quad \delta_{\hat{\mathbf{S}}}(\cdot) = \frac{\partial(\cdot)}{\partial \hat{\mathbf{S}}} \delta_x \hat{\mathbf{S}}.\tag{6.17}$$

6.3 Discretised relations

Material residual and pseudo load are discretised in this section. Computation of the sensitivity matrix is explored. Discretisation of Cauchy stress is presented.

6.3.1 Preliminaries

Derivatives of transformation matrices, approximation of a divergence and definition of a special product are necessary to discretise pseudo load and material residual.

Approximation of a divergence. The term $\text{Div} \delta \mathbf{X}$ is approximated as follows

$$(\text{Div} \delta \mathbf{X})^h = \mathbf{D} \delta \hat{\mathbf{X}}_e \quad \text{with} \quad \mathbf{D} = [\mathbf{d}_1, \dots, \mathbf{d}_8] \quad \text{and} \quad \mathbf{d}_I = [N_{I,1} \quad N_{I,2} \quad N_{I,3}].\tag{6.18}$$

Derivatives of \mathbf{T} . The first derivative of the transformation matrix \mathbf{T} , see equation (5.15), with respect to $\hat{\mathbf{X}}_e$ is denoted with $\mathbb{T} \in \mathbb{R}^{6 \times 6 \times 24}$ and its coefficients are

$$\mathbb{T}_{ijk_1(I)} := H_{ij}^1(I), \quad \mathbb{T}_{ijk_2(I)} := H_{ij}^2(I), \quad \mathbb{T}_{ijk_3(I)} := H_{ij}^3(I)\tag{6.19}$$

with $k_1(I) = 3I - 2$, $k_2(I) = 3I - 1$, $k_3(I) = 3I$, $I = 1, \dots, 8$ and

$$\begin{aligned}
 \mathbf{H}^1(I) &= [\mathbf{H}^{11} \ \mathbf{H}^{12}] \quad \text{with} \quad \mathbf{H}^{11} = \begin{bmatrix} 2J_{11}N_{I,1} & 2J_{12}N_{I,2} & 2J_{13}N_{I,3} \\ 0 & 0 & 0 \\ 0 & 0 & 0 \\ J_{21}N_{I,1}b & J_{22}N_{I,2}b & J_{23}N_{I,3}b \\ J_{31}N_{I,1}b & J_{32}N_{I,2}b & J_{33}N_{I,3}b \\ 0 & 0 & 0 \end{bmatrix} \quad \text{and} \\
 \mathbf{H}^{12} &= \begin{bmatrix} J_{11}N_{I,2}a + J_{12}N_{I,1}a & J_{11}N_{I,3}a + J_{13}N_{I,1}a & J_{12}N_{I,3}a + J_{13}N_{I,2}a \\ 0 & 0 & 0 \\ 0 & 0 & 0 \\ J_{21}N_{I,2} + J_{22}N_{I,1} & J_{21}N_{I,3} + J_{23}N_{I,1} & J_{22}N_{I,3} + J_{23}N_{I,2} \\ J_{31}N_{I,2} + J_{32}N_{I,1} & J_{31}N_{I,3} + J_{33}N_{I,1} & J_{32}N_{I,3} + J_{33}N_{I,2} \\ 0 & 0 & 0 \end{bmatrix}, \\
 \mathbf{H}^2(I) &= [\mathbf{H}^{21} \ \mathbf{H}^{22}] \quad \text{with} \quad \mathbf{H}^{21} = \begin{bmatrix} 0 & 0 & 0 \\ 2J_{21}N_{I,1} & 2J_{22}N_{I,2} & 2J_{23}N_{I,3} \\ 0 & 0 & 0 \\ J_{11}N_{I,1}b & J_{12}N_{I,2}b & J_{13}N_{I,3}b \\ 0 & 0 & 0 \\ J_{31}N_{I,1}b & J_{32}N_{I,2}b & J_{33}N_{I,3}b \end{bmatrix} \quad \text{and} \\
 \mathbf{H}^{22} &= \begin{bmatrix} 0 & 0 & 0 \\ J_{21}N_{I,2}a + J_{22}N_{I,1}a & J_{21}N_{I,3}a + J_{23}N_{I,1}a & J_{22}N_{I,3}a + J_{23}N_{I,2}a \\ 0 & 0 & 0 \\ J_{11}N_{I,2} + J_{12}N_{I,1} & J_{11}N_{I,3} + J_{13}N_{I,1} & J_{12}N_{I,3} + J_{13}N_{I,2} \\ 0 & 0 & 0 \\ J_{31}N_{I,2} + J_{32}N_{I,1} & J_{31}N_{I,3} + J_{33}N_{I,1} & J_{32}N_{I,3} + J_{33}N_{I,2} \end{bmatrix}, \\
 \mathbf{H}^3(I) &= [\mathbf{H}^{31} \ \mathbf{H}^{32}] \quad \text{with} \quad \mathbf{H}^{31} = \begin{bmatrix} 0 & 0 & 0 \\ 0 & 0 & 0 \\ 2J_{31}N_{I,1} & 2J_{32}N_{I,2} & 2J_{33}N_{I,3} \\ 0 & 0 & 0 \\ J_{11}N_{I,1}b & J_{12}N_{I,2}b & J_{13}N_{I,3}b \\ J_{21}N_{I,1}b & J_{22}N_{I,2}b & J_{23}N_{I,3}b \end{bmatrix} \quad \text{and} \\
 \mathbf{H}^{32} &= \begin{bmatrix} 0 & 0 & 0 \\ 0 & 0 & 0 \\ J_{31}N_{I,2}a + J_{32}N_{I,1}a & J_{31}N_{I,3}a + J_{33}N_{I,1}a & J_{32}N_{I,3}a + J_{33}N_{I,2}a \\ 0 & 0 & 0 \\ J_{11}N_{I,2} + J_{12}N_{I,1} & J_{11}N_{I,3} + J_{13}N_{I,1} & J_{12}N_{I,3} + J_{13}N_{I,2} \\ J_{21}N_{I,2} + J_{22}N_{I,1} & J_{21}N_{I,3} + J_{23}N_{I,1} & J_{22}N_{I,3} + J_{23}N_{I,2} \end{bmatrix}.
 \end{aligned}$$

Here, \mathbb{T}^T means that $\mathbb{T}_{ijk}^T = \mathbb{T}_{jik}$ is considered. The quantities $\mathbb{T}_S = \mathbb{T}(a = 2, b = 1)$ and $\mathbb{T}_E = \mathbb{T}(a = 1, b = 2)$ are also available now. We note that $T_{ij, \hat{x}_k} = \mathbb{T}_{ijk}$.

Derivatives of \mathbf{T}_M . The first derivative of the transformation matrix \mathbf{T}_M , see equation (5.24), with respect to $\hat{\mathbf{X}}_e$ is $\mathbb{T}_M \in \mathbb{R}^{6 \times 6 \times 24}$. With $(\mathbb{T}_M)_{ij, \hat{\mathbf{X}}_k} = (\mathbb{T}_M)_{ijk}$ the quantity $(\mathbf{T}_M)_{, \hat{\mathbf{X}}_k}$ is defined. With $\mathbf{J} = [\mathbf{G}_1 \mathbf{G}_2 \mathbf{G}_3]$ and $\mathbf{J}^0 = [\mathbf{G}_1^0 \mathbf{G}_2^0 \mathbf{G}_3^0]$ one obtains

$$\begin{aligned} (\mathbf{T}_M)_{, \hat{\mathbf{X}}_k} = \frac{|\mathbf{J}^0|}{|\mathbf{J}|} & \left(\left((\mathbf{J}^0)^{-T} : \mathbf{J}_{, \hat{\mathbf{X}}_k}^0 - \mathbf{J}^{-T} : \mathbf{J}_{, \hat{\mathbf{X}}_k} \right) (\mathbf{T}_S^0)^{-T} \right. \\ & \left. - (\mathbf{T}_S^0)^{-T} (\mathbf{T}_S^0)_{, \hat{\mathbf{X}}_k}^T (\mathbf{T}_S^0)^{-T} \right). \end{aligned} \quad (6.20)$$

Scalar product $(\cdot : \cdot)$ is here applied to matrices in the same manner, as it is defined for tensors. Additionally, the following relations are used

$$|\mathbf{A}'| = |\mathbf{A}| \mathbf{A}^{-T} : \mathbf{A}', \quad (\mathbf{A}^{-1})' = -\mathbf{A}^{-1} \mathbf{A}' \mathbf{A}^{-1}. \quad (6.21)$$

The computation of $\mathbf{J}_{, \hat{\mathbf{X}}_k}^0$ and $\mathbf{J}_{, \hat{\mathbf{X}}_k}$ is straightforward and details are omitted.

A special product. To reduce the amount of writing and to avoid the index notation, a special product is introduced. For any $z \in \mathbb{N}^+$, $\mathbf{M} \in \mathbb{R}^{z \times 6}$, $\mathbb{T} \in \mathbb{R}^{6 \times 6 \times 24}$ and $\mathbf{V} \in \mathbb{R}^6$ the mapping \mathcal{P} is defined as follows

$$\begin{aligned} \mathcal{P} : \mathbb{R}^{z \times 6} \times \mathbb{R}^{6 \times 6 \times 24} \times \mathbb{R}^6 & \longrightarrow \mathbb{R}^{z \times 24} \\ (\mathbf{M}, \mathbb{T}, \mathbf{V}) & \longrightarrow \mathbf{Q} \quad \text{with} \end{aligned} \quad (6.22)$$

$$Q_{kn} = \sum_{l=1}^6 \sum_{m=1}^6 M_{kl} \mathbb{T}_{lmn} V_m, \quad k = 1, \dots, z \quad \text{and} \quad n = 1, \dots, 24. \quad (6.23)$$

Derivatives of local strains. The first derivative of \mathbf{E}_L^h with respect to $\hat{\mathbf{X}}_e$ reads $(\mathbf{E}_L^h)_{, \hat{\mathbf{X}}} = \mathbf{Q} = [\mathbf{Q}_1, \dots, \mathbf{Q}_8]$ with

$$\mathbf{Q}_I = \begin{bmatrix} N_{I,1}(\mathbf{u}_1^h)^T \\ N_{I,2}(\mathbf{u}_2^h)^T \\ \sum_{L=i}^{iv} \frac{1}{4} (1 + \xi_L^1 \xi^1) (1 + \xi_L^2 \xi^2) N_{I,3}^L(\mathbf{u}_3^L)^T \\ N_{I,1}(\mathbf{u}_2^h)^T + N_{I,2}(\mathbf{u}_1^h)^T \\ \frac{1}{2} ((1 - \xi^2) (N_{I,1}^B(\mathbf{u}_3^B)^T + N_{I,3}^B(\mathbf{u}_1^B)^T) + (1 + \xi^2) (N_{I,1}^D(\mathbf{u}_3^D)^T + N_{I,3}^D(\mathbf{u}_1^D)^T)) \\ \frac{1}{2} ((1 - \xi^1) (N_{I,2}^A(\mathbf{u}_3^A)^T + N_{I,3}^A(\mathbf{u}_2^A)^T) + (1 + \xi^1) (N_{I,2}^C(\mathbf{u}_3^C)^T + N_{I,3}^C(\mathbf{u}_2^C)^T)) \end{bmatrix}. \quad (6.24)$$

6.3.2 Approximation of material residual

Considering the above introduced interpolations, the approximation of the material residual V , see equation (6.2), reads $V^h(\mathbf{v}, \mathbf{X}; \delta \mathbf{X}) = \mathbf{V}_e \delta \hat{\mathbf{X}}_e$ with

$$\begin{aligned}
\mathbf{V}_e = & \int_{\Omega_{R_e}} \left(W_{R_e} + (\hat{\mathbf{S}}^h)^T \mathbf{E}^h - (\hat{\mathbf{S}}^h)^T \hat{\mathbf{E}}^h - \hat{\mathbf{u}}_e^T \mathbf{N}^T \mathbf{b} \right) \mathbf{D}^T d\Omega_e \\
& + \int_{\Omega_{R_e}} \left(\mathcal{P} \left((\hat{\mathbf{S}}^h)^T, \mathbb{T}_E^0, \mathbf{N}_L \boldsymbol{\alpha}_e^1 \right)^T + \mathcal{P} \left((\hat{\mathbf{S}}^h)^T, \mathbb{T}_M, \mathbf{M} \boldsymbol{\alpha}_e^2 \right)^T \right) d\Omega_e \\
& + \int_{\Omega_{R_e}} \mathcal{P} \left(\boldsymbol{\beta}_e^T \mathbf{N}_L^T, (\mathbb{T}_S^0)^T, \mathbf{E}^h \right)^T d\Omega_e \\
& + \int_{\Omega_{R_e}} \left(-\mathcal{P} \left((\hat{\mathbf{S}}^h)^T \mathbf{T}_S^{-T}, \mathbb{T}_S^T, \mathbf{T}_S^{-T} \mathbf{E}_L^h \right)^T + (\hat{\mathbf{S}}^h)^T \mathbf{T}_S^{-T} \mathbf{Q} \right) d\Omega_e \\
& - \int_{\Omega_{R_e}} \left(\mathcal{P} \left(\boldsymbol{\beta}_e^T \mathbf{N}_L^T, (\mathbb{T}_S^0)^T, \hat{\mathbf{E}}^h \right)^T + \mathcal{P} \left((\hat{\mathbf{S}}^h)^T, \mathbb{T}_E^0 \mathbf{N}_L \boldsymbol{\alpha}_e^1 \right)^T \right) d\Omega_e.
\end{aligned} \tag{6.25}$$

6.3.3 Sensitivity and pseudo load matrices

The parts of the pseudo load are approximated as $p_u^h = \delta \hat{\mathbf{u}}_e \mathbf{P}_u^e \delta \hat{\mathbf{X}}_e$, $p_s^h = \delta \hat{\mathbf{S}}^h \mathbf{P}_s^e \delta \hat{\mathbf{X}}_e$ and $p_{\hat{\mathbf{E}}}^h = \delta \hat{\mathbf{E}}^h \mathbf{P}_{\hat{\mathbf{E}}}^e \delta \hat{\mathbf{X}}_e + \delta \tilde{\mathbf{E}}^h \tilde{\mathbf{P}}_{\hat{\mathbf{E}}}^e \delta \hat{\mathbf{X}}_e$ with

$$\begin{aligned}
\mathbf{P}_u^e = & \int_{\Omega_{R_e}} \left(\mathbf{B}^T \hat{\mathbf{S}}^h - \mathbf{N}^T \mathbf{b} \right) \mathbf{D} d\Omega_e \\
& + \int_{\Omega_{R_e}} \left(\mathbf{G} + \mathcal{P} \left(\mathbf{B}^T, \mathbb{T}_S^0, \mathbf{N}_L \boldsymbol{\beta}_e \right) - \mathcal{P} \left(\mathbf{B}_L^T \mathbf{T}_S^{-1}, \mathbb{T}_S, \mathbf{T}_S^{-1} \hat{\mathbf{S}}^h \right) \right) d\Omega_e,
\end{aligned} \tag{6.26}$$

$$\begin{aligned}
\mathbf{P}_s^e = & \int_{\Omega_{R_e}} \left(\mathbf{N}_S^T (\mathbf{E}^h - \hat{\mathbf{E}}^h) \right) \mathbf{D} d\Omega_e \\
& + \int_{\Omega_{R_e}} \left(\mathcal{P} \left(\mathbf{N}_L^T, (\mathbb{T}_S^0)^T, (\mathbf{E}^h - \hat{\mathbf{E}}^h) \right) - \mathcal{P} \left(\mathbf{N}_S^T, \mathbb{T}_E^0, \mathbf{N}_L \boldsymbol{\alpha}_e^1 \right) \right) d\Omega_e \\
& + \int_{\Omega_{R_e}} \left(\mathbf{N}_S^T \mathbf{T}_S^{-T} \mathbf{Q} - \mathcal{P} \left(\mathbf{N}_S^T \mathbf{T}_S^{-T}, \mathbb{T}_S^T, \mathbf{T}_S^{-T} \mathbf{E}_L^h \right) \right) d\Omega_e,
\end{aligned} \tag{6.27}$$

$$\begin{aligned}
 \mathbf{P}_{\hat{E}}^e &= \int_{\Omega_{R_e}} \left(\mathbf{N}_E^T (\bar{\mathbf{S}}^h - \hat{\mathbf{S}}^h) \right) \mathbf{D} d\Omega_e \\
 &+ \int_{\Omega_{R_e}} \left(\mathcal{P} \left(\mathbf{N}_L^T, (\mathbb{T}_E^0)^T, (\bar{\mathbf{S}}^h - \hat{\mathbf{S}}^h) \right) + \mathcal{P} \left(\mathbf{N}_E^T \bar{\mathbf{C}}, \mathbb{T}_E^0, \mathbf{N}_L \boldsymbol{\alpha}_e^1 \right) \right) d\Omega_e \quad (6.28) \\
 &+ \int_{\Omega_{R_e}} \left(\mathcal{P} \left(\mathbf{N}_E^T \bar{\mathbf{C}}, \mathbb{T}_M, \mathbf{M} \boldsymbol{\alpha}_e^2 \right) - \mathcal{P} \left(\mathbf{N}_E^T, \mathbb{T}_S^0, \mathbf{N}_L \boldsymbol{\beta}_e \right) \right) d\Omega_e,
 \end{aligned}$$

$$\begin{aligned}
 \mathbf{P}_{\hat{E}}^e &= \int_{\Omega_{R_e}} \left(\mathbf{M}_E^T \bar{\mathbf{S}}^h \right) \mathbf{D} d\Omega_e + \int_{\Omega_{R_e}} \left(\mathcal{P} \left(\mathbf{M}^T, \mathbb{T}_M^T, \bar{\mathbf{S}}^h \right) \right) d\Omega_e \quad (6.29) \\
 &+ \int_{\Omega_{R_e}} \left(\mathcal{P} \left(\mathbf{M}_E^T \bar{\mathbf{C}}, \mathbb{T}_E^0, \mathbf{N}_L \boldsymbol{\alpha}_e^1 \right) + \mathcal{P} \left(\mathbf{M}_E^T \bar{\mathbf{C}}, \mathbb{T}_M, \mathbf{M} \boldsymbol{\alpha}_e^2 \right) \right) d\Omega_e.
 \end{aligned}$$

The element pseudo load and sensitivity matrices \mathbf{P}_e and \mathbf{S}_e are defined as

$$\mathbf{P}_e := \begin{bmatrix} \mathbf{P}_u^e \\ \mathbf{P}_{\hat{E}}^e \\ \mathbf{P}_{\hat{E}}^e \\ \mathbf{P}_{\hat{S}}^e \end{bmatrix}, \quad \mathbf{S}_e := \begin{bmatrix} \mathbf{S}_u^e \\ \mathbf{S}_{\hat{E}}^e \\ \mathbf{S}_{\hat{E}}^e \\ \mathbf{S}_{\hat{S}}^e \end{bmatrix}. \quad (6.30)$$

These matrices are connected corresponding to the following relation

$$\mathbf{A}_{e=1}^{nelm} \begin{bmatrix} \mathbf{K}_e & \mathbf{0} & \mathbf{0} & \mathbf{L}_e^T \\ \mathbf{0} & \mathbf{A}_e^{11} & \mathbf{A}_e^{12} & -\mathbf{C}_e \\ \mathbf{0} & \mathbf{A}_e^{21} & \mathbf{A}_e^{22} & \mathbf{0} \\ \mathbf{L}_e & -\mathbf{C}_e & \mathbf{0} & \mathbf{0} \end{bmatrix} \mathbf{A}_{e=1}^{nelm} \begin{bmatrix} \mathbf{S}_u^e \\ \mathbf{S}_{\hat{E}}^e \\ \mathbf{S}_{\hat{E}}^e \\ \mathbf{S}_{\hat{S}}^e \end{bmatrix} = -\mathbf{A}_{e=1}^{nelm} \begin{bmatrix} \mathbf{P}_u^e \\ \mathbf{P}_{\hat{E}}^e \\ \mathbf{P}_{\hat{E}}^e \\ \mathbf{P}_{\hat{S}}^e \end{bmatrix}. \quad (6.31)$$

Static condensation on element level, see equation (5.34), can be applied to the above relation and yields \mathbf{K}_{T_e} and \mathbf{P}_{T_e} with

$$\mathbf{P}_{T_e} = \mathbf{P}_u^e + \mathbf{L}_e^T \mathbf{C}_e^{-T} \mathbf{A}_e \mathbf{C}_e^{-1} \mathbf{P}_{\hat{S}}^e + \mathbf{L}_e^T \mathbf{C}_e^{-1} \mathbf{P}_E^e \quad (6.32)$$

with $\mathbf{P}_E^e = \mathbf{P}_{\hat{E}}^e - \mathbf{A}_e^{12} (\mathbf{A}_e^{22})^{-1} \mathbf{P}_{\hat{E}}^e$. After assembly over all elements $\mathbf{K}_T = \mathbf{A}_{e=1}^{nelm} \mathbf{K}_{T_e}$, $\mathbf{S}_u = \mathbf{A}_{e=1}^{nelm} \mathbf{S}_u^e$ and $\mathbf{P}_T = \mathbf{A}_{e=1}^{nelm} \mathbf{P}_{T_e}$ one obtains the following system of equations

$$\mathbf{K}_T \mathbf{S}_u = -\mathbf{P}_T \quad (6.33)$$

with the unknown displacement sensitivities. After solving this system, the sensitivities of stresses and strains can be calculated as follows

$$\begin{aligned}
 \mathbf{S}_{\hat{E}}^e &= \mathbf{C}_e^{-1} (\mathbf{L}_e \mathbf{S}_u^e + \mathbf{P}_{\hat{S}}^e), \\
 \mathbf{S}_{\hat{E}}^e &= -(\mathbf{A}_e^{22})^{-1} (\mathbf{P}_{\hat{E}}^e + \mathbf{A}_e^{21} \mathbf{S}_{\hat{E}}^e), \\
 \mathbf{S}_{\hat{S}}^e &= \mathbf{C}_e^{-T} (\mathbf{A}_e \mathbf{S}_{\hat{E}}^e + \mathbf{P}_E^e).
 \end{aligned} \quad (6.34)$$

6.3.4 Sensitivity of Cauchy stress

The total derivative of Cauchy stress with respect to node coordinate i is

$$\frac{d\boldsymbol{\sigma}^h}{d\hat{X}_i} = \frac{\partial\boldsymbol{\sigma}^h}{\partial\hat{X}_i} + \sum_{j=1}^{nu} \frac{\partial\boldsymbol{\sigma}^h}{\partial\hat{u}_j} \frac{d\hat{u}_j}{d\hat{X}_i} + \sum_{j=1}^{ns} \frac{\partial\boldsymbol{\sigma}^h}{\partial\hat{S}_j} \frac{d\hat{S}_j}{d\hat{X}_i} \quad \text{with} \quad \frac{d\hat{u}_j}{d\hat{X}_i} = (S_u)_{ji}, \quad \frac{d\hat{S}_j}{d\hat{X}_i} = (S_{\hat{s}})_{ji}. \quad (6.35)$$

Quantities nu and ns denote the number of displacement degrees of freedom and the number of assumed stress degrees of freedom. Derivatives of Cauchy stress with respect to the assumed strain components are equal to zero. The total derivative of Cauchy stress consists of its partial derivatives, which reads

$$\begin{aligned} \frac{\partial\boldsymbol{\sigma}^h}{\partial\hat{X}_i} &= -\frac{1}{|\mathbf{F}^h|^2} \frac{\partial|\mathbf{F}^h|}{\partial\hat{X}_i} \mathbf{F}^h \hat{\mathbf{S}}_m^h (\mathbf{F}^h)^T + \frac{1}{|\mathbf{F}^h|} \frac{\partial\mathbf{F}^h}{\partial\hat{X}_i} \hat{\mathbf{S}}_m^h (\mathbf{F}^h)^T \\ &\quad + \frac{1}{|\mathbf{F}^h|} \mathbf{F}^h \hat{\mathbf{S}}_m^h \frac{\partial(\mathbf{F}^h)^T}{\partial\hat{X}_i} + \frac{1}{|\mathbf{F}^h|} \mathbf{F}^h \frac{\partial\hat{\mathbf{S}}_m^h}{\partial\hat{X}_i} (\mathbf{F}^h)^T \\ \frac{\partial\boldsymbol{\sigma}^h}{\partial\hat{u}_i} &= -\frac{1}{|\mathbf{F}^h|^2} \frac{\partial|\mathbf{F}^h|}{\partial\hat{u}_i} \mathbf{F}^h \hat{\mathbf{S}}_m^h (\mathbf{F}^h)^T + \frac{1}{|\mathbf{F}^h|} \frac{\partial\mathbf{F}^h}{\partial\hat{u}_i} \hat{\mathbf{S}}_m^h (\mathbf{F}^h)^T \\ &\quad + \frac{1}{|\mathbf{F}^h|} \mathbf{F}^h \hat{\mathbf{S}}_m^h \frac{\partial(\mathbf{F}^h)^T}{\partial\hat{u}_i} \\ \frac{\partial\boldsymbol{\sigma}^h}{\partial\hat{S}_i} &= +\frac{1}{|\mathbf{F}^h|} \mathbf{F}^h \frac{\partial\hat{\mathbf{S}}_m^h}{\partial\hat{S}_i} (\mathbf{F}^h)^T. \end{aligned} \quad (6.36)$$

Further discretisation is straight forward and details are omitted here.

6.4 Example: clamp

The following numerical example is based on the geometry which is pictured in Figure 6.1. The dimensions of the structure (height, width and depth) are $h = 3$, $w = 10$ and $d = 3$. The material properties are Young's modulus $E = 21000$ and Poisson's ratio $\nu = 0.3$. The load $\bar{q} = 1/30$ is a line load. The applied boundary conditions are pictured in Figure 6.1a. We note that the considered model is not doubly symmetric. In contrast to the right side, support on the left side allows rotation of the clamp. The FE-mesh consists of 1200 elements and 2562 nodes with 7686 degrees of freedom.

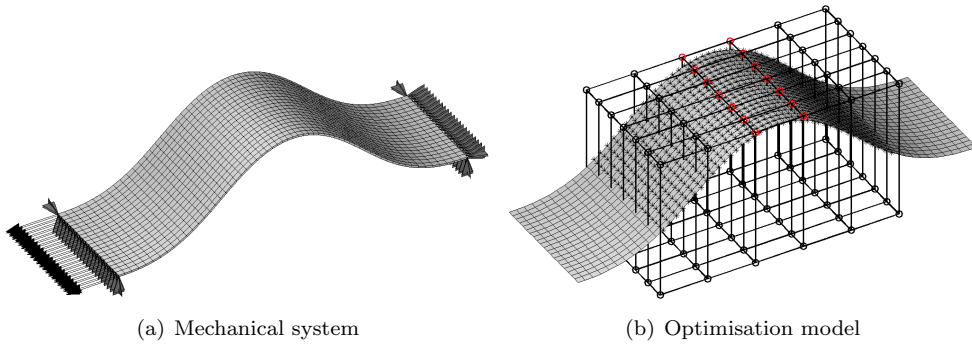


Figure 6.1: Clamp: initial structure

The thickness $t = 0.1$ remains constant during the optimisation. This behaviour is reached computing the middle surface of the shell structure and performing shape optimisation based on its nodes. The modified middle surface mesh is then expanded to 3D finite element mesh. The derivation of corresponding extended velocity fields for sensitivity analysis is straightforward and details are omitted here.

A morphing box is defined by 84 control points and is pictured in Figure 6.1b. Finite element nodes, which are controlled by this box are marked with a star. Vertical positions (z coordinates) of control points, which are marked red are used as design variables. Minimum values of this coordinates ensure a tunnel height of $h_t = 2$.

6.4.1 Compliance minimisation under volume constraint

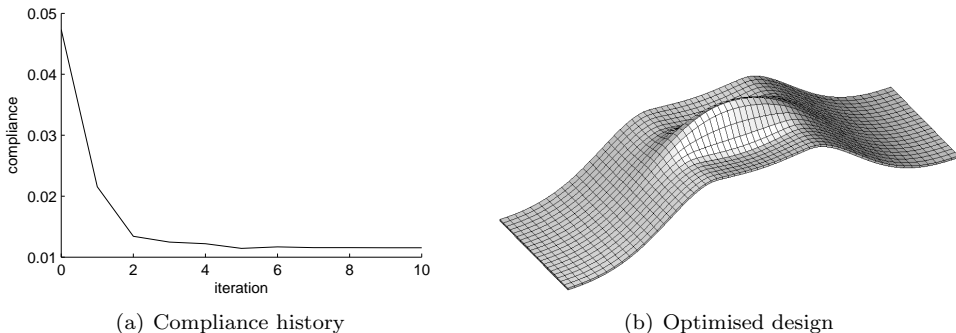


Figure 6.2: Clamp: optimisation results for compliance minimisation

The compliance $J := C := -\Pi$ of the structure, which is pictured in Figure 6.1 is minimised, taking into account a volume constraint $V = V_0$. Here, the quantities V and V_0 denote the current and initial volumes. The algorithm converges after ten iterations. The corresponding iteration history for the objective function is pictured in Figure 6.2a. The compliance is decreased to a quarter of its initial value. The optimised design is presented in Figure 6.2b. The upper half of the structure is stiffened with respect to bending stress. The higher stiffness can be verified considering structural deformation before and after optimisation in Figure 6.3.

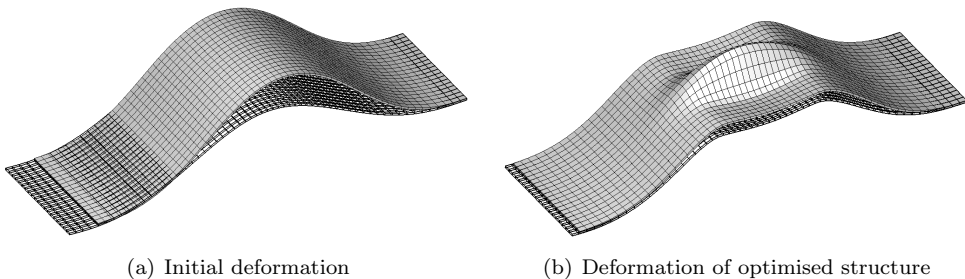


Figure 6.3: Clamp: deformation before and after optimisation

The left and right parts of the structure are not modified by this optimisation because the corresponding finite element nodes are not influenced by the morphing box defined in Figure 6.1b. The transition of optimised part to fixed one is smooth as the left and right two layers of control points are fixed for optimisation.

6.4.2 Volume minimisation under stress constraints

Minimisation of compliance under volume constraint is easy to deal with and leads to structures with high global stiffness. But real world problems necessitate the satisfaction of several local constraints, e.g. stress constraints. Therefore, we consider another model problem of volume minimisation under stress constraints. Stress minimisation at a certain point or at an area can be treated by analogy.

The volume V is chosen as objective function. Stress constraints with limit $\bar{\sigma}$ are necessary from mechanical point of view. The Von Mises stress σ_v is a function of Cauchy stress tensor components σ_{ij} with

$$\sigma_v = \sqrt{\sigma_{11}^2 + \sigma_{22}^2 + \sigma_{33}^2 - \sigma_{11}\sigma_{22} - \sigma_{11}\sigma_{33} - \sigma_{22}\sigma_{33} + 3(\sigma_{12}^2 + \sigma_{13}^2 + \sigma_{23}^2)}. \quad (6.37)$$

We control the Von Mises stress σ_v at all Gaussian points i , that is $\sigma_v^i \leq \bar{\sigma}$. For the considered example the stress limit is $\bar{\sigma} = 65$. Optimisation history for volume and maximum Von Mises stress are pictured in Figure 6.4.

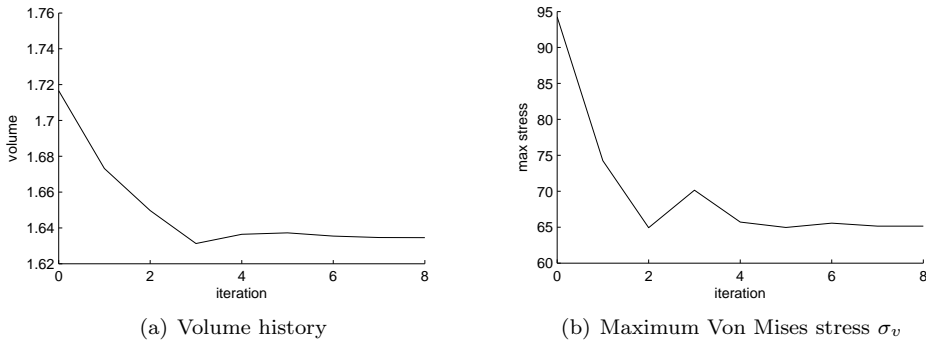
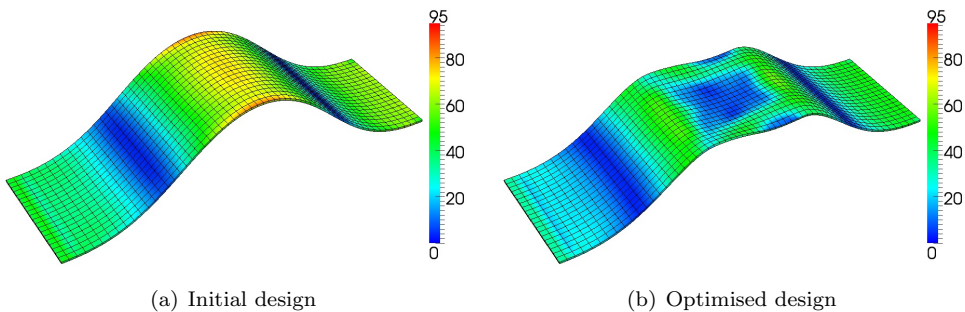


Figure 6.4: Clamp: optimisation results for volume minimisation

The algorithm converges after eight iterations. The volume decrease is about five percent. The stress constraints are satisfied. The maximum Von Mises stress is decreased from value $\max(\sigma_v^i) = 94$ to $\max(\sigma_v^i) = 65$. Von Mises Stress is pictured in Figure 6.5 for the initial and optimised design. We note that the optimisation started with an inadmissible initial design because some stress constraints were violated. It is an important aspect, which must be taken into account choosing the mathematical optimisation algorithm. Not all of them can deal with such situation. The optimised design is not doubly symmetric. This is caused by not symmetric boundary conditions, as mentioned above. Observation of Von Mises stresses in all Gaussian points leads to a large number of constraints and is very expensive. Stresses of only some parts of the structure are usually considered in practical applications.

Figure 6.5: Clamp: Von Mises Stress σ_v

6.5 Summary and concluding remarks

Variational sensitivity analysis of the considered solid shell element is performed and all derived relations are discretised. The pseudo load matrix, the sensitivity matrix and the material residual vector (i.e. vector of configurational forces) are derived. In addition, the sensitivity of stress is considered. Features and capabilities of the presented sensitivity analysis are demonstrated on a numerical example from the field of morphing based shape optimisation.

Sensitivity relations derived in this chapter and all involved quantities must be considered as tools for the nonlinear solid shell element. These tools extend the application range of the solid shell element. An implementation of such tools in existing and future element routines will simplify the exchange of software components for various scientific disciplines.

Possible fields of application. There is a great number of fields where the presented sensitivity relations can be applied. All quantities are derived with respect to coordinates of FE-nodes. Parameter free shape optimisation can be performed based on these derivatives utilising some additional tools like filters and mesh control techniques. Recent works on this topic are [32, 93, 119, 18] and [66]. Gradients for geometry based shape optimisation can be calculated extending the presented sensitivities by the corresponding design velocity fields. R-adaptivity is concerned with improvement of finite element solution on the same mesh. Here, the number of degrees of freedom and mesh topology are fixed. Only the mesh form is changed. A review, much more details and examples on this topic can be found in [100]. Fracture mechanics deals with the propagation of cracks in materials. Here, the strain energy release and the direction of crack growth can be directly derived from the material residuum, which is derived in this chapter. Details and examples on this topic can be found in [99].

Some remarks on the computational effort. In SOP the element pseudo load matrices are computed together with element stiffness matrices in the element routine and assembled parallel to each other. These matrices cause approximately the same numerical effort. The pseudo load matrix is a sparse matrix and its population is comparable with that of the stiffness matrix. In contrast, the sensitivity matrix is a full populated matrix and its computation requires the solution of a linear system of equations with large number of right sides or the inversion of the tangent stiffness matrix. The computation of this matrix is usually avoided employing the adjoint approach to sensitivity analysis. The computation of the material residual vector causes approximately the same numerical effort as the computation of the physical residual.

7 Singular value decomposition (SVD)

The definitions of SVD and *generalised singular value decomposition* (GSVD) are introduced in this chapter. Several applications are demonstrated and features of SVD are explained.

7.1 Introduction

SVD is a mathematical powerful tool which is used in different scientific fields.

7.1.1 State of the art

The basics of singular value decomposition are given in the literature on numerical linear algebra, for example [70]. A summary of the numerical treatment concerning large eigenvalue problems can be found in [69, 141]. SVD algorithms are included in most numerical linear algebra tools. The most important ones are *LAPACK* [15], the *GSL* [6], the library *SVDPACK* [13] and other comparable algorithms in scientific software packages like *MATLAB* [9] or *SCILAB* [12]. Some hints to implementation are given in [20].

SVD is used in *image processing* to reduce the storage space (e.g. [114] and references therein). Hereby, only the most important parts of an image are stored. The rest is quashed. Thus, SVD provides an efficient representation of facial images calculating the so-called eigenfaces, see [103]. Essential influence factors in *statistics* can be determined and interpreted by means of SVD, see e.g. [74]. The most prevailed method in this area is the *principal component analysis* (PCA, see [82]) used for dimension reduction. The power of SVD in conjunction with a special subspace method can be observed in system identification and dynamical behaviour, see [94]. An improved computational approach for linear differential equations such as Laplace and Helmholtz equations motivated by SVD analysis is proposed in [115]. Overall, SVD analysis enhances the eigenvalue analysis in structural dynamics and structural stability and is both, quantitatively and qualitatively well understood.

7.1.2 Special features of the presented research

Within this thesis sensitivity information is analysed by *singular value decomposition* (SVD). Appropriate notation is introduced and different data interpretation techniques are explained on examples in this chapter. SVD of a matrix is interpreted, which is necessary to perceive the concepts presented in subsequent chapters. In addition, an inexpensive SVD of sensitivity matrix is discussed, which is based on GSVD of the stiffness and pseudo load matrices.

7.2 Singular value decomposition

The definition of SVD is presented and some of its applications are briefly described.

7.2.1 Definition and numerical effort of SVD

Let \mathbf{A} be a $m \times n$ real matrix. Then, there exists a factorisation of the form

$$\mathbf{A} = \mathbf{Y}\mathbf{\Sigma}\mathbf{Z}^T = \sum_{i=1}^{\min(m,n)} \sigma_{ii} \mathbf{y}_i \mathbf{z}_i^T, \quad (7.1)$$

where \mathbf{Y} is a $m \times m$ matrix, $\mathbf{\Sigma}$ is a $m \times n$ diagonal matrix with non negative numbers σ_{ii} (*singular values* sorted in decreasing order) on the diagonal and \mathbf{Z} a $n \times n$ matrix. The matrices \mathbf{Y} and \mathbf{Z} contain a set of orthonormal *left* and *right singular vectors* of \mathbf{A} with $\mathbf{Y}^{-1} = \mathbf{Y}^T$ and $\mathbf{Z}^{-1} = \mathbf{Z}^T$. The factorisation in equation (7.1) is the *singular value decomposition* of matrix \mathbf{A} . Singular values are uniquely determined. In contrast, singular vectors can change their signs.

The \mathcal{O} -notation is used to describe the numerical effort for SVD. The full singular value decomposition of a square matrix $\mathbf{A} \in \mathbb{R}^{m \times m}$ requires $\mathcal{O}(m^3)$ floating-point operations (flops). For rectangular matrices $\mathbf{A} \in \mathbb{R}^{m \times n}$ with $m \geq n$ only $\mathcal{O}(mn^2)$ flops are necessary to compute SVD. The computation of only the first k singular vectors reduces the numerical effort. A number of SVD algorithms exists, for example, in *MATLAB*, which makes it possible to work with sparse matrices and to compute only some first k singular values and the corresponding singular vectors. The numerical effort is then approximately of $\mathcal{O}(nmk)$.

7.2.2 Applications of SVD

Matrix approximation. The last term in equation (7.1) shows that any matrix \mathbf{A} can be decomposed in matrices \mathbf{w}_i of rank one weighted with singular values with

$$\mathbf{A} = \sum_{i=1}^{\min(m,n)} \sigma_{ii} \mathbf{y}_i \mathbf{z}_i^T = \sum_{i=1}^{\min(m,n)} \sigma_{ii} \mathbf{w}_i. \quad (7.2)$$

As far as the singular values are sorted in decreasing order and the values of all matrices \mathbf{w}_i have the same ballpark, because the vectors \mathbf{y} and \mathbf{z} are normalised, the main parts of the given matrix, which are the first k parts, can be determined and used for a matrix approximation

$$\tilde{\mathbf{A}} = \sum_{i=1}^k \sigma_{ii} \mathbf{y}_i \mathbf{z}_i^T = \sum_{i=1}^k \sigma_{ii} \mathbf{w}_i, \quad (7.3)$$

with $k \leq r \leq \min(m, n)$. Here, r denotes the rank of the matrix \mathbf{A} . This technique is applied in image compression to reduce storage space. An image is a matrix which contains colour values. As an example, we perform a matrix approximation of an image $\mathbf{B} \in \mathbb{R}^{331 \times 484}$ for different values k . The results are pictured in Figure 7.1. It is very interesting to observe that with $k = 50$ (equal to 16% of all information) one can hardly detect significant differences between the images, and with $k = 15$ (equal to 5% of all information) one can still recognise the most important parts of the image (i.e. house, door, fences, etc.).

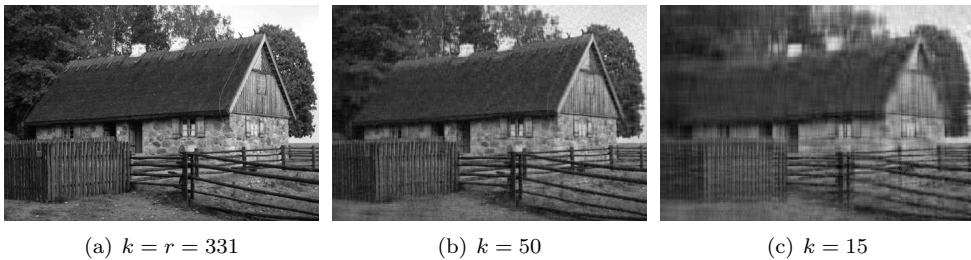


Figure 7.1: Image compression depending on k (photo: © 2009, W. Kijanski)

Pseudo inverse of a matrix. As already mentioned before, any matrix $\mathbf{A} \in \mathbb{R}^{m \times n}$ can be decomposed corresponding to equation (7.1). With $\mathbf{Y}^{-1} = \mathbf{Y}^T$ and $\mathbf{Z}^{-1} = \mathbf{Z}^T$ we obtain

$$\tilde{\mathbf{A}}^{-1} = [\mathbf{Y} \tilde{\Sigma} \mathbf{Z}^T]^{-1} = (\mathbf{Z}^T)^{-1} (\mathbf{Y} \tilde{\Sigma})^{-1} = \mathbf{Z} \tilde{\Sigma}^{-1} \mathbf{Y}^T = \sum_{i=1}^{k \leq r} \frac{1}{\sigma_i} \mathbf{z}_i \mathbf{y}_i^T \quad (7.4)$$

the pseudo inverse (for $k = r = m = n$ the inverse) of the matrix \mathbf{A} . Here, r denotes the rank of the matrix \mathbf{A} and matrix $\tilde{\Sigma}^{-1} \in \mathbb{R}^{n \times m}$ is a diagonal one and consists of reciprocal first k singular values σ_i . The pseudo inverse is defined for singular, quasi-singular and rectangular matrices. Under and over estimated linear systems of equations can be solved utilising the pseudo inverse of a matrix.

Principal component analysis (PCA). Visualisation, interpretation and reduction of large data sets can be performed by principal component analysis. PCA is defined

as an orthogonal linear transformation that transforms the data to a new coordinate system. This transformation is usually delivered by SVD of the data matrix. Here, the greatest variance by projecting of the data comes to lie on the first coordinate (called the first principal component), the second greatest variance on the second coordinate, and so on. This method is explained on the example of a cluster of points. We consider the data matrix which consists of cluster points coordinates

$$\mathbf{B} = \begin{bmatrix} s_1^1 & s_1^2 & \cdots & s_1^n \\ s_2^1 & s_2^2 & \cdots & s_2^n \end{bmatrix}^T. \quad (7.5)$$

These points are pictured in Figure 7.2a. We assume that the perimeter of the cluster is approximated using the function $P(s_1, s_2) = 2(\Delta s_1 + \Delta s_2)$.

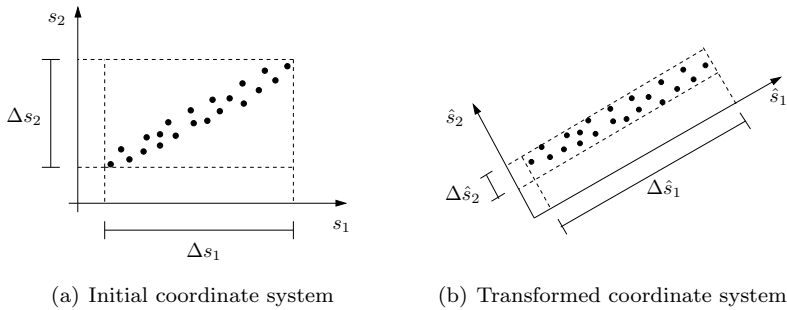


Figure 7.2: Cluster of points

In case that the coordinate system in Figure 7.2a is turned according to Figure 7.2b, the approximation of the perimeter function reads $\hat{P}(\hat{s}_1, \hat{s}_2) = 2(\Delta \hat{s}_1 + \Delta \hat{s}_2)$. The new function approximates the perimeter in a better way and can be obtained using SVD. Therefore, the data matrix \mathbf{B} is decomposed as

$$\mathbf{B} = \begin{bmatrix} s_1^1 & s_1^2 & \cdots & s_1^n \\ s_2^1 & s_2^2 & \cdots & s_2^n \end{bmatrix}^T = \mathbf{Y} \mathbf{\Sigma} \mathbf{Z}^T = \mathbf{Y} \begin{bmatrix} \sigma_{11} & 0 \\ 0 & \sigma_{22} \\ 0 & 0 \\ \vdots & \vdots \\ 0 & 0 \end{bmatrix} \mathbf{Z}^T. \quad (7.6)$$

With this decomposition one can perform the following transformation

$$\hat{\mathbf{B}} = \mathbf{B} \mathbf{Z} = \begin{bmatrix} \hat{s}_1^1 & \hat{s}_1^2 & \cdots & \hat{s}_1^n \\ \hat{s}_2^1 & \hat{s}_2^2 & \cdots & \hat{s}_2^n \end{bmatrix}^T \quad (7.7)$$

and obtain the data matrix $\hat{\mathbf{B}}$ in a new coordinate system \mathbf{Z} . Here the columns of \mathbf{Z} are unit vectors of this system and the corresponding coordinates are called *principal*

components. Singular values σ_{11} and σ_{22} describe the variance of new coordinates. In order to carry out a model reduction, the following implication is used

$$\sigma_{22} \ll \sigma_{11} \longrightarrow \Delta \hat{s}_2 \ll \Delta \hat{s}_1 \longrightarrow \hat{P}(\hat{s}_1, \hat{s}_2) \approx \bar{P}(\hat{s}_1) = 2\Delta \hat{s}_1. \quad (7.8)$$

Moreover, the transformation $\hat{\mathbf{s}} = \mathbf{Z}^T \mathbf{s}$ provides new variables, which are sorted at the extent of their variance. Components of column vectors of \mathbf{Z} define the influence of the old variables on the new ones and are called *loading factors*.

7.2.3 Analysis of input-output systems

Any real matrix $\mathbf{A} \in \mathbb{R}^{m \times n}$ defines an input-output system as follows

$$\mathbf{c} = \mathbf{A}\mathbf{b} \quad \text{with} \quad \mathbf{b} \in \mathbb{R}^n \quad \text{and} \quad \mathbf{c} \in \mathbb{R}^m. \quad (7.9)$$

Here, the inputs and the corresponding outputs are denoted with \mathbf{b} and \mathbf{c} . In this situation it is important to know which input vectors lead to outputs with the largest or with the smallest norm. Singular value decomposition of matrix \mathbf{A} , see equation (7.1), is utilised to analyse this input-output system. If the input corresponds to the k -th right singular vector which is scaled by a factor d with $\mathbf{b} = d\mathbf{z}_k$, we obtain the corresponding output as follows

$$\mathbf{c} = \left(\sum_{i=1}^{\min(m,n)} \sigma_i \mathbf{y}_i \mathbf{z}_i^T \right) d\mathbf{z}_k = d\sigma_k \mathbf{y}_k \quad \text{with} \quad \|\mathbf{c}\|_2 = \|d\sigma_k \mathbf{y}_k\|_2 = d\sigma_k. \quad (7.10)$$

These relations are valid due to the orthonormal bases \mathbf{z}_i and \mathbf{y}_i . We note that inputs which correspond to the largest singular values have an extraordinary impact on outputs. Inputs which correspond to $\sigma = 0$, produce zero valued vectors as output.

7.3 Generalised singular value decomposition

The definition of GSVD is presented. An inexpensive SVD of sensitivity matrix is outlined which is based on GSVD of the pseudo load matrix and the stiffness matrix.

7.3.1 Definition of GSVD

Let $\mathbf{A} \in \mathbb{R}^{l \times m}$ and $\mathbf{B} \in \mathbb{R}^{n \times m}$ be real matrices. The factorisation

$$\mathbf{A} = \mathbf{Z}\mathbf{M}\mathbf{X}^T, \quad \mathbf{B} = \mathbf{Y}\mathbf{Q}\mathbf{X}^T, \quad \mathbf{M}^T \mathbf{M} + \mathbf{Q}^T \mathbf{Q} = \mathbf{I} \quad (7.11)$$

is the *generalised singular value decomposition* (GSVD) of \mathbf{A} and \mathbf{B} . Here, $\mathbf{Z} \in \mathbb{R}^{l \times l}$ and $\mathbf{Y} \in \mathbb{R}^{n \times n}$ are orthonormal matrices. The matrices $\mathbf{M} \in \mathbb{R}^{l \times m}$ and $\mathbf{Q} \in \mathbb{R}^{n \times m}$ are diagonal matrices and contain singular values which are sorted in decreasing or increasing order. The matrix $\mathbf{X} \in \mathbb{R}^{m \times m}$ is a real matrix.

7.3.2 Inexpensive SVD of sensitivity matrix

Sensitivity analysis in structural optimisation sometimes requires the computation of, the so called, *sensitivity matrix* $\mathbf{S} \in \mathbb{R}^{n \times m}$ with

$$\mathbf{S} = \mathbf{K}^{-1} \mathbf{P} \Leftrightarrow \mathbf{S}^T = \mathbf{P}^T \mathbf{K}^{-T}. \quad (7.12)$$

Here, the matrices $\mathbf{K} \in \mathbb{R}^{n \times n}$ and $\mathbf{P} \in \mathbb{R}^{n \times m}$ denote the so called *stiffness matrix* and *pseudo load matrix*. Both matrices are sparsely populated and can be assembled with relatively low numerical effort. In contrast, the computation of sensitivity matrix \mathbf{S} is expensive and requires either the solution of m linear systems of equations or the inversion of the stiffness matrix \mathbf{K} . Furthermore, sensitivity matrix is fully populated and a lot of storage space is necessary for practical applications. Within this thesis SVD of sensitivity matrix is required to perform model reduction and adaptation. Generalised singular value decomposition of stiffness and pseudo load matrices is able to provide SVD of \mathbf{S} without its computation. GSVD of \mathbf{P}^T and \mathbf{K}^T reads

$$\text{GSVD}(\mathbf{P}^T, \mathbf{K}^T) \longrightarrow [\mathbf{Z} \ \mathbf{Y} \ \mathbf{X} \ \mathbf{M} \ \mathbf{Q}]. \quad (7.13)$$

Following relations hold true for decomposed matrices

$$\mathbf{P}^T = \mathbf{Z} \mathbf{M} \mathbf{X}^T, \quad \mathbf{K}^T = \mathbf{Y} \mathbf{Q} \mathbf{X}^T \Leftrightarrow \mathbf{X}^T = \mathbf{Q}^{-1} \mathbf{Y}^T \mathbf{K}^T. \quad (7.14)$$

The last expression is inserted in the first one and we obtain

$$\begin{aligned} \mathbf{P}^T &= \mathbf{Z} \mathbf{M} \mathbf{Q}^{-1} \mathbf{Y}^T \mathbf{K}^T, \\ \Leftrightarrow \mathbf{P}^T \mathbf{K}^{-T} &= \mathbf{Z} \mathbf{M} \mathbf{Q}^{-1} \mathbf{Y}^T, \\ \Leftrightarrow \mathbf{S}^T &= \mathbf{Z} \mathbf{\Sigma}^T \mathbf{Y}^T \quad \text{with} \quad \mathbf{\Sigma}^T = \mathbf{M} \mathbf{Q}^{-1}, \\ \Leftrightarrow \mathbf{S} &= \mathbf{Y} \mathbf{\Sigma} \mathbf{Z}^T. \end{aligned} \quad (7.15)$$

The last expression is the SVD of the sensitivity matrix. The full generalised singular value decomposition of square matrices $\mathbf{A} \in \mathbb{R}^{m \times m}$ and $\mathbf{B} \in \mathbb{R}^{m \times m}$ requires $\mathcal{O}(2m^3)$ floating-point operations and no advantage is reached so far. Enhanced sensitivity analysis which is presented in this thesis requires only the computation of some largest singular values and the corresponding vectors of sensitivity matrix. For such situations, an algorithm was presented in [80] which can deal with sparse matrices and saves a lot of numerical effort considering practical applications. We note that this algorithm is not yet implemented in *MATLAB*, where only full GSVD is available.

7.4 Summary and concluding remarks

SVD is used to sort out the valuable part of information which is packed in matrices. Techniques like the analysis of input-output systems, model reduction and coordinate transformation are explained, which are the prerequisites of the subsequent chapters. Numerical effort of SVD and the treatment of sparse matrices are discussed. Inexpensive computation of SVD of the sensitivity matrix is outlined.

8 Sensitivity based imperfections for nonlinear buckling analysis

This chapter outlines a technique to generate ‘worst case’ imperfections for nonlinear buckling analysis. It is based on the analytical derivation and efficient computation of the Fréchet derivatives of the physical residual with respect to the full space of all possible design parameters. This overhead of sensitivity information is examined by a singular value decomposition (SVD) in order to detect design changes with major and minor influences on equilibrium. This knowledge enables the engineer to understand and improve structural behaviour and to detect relevant geometrical conditions for buckling analysis.

8.1 Introduction

The *pseudo load matrix* (Fréchet derivative) is a well known quantity in sensitivity analysis of shape optimisation problems, see chapter 6. This matrix is analysed by a singular value decomposition (SVD) to demonstrate that it contains additional valuable information, which can be used to create imperfection modes for nonlinear buckling analysis. Right singular vectors which correspond to the largest singular values are used as imperfection modes. Local and global imperfections can be distinguished. Geometrical constraints like prescribed denting shapes and thickness imperfections can be considered to study the corresponding effects on buckling. The most unfavourable imperfection can also be found in situations, where the mentioned properties are combined. The generic concept is applied to structures modelled using nonlinear solid shell element, which is presented in chapter 5. This approach is also proposed by the author in [64]. Nonlinear elastic problems, which are time independent are considered in this chapter. The central aspects of the presented approach are commented on with references to literature.

8.1.1 State of the art

Buckling is a process whereby a loaded structure suddenly changes its shape. The structure is often destroyed after this process if stability was lost.

Classical buckling analysis.

Beginning with the pioneer work of Koiter [92] in 1945, a lot of research was done to understand the buckling and post-buckling behaviour of structures (also called *structural stability analysis*). Overview articles on this topic are, for example [52] and [117]. Branch switching, direct calculation of critical points and path-following are widespread strategies in this field. A simple load control technique and supervision of the smallest eigenvalue of the tangent matrix are satisfactory to solve the problems in this contribution.

Imperfections.

Small deviations from the ideal shape are called *geometrical imperfections* or short *imperfections*. Only those (geometrical) imperfections are considered here. Imperfections may cause a dramatic reduction of the buckling load and lead to a catastrophic failure. Modern structural analysis software allows to study nonlinear buckling behaviour in the presence of imperfections. Here, the question arises what shape should have the applied imperfection (for a given amplitude) to lead to the smallest load-carrying capacity. In other words, what is the ‘worst’ imperfection? As noted in [117], Koiter expected the most important influence on the behaviour of imperfect structure from mode shapes that correspond to the buckling mode of the perfect structure. This is the most often used assumption analysing the structural stability up today, see for example international standards [53, 54]. The corresponding approach ‘is neither robust nor reliably accurate’ as discussed for shells in [132]. Therefore, understanding the nature and effects of imperfections considering thin walled structures remains to be an area of interest today. A survey of this research field is given in [17] and [52].

Imperfections in context of structural optimisation.

Structural optimisation is often used to increase the load-carrying capacity and the efficiency of thin walled structures. Unfortunately, such optimised structures are highly sensitive with respect to imperfections as demonstrated in [134]. More details and examples on this topic are presented in [135]. In order to treat this problem, authors in [116, 26] insert the imperfection sensitivity into the optimisation model. Stable designs are obtained maximising the buckling load. In conclusion of that work a possible computation of the ‘worst’ imperfection shape is outlined. For this purpose, the failure load must be minimised for a given structural design and varying imperfection shape. A similar strategy was, for example, followed in [50]. Several

approaches are proposed, where unfavourable imperfections are computed as solutions of inverse problems, see for example [132].

8.1.2 Special features of the presented research

In contrast to the concept presented in [132], no optimisation problem is solved by the approach proposed in this chapter. However, only a quantity which usually appears in gradient based structural optimisation is used to create imperfections. Thus, this approach does not cause extra iterations. It is well known, that the ‘worst case’ imperfection in its true sense does not exist, see [120]. Nevertheless, the term ‘worst’ is used in the specified sense described below. From the optimisation point of view, imperfections are variations of design. We consider a perfect structure, which is in equilibrium with applied loads and hold the state functions fixed. In this situation, shape changes, which would disturb equilibrium most of all are considered to be the best candidates for imperfections. The pseudo load matrix describes how the equilibrium reacts (*output*) on an imposed design modification (*input*). We analyse this *input-output system* by a singular value decomposition (SVD), see chapter 7. This way the ‘worst’ imperfection or the one with the biggest influence on equilibrium can be found. The corresponding imperfect structure is analysed and the critical load is computed. In this contribution design velocity fields, see chapter 4, are used to transform the pseudo load matrix into different design descriptions and to create ‘worst’ imperfections of only some parts of a structure.

8.2 Stability of equilibrium

Stability conditions for equilibrium are presented for variational and discretised cases.

8.2.1 Variational relations

In context of structural optimisation $\Pi(\mathbf{v}, \mathbf{X})$ is the energy (Hu-Washizu) functional, which is nonlinear with respect to variables $\mathbf{v} \in \mathcal{V}$ and $\mathbf{X} \in \mathcal{X}$, see chapter 5. It is defined on Hilbert spaces \mathcal{V} and \mathcal{X} , i.e. $J : \mathcal{V} \times \mathcal{X} \rightarrow \mathbb{R}$. Generalised functions for the state \mathbf{v} and for the design \mathbf{X} are introduced here in an abstract sense. If $\Pi(\cdot)$ is a differentiable functional on \mathcal{V} , the following notation, see also [98], is used for the first and second partial variations (i.e. *directional derivatives* or *Gâteaux derivatives*) with respect to the state

$$\Pi'_v(\mathbf{v}, \mathbf{X}; \boldsymbol{\eta}) := \left. \frac{d}{d\varepsilon} \Pi(\mathbf{v} + \varepsilon \boldsymbol{\eta}, \mathbf{X}) \right|_{\varepsilon=0}, \quad (8.1)$$

$$\Pi''_{vv}(\mathbf{v}, \mathbf{X}; \boldsymbol{\eta}, \boldsymbol{\mu}) := \left. \frac{d}{d\varepsilon} \Pi'_v(\mathbf{v} + \varepsilon \boldsymbol{\mu}, \mathbf{X}; \boldsymbol{\eta}) \right|_{\varepsilon=0}. \quad (8.2)$$

The quantity $R := \Pi'_v(\mathbf{v}, \mathbf{X}; \boldsymbol{\eta})$ is linear with respect to $\boldsymbol{\eta}$ and is called *physical residual*. The *tangent physical stiffness operator* is defined as $k := \Pi''_{vv}(\mathbf{v}, \mathbf{X}; \boldsymbol{\eta}, \boldsymbol{\mu})$ and is linear with respect to $\boldsymbol{\eta}$ and $\boldsymbol{\mu}$. A stable solution of a nonlinear structural analysis problem is reached if the energy functional obtains a strong local minimum with respect to \mathbf{v} . This state is characterised by the following conditions

$$R = 0 \quad \text{and} \quad k > 0. \quad (8.3)$$

Here, the first condition forces the equilibrium of the structure. The second one, means that small perturbations of \mathbf{v} should not lead to an energy decrease.

8.2.2 Discretised relations

Systems of nonlinear, partial differential equations are usually solved by using the finite element method, see for example [152]. The corresponding discretisation and the subsequent assembly of all element contributions lead to the physical residual vector $\mathbf{R} \in \mathbb{R}^n$ and to the symmetric, tangent physical stiffness matrix $\mathbf{K} \in \mathbb{R}^{n \times n}$ with the number of degrees of freedom n . Taking displacement boundary conditions into account, one obtains a reduced stiffness matrix $\mathbf{K}_r \in \mathbb{R}^{r \times r}$ with $r < n$. In the following, the smallest eigenvalue of \mathbf{K}_r is noted by γ . Stability conditions given in equation (8.3) can be formulated considering discrete quantities

$$\mathbf{R} = \mathbf{0} \quad \text{and} \quad \gamma > 0. \quad (8.4)$$

Hereby, the equilibrium is expressed by n equations and stability is forced by positive definiteness of \mathbf{K}_r . The loads are usually scaled by a parameter $\lambda > 0$ to compute load deflection curves considering nonlinear behaviour. Therefore, the eigenvalue $\gamma(\lambda)$ depends on the load parameter. Unstable states are indicated by $\gamma(\lambda) \leq 0$. In this thesis only the computation of the first instability point is considered. In this case, the load parameter is gradually increased in an interval $0 < \lambda \leq \lambda_c$. The value λ_c with $\gamma(\lambda_c) = 0$ indicates the first instability point and is called the critical load (only in this context). The *bisection method* is well known in context of line search in optimisation, see for example [105]. This method is used to compute an accurate value λ_c and to reduce the numerical effort. An eigenvector of the reduced stiffness matrix \mathbf{K}_r which corresponds to $\gamma(\lambda_c) = 0$ is called *buckling mode*.

8.3 Sensitivity based imperfections

One has to violate the conditions (8.4) to create ‘worst’ imperfections. Most of the proposed techniques on this topic try to affect the smallest eigenvalue γ of the tangent physical stiffness operator, see for example [79, 26, 137, 116, 50, 148, 132]. The strategy followed in this contribution is to disturb the equilibrium condition $\mathbf{R} = \mathbf{0}$.

8.3.1 Global imperfections

Variational design sensitivity analysis is a branch of structural optimisation. Here, variations of the material configuration $\delta\mathbf{X}$ are considered and the changes of an arbitrary objective functional $J(\mathbf{v}(\mathbf{X}), \mathbf{X})$ are observed. Its total partial variation with respect to \mathbf{X} contains the variation of the state $\delta\mathbf{v} = \frac{d\mathbf{v}}{d\mathbf{X}} \cdot \delta\mathbf{X}$ with respect to design. The variational equation for the sensitivity of the state due to changes in the design, see chapter 6, is given as follows

$$k(\mathbf{v}, \mathbf{X}; \delta\mathbf{v}, \delta\bar{\mathbf{v}}) = -p(\mathbf{v}, \mathbf{X}; \delta\mathbf{v}, \delta\bar{\mathbf{X}}). \quad (8.5)$$

For a given variation in the design $\delta\bar{\mathbf{X}}$, the variation in the state $\delta\bar{\mathbf{v}}$ is obtained. This is the main purpose of the pseudo load p . Discretisation of operator p leads to the pseudo load matrix $\mathbf{P} \in \mathbb{R}^{n \times m}$ with the number of design variables m and with the number of degrees of freedom n . This matrix defines an input-output system

$$d_{\hat{\mathbf{X}}}\mathbf{R} = \mathbf{P} d\hat{\mathbf{X}}. \quad (8.6)$$

A given perturbation in design $d\hat{\mathbf{X}}$ (input) yields perturbation in equilibrium $d_{\hat{\mathbf{X}}}\mathbf{R}$ (output). As only the partial derivative is considered, the notation $d_{\hat{\mathbf{X}}}$ is utilised. Singular value decomposition is utilised to analyse this input-output system. If the perturbation in design is equal to the k -th right singular vector $d\hat{\mathbf{X}} = \mathbf{z}_k$, we obtain the corresponding perturbation in equilibrium as follows

$$d_{\hat{\mathbf{X}}}\mathbf{R} = \left(\sum_{i=1}^{\min(n,m)} \sigma_i \mathbf{y}_i \mathbf{z}_i^T \right) \mathbf{z}_k = \sigma_k \mathbf{y}_k \quad \text{with} \quad \|d_{\hat{\mathbf{X}}}\mathbf{R}\|_2 = \|\sigma_k \mathbf{y}_k\|_2 = \sigma_k. \quad (8.7)$$

These relations are valid because of the orthonormal bases \mathbf{z}_i and \mathbf{y}_i . We note that inputs (shapes) which correspond to the largest singular values have an extraordinary impact on equilibrium. Taking these observations into account, SVD based procedure, which is pictured in Figure 8.1 can be utilised to generate imperfections. Here, the first instability point of the perfect structure is determined. The corresponding load parameter λ_c and the state function \mathbf{v} are considered to be fixed. What shape changes would disturb equilibrium most of all in this situation? The pseudo load matrix \mathbf{P} is computed for load level λ_c to answer this question. The most unfavourable values of the chosen design variables are obtained by using SVD and computing right singular vectors which corresponds to the largest singular values of the pseudo load matrix. The amplitude of such an imperfection must be chosen by the engineer. The corresponding imperfect model is analysed again to detect the first instability point or to evaluate some failure criteria.

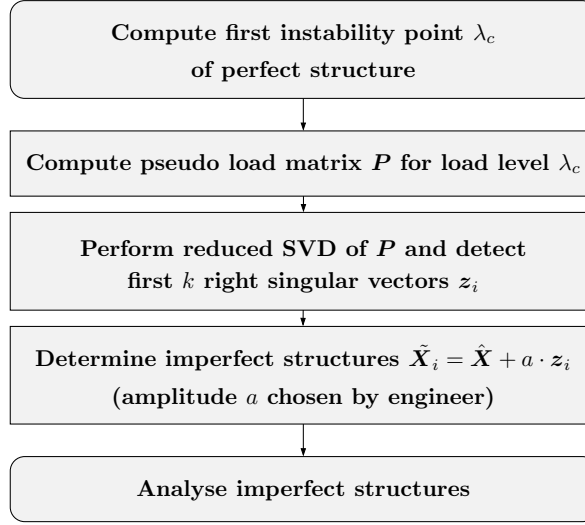


Figure 8.1: Generation of SVD based imperfections

8.3.2 Local imperfections

The pseudo load matrix is usually calculated with respect to coordinates of all finite element nodes $\hat{\mathbf{X}}$ as design variables. In this case, the highest degree of freedom for design changes is considered. Such design space is used, for example, in [50] to create imperfections. In different situations one is interested in local design changes like imperfections of certain parts of a structure or in thickness imperfections only. In other cases one wants to study certain shapes of imperfections like waves or denting, see for example [132]. These cases delineate the main application area of the presented method. Hence, the concept of so called *design velocity fields*, which are well-known in shape optimisation, see chapter 3 and 4, is utilised to modify the pseudo load matrix, which was computed with respect to node coordinates. Following this concept, a map is defined

$$\hat{\mathbf{X}} = \Phi(\mathbf{w}) \quad \text{with} \quad \Phi : \mathbb{R}^s \longrightarrow \mathbb{R}^m, \quad (8.8)$$

where the coordinates of FE nodes are functions of s new design variables \mathbf{w} . Utilising the chain rule we obtain the pseudo load matrix with respect to new design variables

$$\bar{\mathbf{P}} = \mathbf{P} \frac{d\hat{\mathbf{X}}}{d\mathbf{w}} = \mathbf{P}\Psi \quad \text{with} \quad \bar{\mathbf{P}} \in \mathbb{R}^{n \times s}. \quad (8.9)$$

Here, the quantity $\Psi \in \mathbb{R}^{m \times s}$ is called design velocity fields matrix, where the i -th column is the velocity field for the new design variable w_i . The procedure presented in Figure 8.1 is also valid for using $\bar{\mathbf{P}}$ instead of \mathbf{P} . In cases, where only imperfections

of some parts of a structure are considered, design velocity fields matrix is a simple Boolean matrix and can be created using standard selection tools. We note that design velocity fields usually reduce the number of variables which is beneficial for the numerical effort of the utilised SVD.

8.4 Example: compressed cylinder

The proposed strategy is clarified by considering the structure in Figure 8.2.

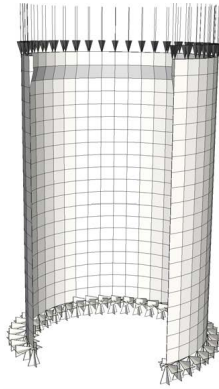


Figure 8.2: Compressed cylinder

Here, only $3/4$ of the model is visualised. The example is unit less, but the dimensions and material properties are chosen in a way that the structure corresponds to a part of a PET bottle. The height is $h = 12$, the radius is $r = 4$ and the thickness is $t = 0.015$. The free edge of the structure is stiffened with a ring ($h_r = 1.2$, $t_r = 0.15$) to enforce buckling within the surface. All bottom nodes are fixed in all directions. A St. Venant material with Young's modulus $E = 350$ and Poisson's ratio $\nu = 0.4$ is assumed. The critical load λ_c is the load resultant and is to be calculated for perfect and imperfect designs.

8.4.1 Analysis of the perfect structure

The critical load parameter λ_c of the perfect structure is determined for different mesh sizes, see Figure 8.3a. A good approximation is reached using a mesh with 6050 elements. The eigenvalue decomposition of the reduced tangent stiffness matrix at load level λ_c provides eigenvectors which are the buckling modes. For meshes with 800 and 6050 elements the corresponding buckling modes are pictured in Figure 8.3b-c.

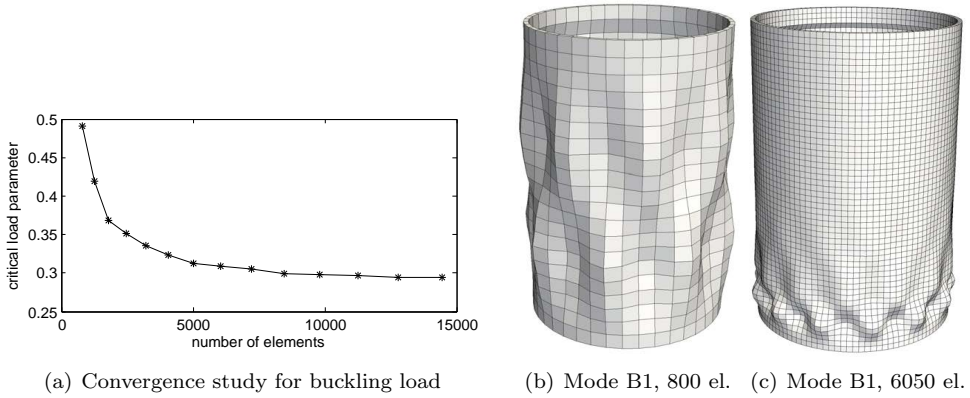


Figure 8.3: Buckling loads and modes of the perfect structure

8.4.2 SVD of pseudo load matrix

The pseudo load matrix is also computed at the load level λ_c and is decomposed by singular value decomposition. The corresponding singular value distribution is pictured in Figure 8.4a for a mesh with 6050 elements. The first and last data points are marked with a star. As one can recognize, some first right singular vectors as inputs have an extraordinary impact on outputs. The first singular vectors are pictured for different meshes in Figure 8.4b-c. These modes show the same mesh dependency as the buckling modes in Figure 8.3b-c.

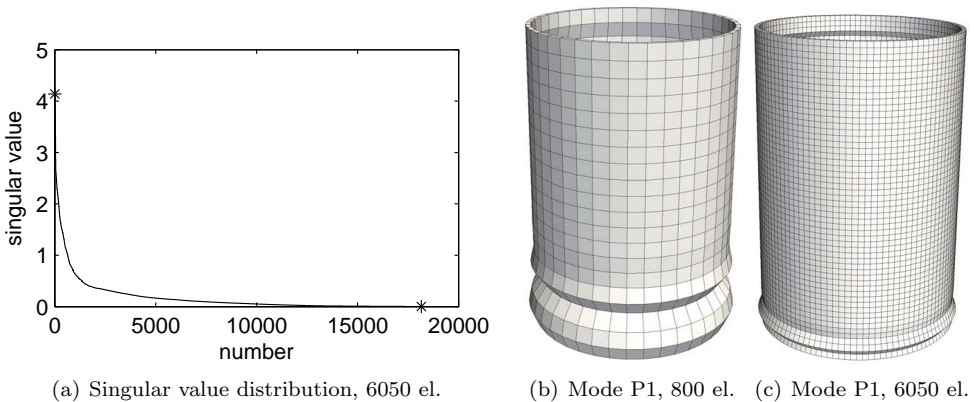


Figure 8.4: Singular value decomposition of the pseudo load matrix

8.4.3 Analysis of the imperfect structure

The buckling mode B1 pictured in Figure 8.3c, the first singular vector P1 pictured in Figure 8.4c and the second vector P2 are scaled to a certain amplitude and applied as imperfections to the cylinder. The corresponding imperfect structures are analysed again and the critical load parameters are computed. For amplitudes $0 \leq a \leq \frac{h}{200}$ the corresponding critical loads λ_c are pictured in Figure 8.5a.

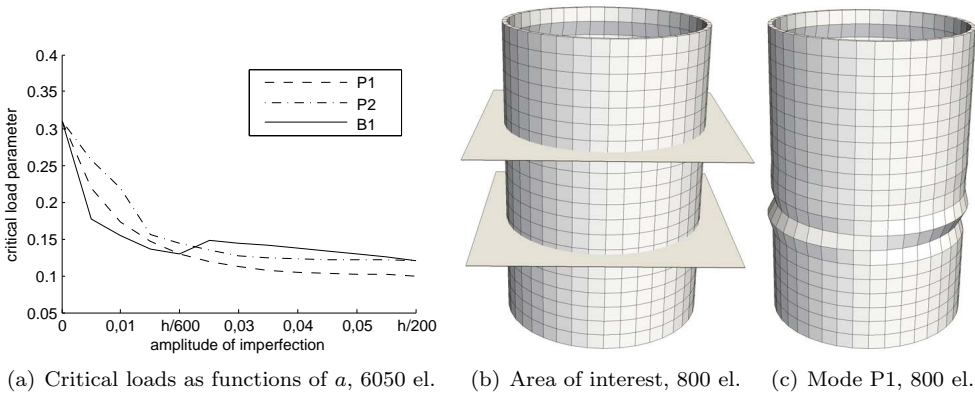


Figure 8.5: Properties of SVD based imperfections

These curves result from parameter studies and should not be confused with convergence plots. As one can see, buckling mode $B1$ provides ‘worst case’ imperfection for amplitudes $0 \leq a \leq \frac{h}{600}$. If the amplitude is $a \geq \frac{h}{600}$, vectors $P1$ and $P2$ are the better choice to create imperfections.

The main result of this study is that right singular vectors of the pseudo load matrix are suitable to create imperfections. Following this idea, it is possible to generate the ‘worst’ imperfections of only some parts of a structure.

For example, we consider the area of the cylinder between the planes in Figure 8.5b. The ‘worst case’ imperfection of this area is pictured in Figure 8.5c and is determined as the first right singular vector of the modified pseudo load matrix \bar{P} corresponding to equation (8.9).

8.5 Summary and concluding remarks

The pseudo load matrix evaluated at the critical load level contains full sensitivity information which can be analysed and interpreted using its singular value decomposition. This matrix defines an input-output system with changes in design as input

and distortions in equilibrium as output quantities. The most significant modes can be identified and used as imperfections for nonlinear buckling analysis. In contrast to buckling modes, it is possible to analyse the ‘worst’ imperfections of only some parts of a structure and of design parameters like thickness. For this reason the pseudo load matrix is transformed employing design velocity fields known in shape optimisation. Despite of using SVD the numerical effort for such modes is comparable with the computation of buckling modes since only some first singular values and vectors are computed. Furthermore, pseudo load matrix is sparsely populated and the corresponding algorithms can be utilised.

The proposed techniques are implemented in *MATLAB* based *structural optimisation program* (SOP). Here, different kinds of design velocity fields are available for structural optimisation purposes and can be utilised to transform the pseudo load matrix for structural stability analysis.

9 Model reduction based on SVD of sensitivity information

A model reduction technique for structural optimisation problems is presented in this chapter. It is based on the singular value decomposition (SVD) of the pseudo load and sensitivity matrices. The corresponding optimisation algorithm is outlined.

9.1 Introduction

The simulation and optimisation of real-world problems induce a high demand on computer power. Hence, the need for model reduction (also called *approximate models*, *surrogate models*, *meta models* or *response surface models*) arises. Numerous approaches to reduce the dimension of the problem have been developed.

9.1.1 State of the art

The *analysis approximation methods* reduce the number of degrees of freedom of the analysis model by means of transformations (projections) into a lower dimensional space to speed up structural analysis. These methods are often used to analyse large-scale dynamical systems or time dependent models. Here, the SVD-based, the Krylov-based and the SVD-Krylov-based approximation methods are known, see [16].

The *optimisation approximation methods* tackle the optimisation problem and replace the original one by an approximation, which is easier to solve. In general, the number of design variables is reduced. Here, two categories of approximations can be highlighted. *Local approximations* are significant in the neighbourhood of the considered point and *global approximations* are valid for the whole space or large areas of it, see [22] for an overview. The disadvantage of all mentioned approximation methods is the lack of sufficient *training data*. This central *matrix of snapshots* requires multiple evaluations of the original problem and is computationally very expensive. This

problem is increased with the number of design variables, e.g. especially in topology optimisation and nodal based shape optimisation. A great number of training vectors is necessary to achieve a model with sufficient approximation accuracy. The method proposed in this chapter requires neither the matrix of snapshots nor training vectors.

9.1.2 Special features of the presented research

The pseudo load matrix and the sensitivity matrix dominate design sensitivity analysis of shape optimisation problems. They describe how a structure reacts on an imposed design modification. These matrices are commonly used to derive and to calculate the gradients of objective functions and of constraints. Pseudo load and sensitivity matrices are analysed for the model problem of morphing based shape optimisation by a singular value decomposition (SVD). It is demonstrated that these matrices contain additional valuable information, which is not yet used either in theory or algorithms for shape optimisation. To formulate reduced quadratic sub-problems within the *sequential quadratic programming* (SQP) approach, the information on the inner structure of the sensitivities is used. Similar techniques are proposed by the author in [66] for nodal based shape optimisation and in [63] for topology optimisation.

9.2 Inner structure of shape sensitivities

To derive sensitivity relations for arbitrary objective functions and constraints, the pseudo load matrix \mathbf{P}_T and the sensitivity matrix \mathbf{S}_u must be calculated, see chapter 6. These matrices are usually calculated with respect to coordinates of all FE-nodes $\hat{\mathbf{X}}$ as design variables. In this case, the highest degree of freedom for design changes is considered. Such design space is, for example, considered in *FE-node based* or also called *parameter-free* shape optimisation, see [32, 119, 93, 66]. In context of morphing based shape parametrisation, the concept of, so called, *design velocity fields* well-known in shape optimisation, see chapter 3 and 4, is utilised to calculate the pseudo load matrix $\bar{\mathbf{P}}_T$ and the sensitivity matrix $\bar{\mathbf{S}}_u$ with respect to free coordinates of control points \mathbf{w} as design variables. Following this concept, a map is defined

$$\hat{\mathbf{X}} = \Phi(\mathbf{w}) \quad \text{with} \quad \Phi : \mathbb{R}^s \longrightarrow \mathbb{R}^m, \quad (9.1)$$

where the coordinates of FE nodes are functions of s free coordinates of control points \mathbf{w} . Utilising the chain rule we obtain the desired matrices

$$\begin{aligned} \bar{\mathbf{P}}_T &= \mathbf{P}_T \frac{d\hat{\mathbf{X}}}{d\mathbf{w}} = \mathbf{P}_T \mathbf{\Psi} \quad \text{with} \quad \bar{\mathbf{P}}_T \in \mathbb{R}^{n \times s}, \\ \bar{\mathbf{S}}_u &= \mathbf{S}_u \frac{d\hat{\mathbf{X}}}{d\mathbf{w}} = \mathbf{S}_u \mathbf{\Psi} \quad \text{with} \quad \bar{\mathbf{S}}_u \in \mathbb{R}^{n \times s}. \end{aligned} \quad (9.2)$$

Here, the quantity $\mathbf{\Psi} \in \mathbb{R}^{m \times s}$ is called design velocity fields matrix, where the i -th column is the velocity field for the variable w_i . We note that design velocity fields

usually reduce the number of variables, which is beneficial for the numerical effort of the utilised SVD. In contrast to the concept presented by the author in [63], the number of design variables does not depend on the chosen discretisation. Hence, the optimised shapes are FE-mesh independent. Numerical defects like mesh distortions and jagged boundaries do not appear due to morphing based design parametrisation. Next up, a simple example of shape optimisation is introduced, which is used for the SVD based exploration of sensitivity information in this section.

9.2.1 Example: uniaxial strained shell

The compliance of the structure pictured in Figure 9.1 is to be minimised considering a constant volume constraint. The dimensions of the structure (width and depth) are $a = 200$ and $b = 100$. The thickness $t = 0.3$ must remain constant during the optimisation. The material properties are Young's modulus $E = 21000$ and Poisson's ratio $\nu = 0.3$. The load $\bar{q} = 1/20000$ is a surface load. The applied boundary conditions are pictured in Figure 9.1a. The finite element mesh consists of 800 elements and 1722 nodes with 5166 degrees of freedom. A morphing box is defined by 400 control points and is pictured in Figure 9.1b. Vertical positions (z coordinates) of 144 control points, which are marked red, are used as design variables.

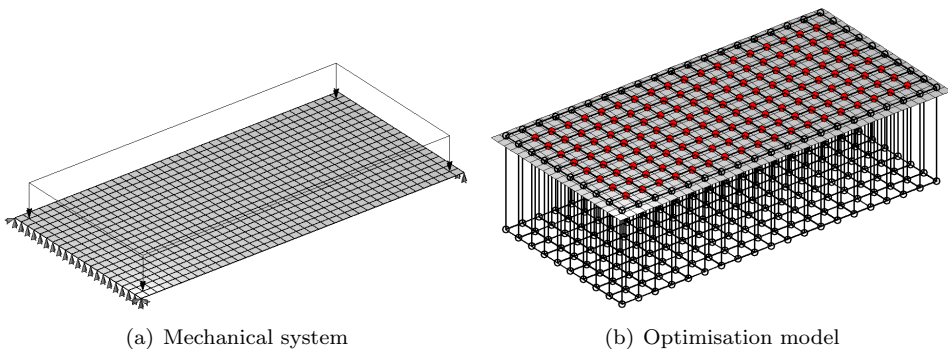


Figure 9.1: Uniaxial strained shell: initial structure

The large number of control points ensures a high degree of freedom for design changes. A reasonable model reduction technique should preserve this property and can not be based on a model with less control points.

9.2.2 SVD of the sensitivity matrix

The sensitivity matrix $\bar{\mathcal{S}}_u$ is computed for the initial design of the structure pictured in Figure 9.1. The columns j are the variations of the displacement field with respect

to a variation of the design variable w_j . They are local changes in the displacement field and are ordered according to the node numbers. Singular value decomposition provides an enhanced interpretation of the sensitivity matrix

$$\bar{\mathbf{S}}_u = \mathbf{Y}\mathbf{\Sigma}\mathbf{Z}^T \quad \text{with} \quad \mathbf{Y} \in \mathbb{R}^{5166 \times 5166}, \quad \mathbf{\Sigma} \in \mathbb{R}^{5166 \times 144}, \quad \mathbf{Z} \in \mathbb{R}^{144 \times 144}. \quad (9.3)$$

The right singular vectors (inputs) can be interpreted as design modes (shape modes) and the left singular vectors as the corresponding displacement responses (outputs). The singular values of $\bar{\mathbf{S}}_u$ are pictured in Figure 9.2. These values can be used to identify such design modes, which effect global changes in displacement field. One can recognize, that about five first design modes have an extraordinary impact on the displacement field. To give an example, the first design mode and the corresponding perturbation in displacements are pictured in Figure 9.3a and b.

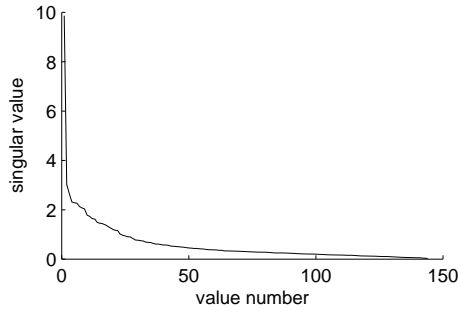


Figure 9.2: Uniaxial strained shell: singular value distribution of $\bar{\mathbf{S}}_u$

From mechanical point of view, design changes pictured in Figure 9.3a stiffen the structure and the displacements are decreased as shown in 9.3b. Singular values with numbers in the range about 5 – 50 are much smaller than the first five, but they distinctly differ from zero.

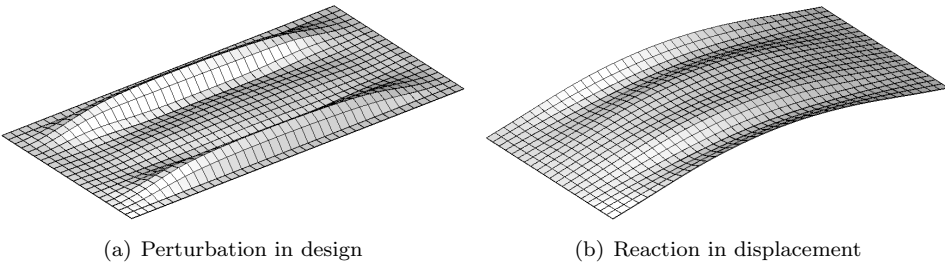


Figure 9.3: Uniaxial strained shell: the first left and right singular vectors of $\bar{\mathbf{S}}_u$

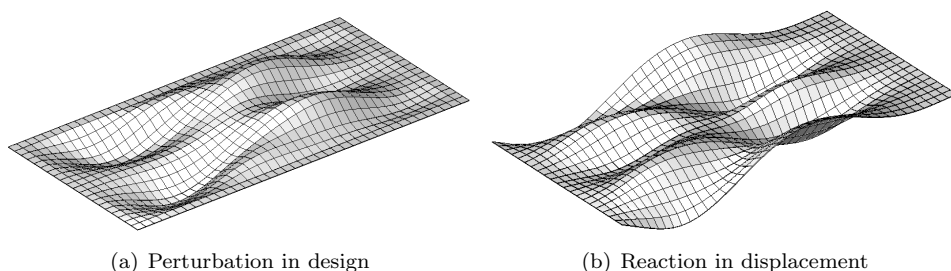


Figure 9.4: Uniaxial strained shell: the 14th left and right singular vectors of $\bar{\mathbf{S}}_u$

The corresponding design modes are also smooth ones, but they can not be interpreted from mechanical point of view. One representative of this group is pictured in Figure 9.4a with its displacement response in 9.4b. The rest of the design modes represent high oscillating changes in design which are meaningless. For example, the design mode 100 and the corresponding displacement mode are pictured in Figure 9.5.

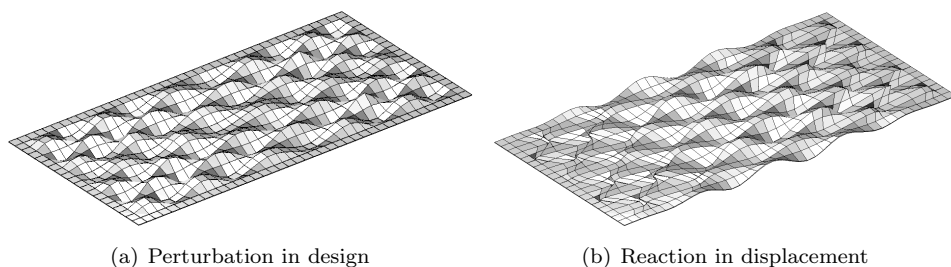


Figure 9.5: Uniaxial strained shell: the 100th left and right singular vectors of $\bar{\mathbf{S}}_u$

These modes can be neglected in an optimisation process. Hence, the valuable parts of the sensitivity matrix $\bar{\mathbf{S}}_u$ are extracted using the singular value decomposition.

9.2.3 SVD of the pseudo load matrix

The interpretation of the pseudo load matrix $\bar{\mathbf{P}}_T$ and its SVD is very similar to that of $\bar{\mathbf{S}}_u$, see [66]. Hence, only some remarks are given in this section and details are omitted. The column vectors j of matrix $\bar{\mathbf{P}}_T$ describe the changes of the physical residual \mathbf{R} as a response to the perturbation in design variable w_j . SVD of the pseudo load matrix can be utilised to identify shape modes, which have an extraordinary impact on physical residual. Compared with the distribution of the singular values of the sensitivity matrix, the singular value distribution of the pseudo load matrix can not be separated in regions with high and small values. The curve is usually

monotonically decreasing. The corresponding shape modes look very similar to those pictured in figures 9.3, 9.4 and 9.5, but they are arbitrary distributed over the whole spectrum. They are sorted according to their impact on the physical residual.

9.3 Shape optimisation based on SVD

Model reduction presented in this chapter is based on the idea of using right singular vectors from SVD of the sensitivity matrix or of the pseudo load matrix as shape modes within the shape optimisation procedure. For this reason a subset of these modes is chosen and changes in design of the structure are described as linear combination of them. The corresponding scaling factors are used as design variables in the modified optimisation procedure.

9.3.1 Selection of shape (design) modes

The singular value decomposition of pseudo load matrix or of the sensitivity matrix provides a set \mathbf{Z} of shape modes, which can be used to minimise any objective function J . Singular values of this decomposition indicate modes that influence either the physical residual or the displacement field most of all.

In case of compliance minimisation the objective function is directly related to the displacement field because minimising the compliance is equal to maximising the stiffness of the structure, which is similar to reducing the global deformation (displacements) of the structure. Here, SVD of the sensitivity matrix is beneficial. The corresponding singular values can be used to identify some shape modes, which have an extraordinary impact on the compliance.

Arbitrary objective functions. Considering an arbitrary objective function $J(\mathbf{w})$ with $\mathbf{w} \in \mathbb{R}^s$ and an arbitrary set of shape modes $\mathbf{Z} \in \mathbb{R}^{s \times s}$ some kind of indicators \bar{c}_i with $i = 1, \dots, s$ are needed to select a suitable subset of shape modes. Such indicators are derived as total derivatives of the objective function with respect to the scale factors α_i of shape modes, i.e.

$$\bar{\mathbf{c}} = \frac{dJ}{d\boldsymbol{\alpha}} = \left(\frac{\partial J}{\partial \mathbf{w}} \right) \frac{d\mathbf{w}}{d\boldsymbol{\alpha}} = \left(\frac{\partial J}{\partial \mathbf{w}} \right) \mathbf{Z}, \quad \text{with } \mathbf{w} = \mathbf{Z}\boldsymbol{\alpha}. \quad (9.4)$$

Only absolute values $c_i = |\bar{c}_i|$ should be used as indicators because the sign of singular vectors is not unique. The desired subset $\tilde{\mathbf{Z}}$ of shape modes is obtained by means of the Boolean reduction matrix $\mathbf{B} \in \mathbb{R}^{s \times l}$ with $\tilde{\mathbf{Z}} = \mathbf{Z}\mathbf{B}$. The number of shape modes l to be selected is prescribed by the user. Note, the matrix \mathbf{B} picks those modes which correspond to indicators with the largest values.

Consideration of constraints. Pseudo load matrix and sensitivity matrix do not contain information about constraints. The corresponding shape modes are not necessarily suitable to take into account constraints. General constraints $h_j(\mathbf{w}) \leq 0$ with $j = 1, \dots, m$ are isolines and isosurfaces of the function, which are controlled and they describe the boundary of the design space. These boundaries are exceeded if the constraints are injured. The mathematical optimiser must be able to find the feasible design space. The gradients of constraints ∇h_j with respect to the design variables are orthogonal to the isolines and isosurfaces of the corresponding constraints representing the shortest way to the feasible design space. Hence, it must be possible to express the gradients of constraints as linear combination of the selected shape modes. In the other case, the new basis vectors must be supplemented with the gradients of constraints as follows

$$\bar{\mathbf{Z}} = \begin{bmatrix} \nabla h_1 & \cdots & \nabla h_m & \tilde{\mathbf{Z}} \end{bmatrix}. \quad (9.5)$$

Here, the gradients of constraints should be normalised as the singular vectors are orthonormal ones. Equality constraints are considered in the same way.

9.3.2 Modified optimisation procedure

We perform a coordinate transformation introducing new design variables $\boldsymbol{\kappa} \in \mathbb{R}^{l+m}$, which are scaling factors of the design modes. This transformation reads

$$\mathbf{w} = \bar{\mathbf{Z}}\boldsymbol{\kappa} \quad \text{with} \quad \bar{\mathbf{Z}} \in \mathbb{R}^{s \times (l+m)}. \quad (9.6)$$

The first derivative of this equation with respect to the new variables is the matrix $\bar{\mathbf{Z}}$. Utilising the chain-rule all derivatives which are needed for the mathematical optimiser can be calculated with respect to the new variables, i.e.

$$\frac{d(\bullet)}{d\boldsymbol{\kappa}} = \frac{d(\bullet)}{d\mathbf{w}} \bar{\mathbf{Z}}. \quad (9.7)$$

Several strategies for applying a model reduction are useful. SVD can be applied in each and every iteration or only at one or few specially chosen situations. An optimisation procedure based on SVD is pictured in Figure 9.6. Here, SVD is performed in each n -th iteration.

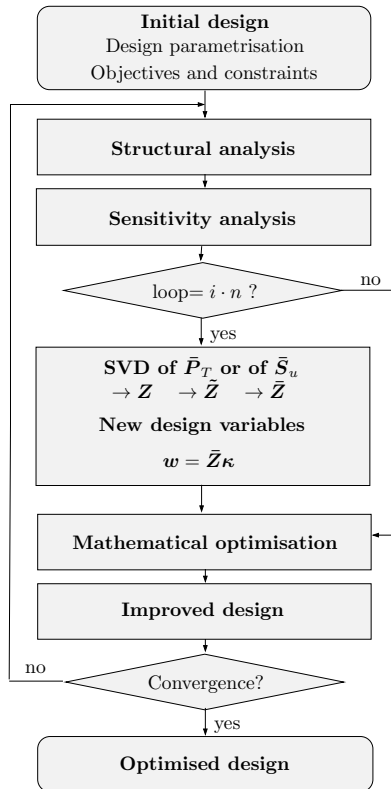


Figure 9.6: Optimisation procedure based on SVD

Variable i denotes an integer value with $i \geq 0$. We notice that it is possible to use SVD of the pseudo load matrix or of the sensitivity matrix to generate shape modes. Furthermore, new initialisation of the BFGS approximation of the Hessian matrix must be performed after each computation of new basis vectors.

9.4 Example: uniaxial strained shell - continued

The compliance of the structure pictured in Figure 9.1 is to be minimised considering a volume constraint. A volume increase of only 5% is allowed. SVD based algorithm presented in Figure 9.6 is utilised. SVD of the sensitivity matrix is performed in each 5th iteration to generate shape modes. Modes, which correspond to largest singular values are selected. Volume gradient is added to the basis vectors to take the constraint into account. Utilising all right singular vectors of sensitivity matrix as shape modes only coordinate transformation takes place and the optimisation results are the same as using the standard optimisation procedure, see Figure 9.7a.

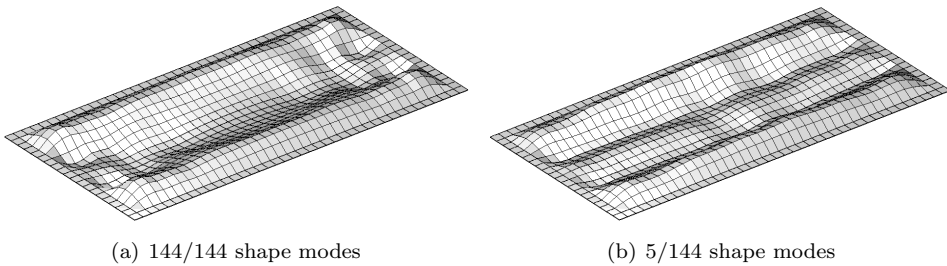


Figure 9.7: Uniaxial strained shell: optimised structure

Model reduction is performed selecting only 5 modes out of 144 ones. The corresponding optimised structure is pictured in Figure 9.7b. It is very interesting to observe that using only about 4% of all possible modes, reasonable results are achieved. Compliance values and compliance decreases with the corresponding errors are summarised in Table 9.1 for different model reduction grades.

Table 9.1: Uniaxial strained shell: compliance after the 40th iteration

number of modes (·)/144	compliance C	compliance decrease C_{diff}	relative error %
5	0.01288	6.6376	0.0286
11	0.01255	6.6380	0.0236
50	0.01233	6.6382	0.0203
144	0.01098	6.6395	0

9.5 Summary and concluding remarks

Singular value decomposition is a tool to sort out great amount of information, which is packed in matrices. It gives the possibility to separate important and unimportant parts of information and provides statements about the influence of model variables on the content of information. For some problem definitions model reduction can be carried out in this way.

The presented SVD based structural optimisation algorithm is developed to demonstrate the information content of quantities which appear in sensitivity analysis and to explore these quantities by means of SVD. Of course, the numerical performance of the algorithm is not optimal for general cases. But in contrast to the approach presented by the author in [66], the second dimension of the pseudo load matrix and of the sensitivity matrix does not depend on the considered finite element mesh. This

dimension corresponds to the number of design variables and can be set up by design engineer. Hence, the effort for SVD depends only on the utilised design description, morphing boxes, for example. For some objectives only the computation of some first singular vectors and values of the sensitivity matrix is necessary, see for example the example in section 9.4. In such cases the generalised singular value decomposition can be utilised to save the storage space and the computational time. See chapter 7, section 7.3 for more details on this topic.

It depends on the considered objective function which matrix should be decomposed by SVD to generate shape modes. The objective function must be interpreted from mechanical point of view and the choice must be made if pseudo load matrix or the sensitivity matrix is to be used. An example where shape modes of both matrices are compared is presented by the author in [66]. The handling of stress constraints is also demonstrated by an example in the mentioned contribution.

The proposed model reduction techniques are implemented in *MATLAB* based *structural optimisation program* (SOP). Shape modes based on SVD of pseudo load matrix and of sensitivity matrix can be selected utilising different kinds of indicators.

10 SVD based design exploration

This chapter is concerned with the exploration of the FE model and of the corresponding design description. Based on singular value decomposition of sensitivity information, interactive tools are derived which facilitate the definition of a structural optimisation problem.

10.1 Introduction

For different kinds of application algorithmic treatment of SVD based sensitivity information is presented in chapter 8 and chapter 9. The corresponding implementation provides *black box* like programs, which require the input of only some parameter values by the user. The optimisation model is considered to be given and all necessary conditions are prescribed and predefined. Techniques which deal with the solution of a given structural optimisation problem only can be improved with respect to their numerical effort, required storage space, convergence speed and computational time.

However, the process of definition of a structural optimisation problem is human controlled and is based on his/her experience and knowledge. Within this process decisions which tackle the kind of design parametrisation, the type and number of design variables and relations between these variables have an extraordinary impact on the quality of optimisation results, on the solubility of the problem and on the corresponding computational effort. The exploration of structural design is utilised to facilitate and substantiate these decisions.

10.1.1 State of the art

In the field of architecture, the exploration of design is outlined in [86] and [61]. Within computational differential geometry, design exploration is utilised to navigate in subspaces of the shape space of constrained meshes, see [150]. In context of software development, an approach for design space exploration was proposed in [84]. Concept

exploration and selection are presented in [101] under a multiobjective optimisation framework in context of product development.

Exploration of the structural design is directly related with topics like *robustness*, *uncertainty* and *reliability analysis*, where sensitivity of structural response with respect to some model parameters is analysed. The aim of uncertainty analysis, see [47, 85], is to show that the considered structure is not sensitive with respect to tolerances of load positions, values and directions, support positions and types, material properties and geometrical quantities. Within robustness analysis, which is reviewed in [109, 46, 138], different load cases are considered. Reliability, as outlined in [113, 140, 37], describes structural safety in the presence of design changes. Techniques presented in this chapter could also be useful within robustness, uncertainty and reliability analysis.

Structural design exploration tools are available in *ANSYS* [2], *AVL* [4] and *BOEING* [5] software environments. They are based on *response surfaces* [128, 83], *meta models* [143, 129], and techniques from the field of *design of experiments* [118]. A recent work on the exploration of the structural design in an aircraft conceptual perspective is [106]. The definition of the optimisation problem is tackled and adaptive formulation of functional and design variable constraints is proposed. This allows the exploration of further promising solutions initially not contained in the feasible design set. Multi objective design exploration for aerodynamic configurations is proposed in [107]. Investigations presented in this chapter highlight the information which has not been used so far in all mentioned algorithms and approaches.

10.1.2 Special features of the presented research

Within this chapter techniques, which facilitate the definition of a structural optimisation problem are presented. These techniques are derived from methods, which are well known in the scope of statistics as well as of applied sciences and are especially based on *principal component analysis*, *factor analysis* and the computation of *variance* and *correlation*, see [41] for more details on this topic.

The above mentioned concepts like response surfaces, meta models and design of experiments require repeated evaluations of objectives, constraints and structural response. The numerical effort increases with the number of design variables as for each variable structural analysis is performed several times. Within this chapter the exploration of design is based on sensitivity information. Structural and the corresponding sensitivity analysis are performed only once at the beginning of exploration.

Usually, exploration of design only tackles the definition of design variables, comparison of different design variants and the numerical effort. In addition, sensitivity based exploration of design space, which is outlined in this chapter, is also able to

detect numerical defects like the appearance of jagged boundaries, mesh distortions and physically meaningless changes in thickness.

Further, not only predefined design descriptive variables are considered, but also the full space of all possible design variants is explored, which is possible considering the coordinates of FE-nodes as design variables.

10.2 A structural optimisation assistant

A software assistant or expert system is a graphical user interface with the objective of supporting a user with a sequence of dialogue boxes leading the user through a series of well-defined steps. During this process the user is provided with carefully condensed information to facilitate his/her decisions. Complex tasks might be easier performed using an assistant. In this section a structural optimisation assistant is presented to support the design engineer during the definition of the optimisation problem. The flow chart of the proposed assistant is pictured in Figure 10.1.

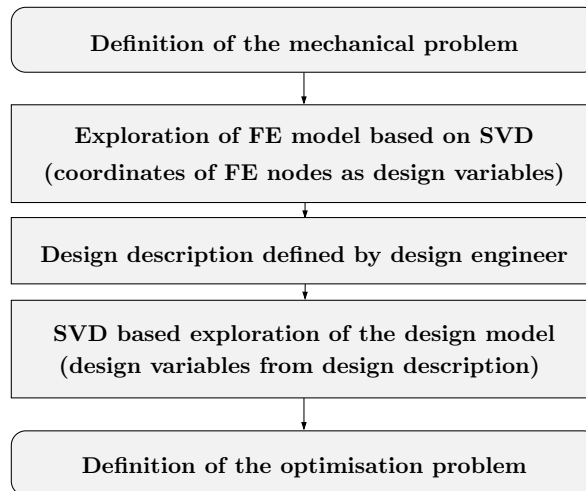


Figure 10.1: Flowchart of SVD based design exploration

In following, the items of this flowchart are explained in detail.

Mechanical problem definition. The definition of a structural optimisation problem requires the formulation of mechanical model. In context of finite element method the kind of boundary value problem, the type of analysis and some technology parameters must be chosen. For example, it has to be decided if elasticity or plasticity theory

should be used, whether the mechanical behaviour does depend on time or not, if the influence of temperature must be considered. Finite element mesh is created, material parameters and boundary conditions are prescribed. The formulated mechanical problem is analysed with respect to plausibility, accuracy and discretisation errors. If necessary, the finite element mesh is refined.

SVD based FE model exploration. Structural response is usually observed considering the displacements, stresses and strains of the deformed model. The design engineer requires information about the sensitivity of these response fields with respect to changes in shape and other parameters of the structure to explore the model. It is well known from FE node based shape optimisation, see for example [32], that maximum design freedom is obtained if coordinates of FE nodes are used as design variables. Utilising such design variables, sensitivity matrices and pseudo load matrices are computed for the initial structure. These matrices contain the desired sensitivity information. Techniques like principal component analysis (PCA), factor analysis (FA) and singular value decomposition (SVD), which are widespread in statistics, are used to analyse this great amount of information. Perturbations of model parameters like thickness, structural shape, support and loading positions with high potential to change the mechanical behaviour of the model, can be detected and explored. In section 10.3 this topic is discussed in detail.

Design description. Parametrisation of design is performed based on observations, which are done exploring the FE model. Parts of the structure, which potentially have high influence on objectives and constraints are considered. The kind of parametrisation is chosen. For this reason techniques from CAD, morphing or FE node based parametrisation are utilised. Details on this topic are presented in chapter 3 and 4.

SVD based design exploration. A large number of parameters, which describe the design of the structure can appear for real world applications. Such parameters can be radii of circles, lengths, widths, heights and thicknesses of structural parts, coordinates and weights of control points, which define NURBS. Within the morphing based parametrisation, the coordinates of control points, which define the morphing boxes are used as design variables. Their number has an extraordinary influence on possible design variations. Also in this situation, the design engineer needs some information about the sensitivity of structural response with respect to design describing parameters. In this case, the sensitivity matrices and the pseudo load matrices are calculated with respect to design parameters. Utilising SVD and other statistical methods, these matrices are analysed and the design model is explored. In addition, the SVD of velocity fields matrices can be helpful to explore the design space. If necessary, the design description can be refined or coarsened. A detailed discussion on this topic is presented in section 10.4.

Optimisation problem definition. Based on observations exploring the design, the definition of optimisation problem can now be finalised. Therefore, some design descriptive parameters are chosen as design variables. Bounds for these variables are defined. If necessary, some relations between design variables are formulated in addition to the original objectives and constraints to enforce symmetry or producibility and to avoid mesh distortions. Such optimisation problem is then solved by a general structural optimisation procedure which is, for example, introduced in chapter 3.

10.3 FE model exploration

FE model exploration is motivated in the previous section. The design engineer is supported by a structural optimisation assistant, which evaluates the great amount of sensitivity information for the initial structure and extracts the significant factors and effects. Based on the observations exploring the FE model, the design engineer can choose the kind of design parametrisation.

Within this section only shape changes are considered as design modifications. Only the displacements sensitivity matrix is analysed. Application of the proposed techniques to pseudo load matrix and to stress sensitivity matrix is straight forward and details are omitted. Using the example of a cantilever shell, which is pictured in Figure 10.2a, FE model exploration is explained.

10.3.1 Cantilever shell: FE model

The compliance $J := C := -\Pi$ of the structure, which is pictured in Figure 10.2a has to be minimised taking a volume constraint $V = 1.05 V_0$ into account. Here, the quantities V and V_0 denote the current and initial volumes.

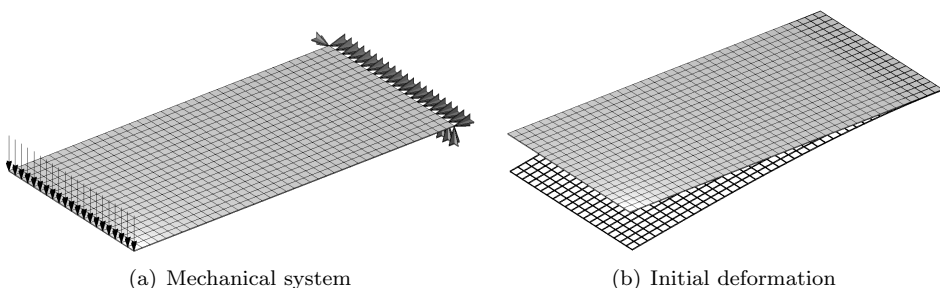


Figure 10.2: Cantilever shell: initial structure

The dimensions of the structure (length and width) are $l = 200$ and $w = 100$. The shell thickness is $t = 0.5$. The material properties are Young's modulus $E = 21000$

and Poisson's ratio $\nu = 0.3$. The load $\bar{q} = 0.002$ is a line load. All finite element nodes on the right side of the structure are fixed in all three directions. The applied boundary conditions are pictured in Figure 10.2a. The finite element mesh consists of 800 elements and 1722 nodes with 5166 degrees of freedom. The initial deformation of the structure is pictured in Figure 10.2b. Due to the low stiffness, the structure is very sensitive with respect to changes in shape. Another advantage of this example is the simple geometry, which allows to present pictorial material using as little as possible images.

10.3.2 Inner structure of the sensitivity matrix

To begin with the exploration of the FE model, the coordinates x , y and z of all finite element nodes are considered as design variables. Only the loaded nodes, x and y coordinates of fixed nodes are excluded from the set of design variables. Such variables enable maximum possible design freedom, as it is known from FE node based shape optimisation, see [32]. The displacements sensitivity matrix is calculated with respect to the mentioned variables. Singular value decomposition of this matrix is performed. Right singular vectors are interpreted as perturbations in design and the corresponding left singular vectors represent reactions in displacements. The first right singular vector (mode) for the considered example corresponds to the largest singular value and is pictured in Figure 10.3a. This mode represents thickness changes, which correlate with the moment curve of the structure. Such changes would stiffen the structure and can be interpreted from mechanical point of view.

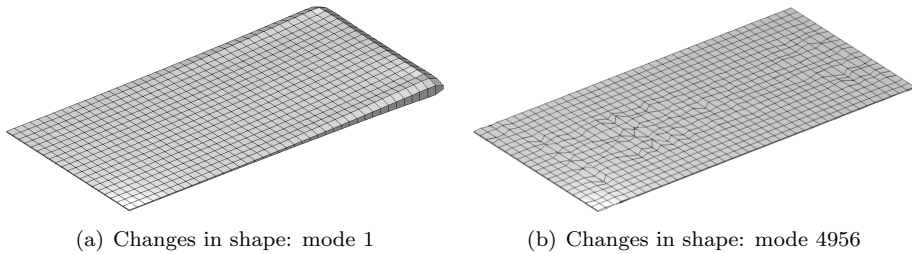


Figure 10.3: Cantilever shell: SVD of sensitivity matrix, where all coordinates of top and bottom finite element nodes are considered as design variables.

The last shape mode corresponds to singular value, which is zero and is pictured in Figure 10.3b. Zero value means that this mode does not have any influence on displacements. As one can recognize, mesh distortions are represented by this mode. These mesh distortions are mainly in the plane of the shell. It is also a well known fact in context of FE node based shape parametrisation. To avoid such problems a so called *in-plane regularisation* is utilised in [32]. The singular value distribution of the considered sensitivity matrix is pictured in Figure 10.4a. From about five thousand

singular values only few ones are significantly greater than zero. That means that the huge design space is described by variables with very slow variance and that a great number of shape changes exists not influencing on the structural response.

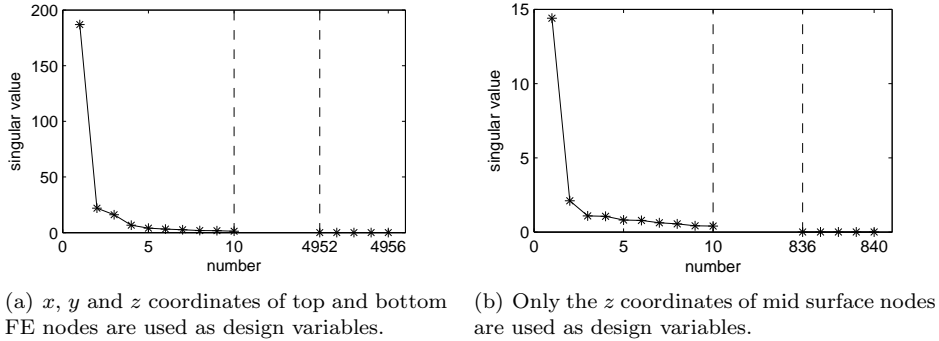


Figure 10.4: Cantilever shell: singular value distribution of sensitivity matrix for different choices of design variables.

Based on the above observations and due to some producibility criteria, the design engineer decides to enforce a constant shell thickness during the optimisation. For this reason a mid surface of the shell is created and coordinates of the corresponding mesh nodes are used as design variables. To exclude in-plane mesh distortions, the design engineer decides to use only the z coordinates of mid surface nodes as design variables. For this new set of design variables the sensitivity matrix is computed. We note that only a transformation of the previous sensitivity matrix is necessary. The modified sensitivity matrix is decomposed utilising SVD and steps described before are repeated. The corresponding singular value distribution is pictured in Figure 10.4b. This distribution is very similar to the previous one, but the design space is now described by six times less variables. Some first shape modes have an extraordinary impact on structural response as indicated by the first few singular values. Nevertheless, the chosen variables also have very slow variance, which can be observed considering the rest singular values near zero. The first shape mode is pictured in Figure 10.5a and represents changes in design, which would increase structural stiffness concurrently keeping the thickness constant. The last shape mode is pictured in Figure 10.5b and represents jagged boundaries. Such effect is also well known in FE node based shape optimisation and is usually prevented utilising, so called, *out-of-plane* regularisation techniques like filters, see [32, 66]. Another way to avoid problems mentioned above is to use CAGD or morphing based shape parametrisation techniques, see chapter 3.

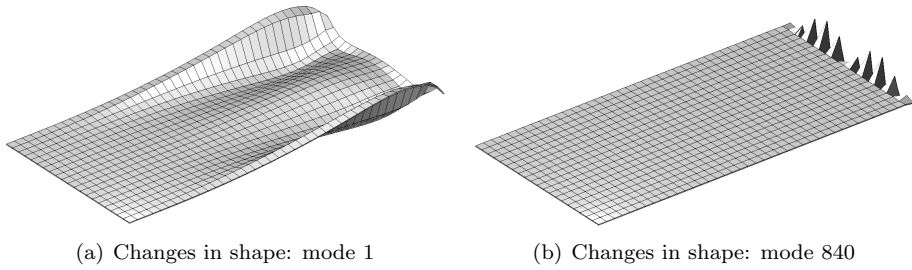


Figure 10.5: Cantilever shell: SVD of sensitivity matrix where z coordinates of mid surface nodes are considered as design variables.

10.4 Design exploration

Based on the above observations the design engineer decides to utilise morphing based shape parametrisation, see chapter 4, to restrict the design space, to obtain smooth solutions and to reduce the number of design variables.

10.4.1 Cantilever shell: design model

To parametrise the shape of the structure, the design engineer creates two similar morphing boxes with different numbers of control points (CPs). These boxes are pictured in Figure 10.6. Only vertical positions of red marked control points are utilised as design variables to avoid mesh distortions.

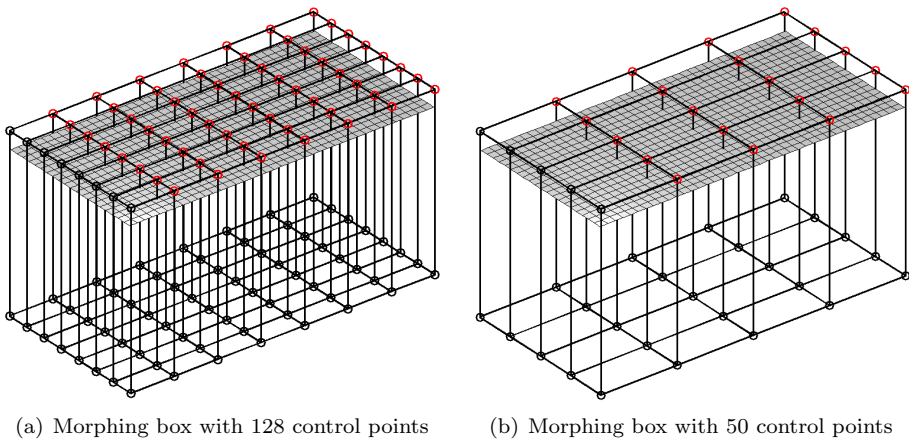


Figure 10.6: Cantilever shell: morphing based design description.

Again, coordinates of mid surface nodes are introduced and are controlled by the morphing box to enforce a constant thickness. Positions of finite element nodes are then defined as functions of mid surface node coordinates.

10.4.2 Inner structure of the transformed sensitivity matrix

Both models in Figure 10.6 are compared by means of SVD based design exploration. The model in Figure 10.6a consists of 128 CPs but only z coordinates of 56 CPs are used as design variables. The corresponding sensitivity matrix is obtained transforming the previous one with respect to the new design description. Right singular vectors represent now perturbations in design (in control point positions) and can be transformed to shape changes (changes in coordinates of finite elements). Shape changes which correspond to the first and the last modes are pictured in Figure 10.7.

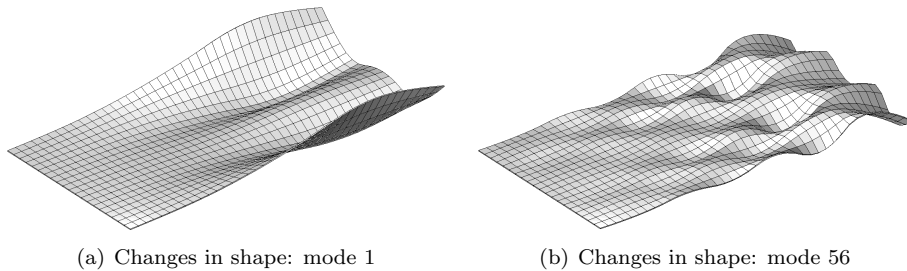


Figure 10.7: Cantilever shell: SVD of sensitivity matrix where z coordinates of control points are considered as design variables. Model with 128 CPs.

Here, the first mode represents a smooth modification of the shape, which preserve the constant thickness and which increases the global structural stiffness. The mode number 56, pictured in Figure 10.7b is also a smooth one and mesh distortions with jagged boundaries do not appear here. The presented shape changes consist of high oscillating shell parts. The last SVD modes usually represent the smallest possible wavelengths of design perturbation and indicate how fine the details of the optimised structure can be. The corresponding singular value distribution is pictured in Figure 10.8a. We notice that much more singular values are now significantly greater than zero compared to the case of using coordinates of finite element nodes as design variables. Nevertheless, a great number of design modifications exist without influence on structural response, as it is indicated by the rest of singular values. Next up, the sensitivity matrix for the model, which is pictured in Figure 10.6b is computed. It consists of only 20 design variables, which are the vertical positions of the red marked CPs. The corresponding singular value distribution is presented in Figure 10.8b.

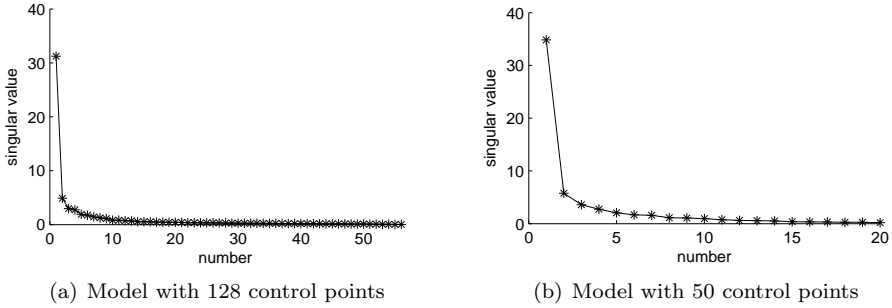


Figure 10.8: Cantilever shell: singular value distribution of sensitivity matrix where z coordinates of control points are used as design variables.

As one can recognize, only about a quarter of singular values are near zero. That means that the chosen variables have great variance on the structural response. We notice that there are only 20 variables. The first shape mode is pictured in Figure 10.9a. This mode shows high correlation with the mode presented in Figure 10.7a but it is not so detailed.

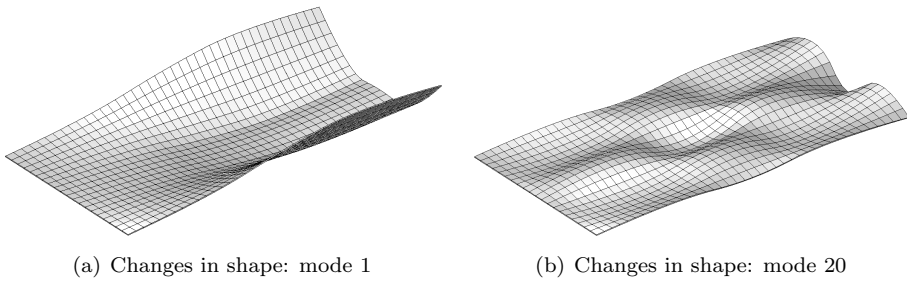


Figure 10.9: Cantilever shell: SVD of sensitivity matrix where z coordinates of control points are considered as design variables. Model with 50 CPs.

This behaviour also appears in FE node based shape optimisation if a filter is used. The greater the filter radius is, the less details the optimised structure consists. In both cases (FE node based shape optimisation using filter and morphing based shape optimisation) the design space is restricted and the nonlinear optimisation problem is regularized, which is beneficial for the convergence of mathematical optimiser. The shape mode number 20 is pictured in Figure 10.9b. As one can recognize, much less oscillations appear here and very smooth shape changes can be obtained. Design engineers often choose models with less design variables to reduce the numerical effort of mathematical optimiser and of sensitivity analysis. In contrast to models in section 10.3, only a fraction of design variables is utilised in morphing based shape

parametrisation. Which of the models presented in Figure 10.6 should be used for the considered example is eventually a design decision. Similar situation appears in FE node based shape optimisation if the size of the filter radius is chosen.

10.4.3 Cantilever shell: optimisation results

In Figure 10.10 for both models the optimised structures are pictured and the corresponding compliance values are given. For both cases thirty iterations are performed to obtain comparable and converged results. We notice that very similar results are obtained and the values of objective function do not differ very much.

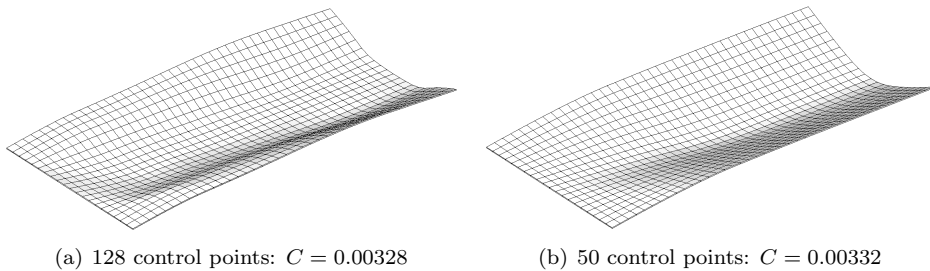


Figure 10.10: Cantilever shell: optimised structure.

In both cases one obtains a smooth solution and mesh distortions with jagged boundaries do not appear. If x and y coordinates of control points are added to the design variables set, SVD based design exploration indicates mesh distortions very similar to the previous section. To avoid great amount of pictorial material, the details on this topic are omitted. Nevertheless, this fact confirms that design exploration step is required despite of foregoing FE model exploration.

10.5 Correlation between design and FE model

In section 10.3 z coordinates of mid surface nodes are considered as design variables to enable maximum design freedom. The corresponding sensitivity information is explored by SVD. In section 10.4 morphing based design parametrisation is performed. The number of control points, their positions and free degrees of freedom are defined based on the design engineers experience and on the observations done within exploration of the model. It is well known, that each kind of design parametrisation, which is not based on FE node coordinates, restricts the design space. Due to these parametrisations, the number of design variables is decreased and some design changes are excluded from the design space. Sometimes, it is very difficult to recognize whether the parametrised model is flexible enough to be able to reach useful

optimised structures and whether unwanted shape changes are really excluded.

Design velocity fields matrix $\Psi \in \mathbb{R}^{n \times m}$ is usually calculated within sensitivity analysis as the last member of the sensitivity chain. The m columns of Ψ represent first derivatives of n FE nodes coordinates with respect to the m design variables. For given small changes in design $d\hat{C}$, changes in FE nodes coordinates $d\hat{X}$ can be computed by $d\hat{X} = \Psi d\hat{C}$.

The chosen design description is flexible enough if quantities like gradients of objectives and constraints or first modes of SVD of sensitivity matrix can be represented in a basis, which is defined by the design velocity fields matrix Ψ . Therefore, for a given gradient or mode $d\hat{X}$ the best possible approximation by the chosen design variables is computed utilising the *pseudo inverse*, see chapter 7, of the design velocity fields matrix with $d\bar{C} = \text{pinv}(\Psi)d\hat{X}$. This corresponds to the solution of an overestimated system of linear equations. In this case, best approximation means that a minimum of a least squares problem is determined. The corresponding approximation of the input quantity $d\bar{X}$ is computed evaluating the modified morphing boxes.

The quality of such an approximation depends directly on the basis Ψ and can be measured by means of the absolute value of the so called *correlation coefficient* ρ , which in case of two vectors is defined as follows

$$\rho^+ = |\rho| = |\cos \alpha| = \left| \frac{\hat{X}^T \bar{X}}{\|\hat{X}\| \|\bar{X}\|} \right| \quad \text{with} \quad 0 \leq \rho^+ \leq 1. \quad (10.1)$$

The absolute value of ρ is utilised because the signs of the modes are not uniquely determined. In case of shape optimisation one can say that the value $\rho^+ \geq 0.9$ indicates a very high correlation between two modes.

In case that some shape modes $d\hat{X}$ are to be excluded from the design space, one has to show, that the vectors $d\hat{X}$ and $d\bar{X}$ are not correlated. For shape optimisation one can say that almost no correlation exists if $\rho^+ \leq 0.1$.

To give an example on this topic, we compute correlation coefficients between the first shape mode from SVD of sensitivity matrix, which is computed with respect to z coordinates of mid surface nodes as design variables, see section 10.3, and the corresponding approximation based on the design velocity fields matrix of different morphing boxes. In Table 10.1 these coefficients are summarised.

Table 10.1: Cantilever shell example: model correlation

number of control points	$10 \times 10 \times 2$ = 200	$8 \times 8 \times 2$ = 128	$5 \times 5 \times 2$ = 50	$3 \times 3 \times 2$ = 18	$2 \times 2 \times 2$ = 8
correlation coefficient ρ^+	0.964	0.960	0.900	0.650	0.0015

In section 10.4 in Figure 10.6 morphing boxes with 128 and with 50 control points are introduced. In Figure 10.11 morphing based design description with 8 control points is presented.

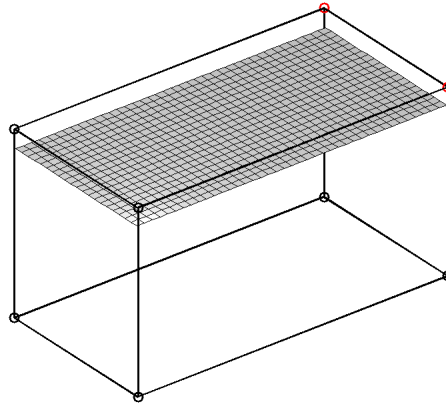


Figure 10.11: Cantilever shell: design description with 8 control points.

In this case it is impossible to change the design in such a way that the structure at least approximately would become similar to shape pictured in Figure 10.5a. This fact is indicated by near zero correlation in Table 10.1. Utilising 18 control points, it is possible to create a curved boundary on the right side of the shell and the corresponding correlation coefficient is drastically increased to a value of $\rho^+ = 0.650$. Models with 128 and 50 control points show a very high correlation with $\rho^+ \geq 0.9$. In case of the model with 200 control points, the number of design variables is greatly increased but the corresponding correlation coefficient is slightly improved. Based on this study, the design engineer decides to use morphing box with 50 control points to hold the number of design variables as few as possible but to have the design space as suitable as possible. In order to check whether unwanted modes are excluded from the model, the correlation coefficient between the mode pictured in Figure 10.5b and the approximated design changes $d\bar{\mathbf{X}}$ for the model with 50 control points is calculated. The corresponding value of $\rho^+ = 0.00018$ indicates that it is impossible to create such a jagged boundary utilising the chosen morphing box.

10.6 Summary and concluding remarks

A structural optimisation assistant is presented, which is implemented in *MATLAB* based *structural optimisation program* (SOP). It is used as a preprocessor tool during the definition of a structural optimisation problem. By means of this tool regions of the structure with high sensitivity with respect to changes in design are highlighted and shape modes with extraordinary impact on structural response are detected. Redundant shape changes and numerical defects like jagged boundaries and mesh distortions are tracked and excluded from the design descriptive model. The design variables set is reduced to the most effective variables, which is advantageous for the numerical effort and for the solubility of the problem. Such an assistant facilitates and substantiates the definition of an optimisation problem.

Due to the linear approximation nature of first derivatives, all decisions based on initial structure derivatives are only valid for moderate changes in design. FE model and design exploration can also be performed at several optimisations stages to improve the quality of predictions. We note that for the presented exploration only first and last modes are utilised within this chapter to reduce the amount of pictorial material. Nevertheless, it could be helpful to observe the intermediate modes to discover further phenomena. Within this thesis only shape changes are considered as design changes. However, the proposed techniques are also valid for other types of variables like material properties or load positions.

Utilising pure displacement formulations, only the sensitivity matrix for displacements and the pseudo load matrix for partial derivative of the energy with respect to displacements are available. In context of mixed finite element formulation the sensitivity matrices of stresses and strains can also be computed. In this case, additional valuable information can be gained for certain objectives and constraints. This topic could be a part of the future work.

As only first and last SVD modes of sensitivity matrix are computed within this approach, a sparse generalised singular value decomposition can be utilised to reduce the computational effort, to save the storage space and to avoid the computation of this matrix. See chapter 7, section 7.3.2 for more details on this topic.

11 Numerical examples

The features and capabilities but also the shortcomings of the proposed techniques are demonstrated on more practical numerical examples in this chapter. Either compliance or volume of the structure is minimised, taking stress and volume constraints into account. All computations are performed utilising the *structural optimisation program* (SOP) where all algorithms outlined in this thesis have been implemented.

11.1 Introduction

Algorithms and techniques proposed in this thesis are demonstrated on practical 3D applications. Structural analysis and optimisation are performed using SOP. Additional 2D examples are presented in [66] and [63].

11.1.1 Considered objectives and constraints

Two types of structural optimisation problems are considered.

Compliance minimisation under volume constraint. Minimising the compliance $C = -\Pi$ of the structure the global structural stiffness, which is expressed by the potential energy is maximised. In chapter 6 the vector of configurational forces, which is also called the discretised material residual is derived. This vector represents the total derivative of the potential energy with respect to coordinates of FE-nodes. Hence, its negative values represent the total derivative of compliance. Objectives like compliance and energy of the structure represent a special case where partial and total derivatives with respect to design are equal. The computation of pseudo load and sensitivity matrices is not necessary. Compliance minimisation problem is restricted introducing a volume constraint to get reasonable optimised structures.

Volume minimisation under stress constraints. Stress is often used as failure criterion within structural analysis. Optimising the shape of a structure, stress constraints must be taken into account. In chapter 6 stress sensitivity is derived. The pseudo load and sensitivity matrices must be computed to obtain stress gradients. Within this chapter structural volume is minimised and Von Mises stress at each Gaussian point is controlled.

In both cases additional geometric constraints can be utilised to enforce symmetry or producibility and to restrict the design space. Furthermore, bounds for the design variables can be taken into account.

11.1.2 Special features of the presented examples

The gradients of objectives and constraints are computed with respect to FE-node coordinates and transformed by means of *design velocity fields matrices*, see chapter 4, to obtain sensitivity with respect to changes in control point positions.

The utilised solid shell element is used either in solid or in shell mode to optimise the shape of 3D structures, which are modelled either by volumes or by surfaces. Examples with cuboidal and freeform morphing boxes are considered to demonstrate the inverse computation of the local coordinates of FE-nodes.

11.2 Compliance and volume minimisation

In chapter 6, section 6.4 the first example for compliance and volume minimisation was introduced. More practical applications are presented in this section.

11.2.1 Reservoir bracket

The compliance $J := C := -\Pi$ of the structure, which is pictured in Figure 11.1 is minimised, taking into account a volume constraint $V = 1.05 V_0$. Here, the quantities V and V_0 denote the current and initial volumes. The inner radius and the outer one are $r_i = 35$ and $r_o = 55$. The height is $h = 2$. The material properties are Young's modulus $E = 21000$ and Poisson's ratio $\nu = 0.3$. The load resultant is $\bar{Q} = 1$. The applied boundary conditions are pictured in Figure 11.1a. The finite element mesh consists of 984 elements and 2110 nodes with 6330 degrees of freedom. The thickness $t = 0.1$ remains constant during the optimisation.

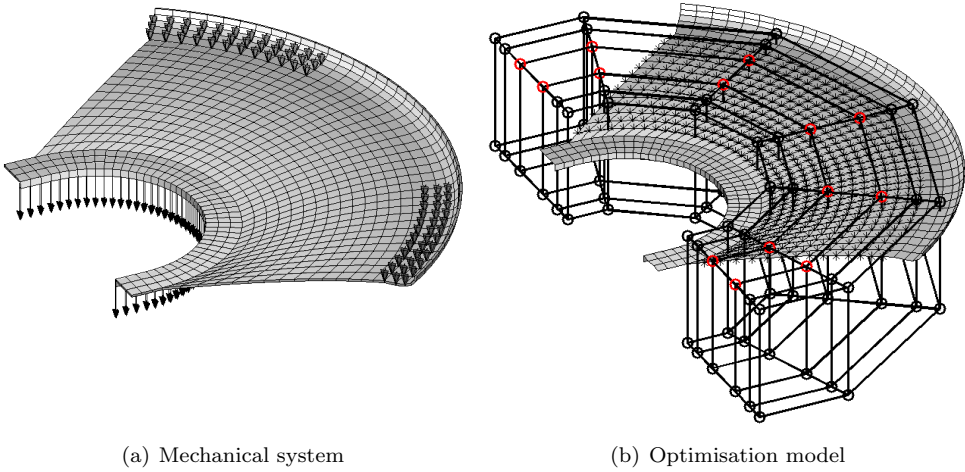


Figure 11.1: Reservoir bracket: model problem

A morphing box is defined by 84 control points and is pictured in Figure 11.1b. Finite element nodes, which are controlled by this box are marked with a star. Vertical positions of control points, which are marked red are used as design variables.

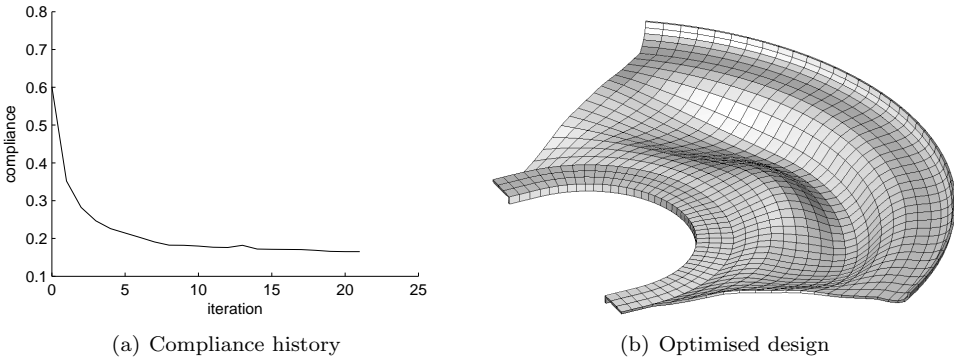


Figure 11.2: Reservoir bracket: optimisation results

The algorithm converges after 21 iterations. The corresponding iteration history for the objective is pictured in Figure 11.2a. The compliance is decreased to a third of its initial value. The optimised design is presented in Figure 11.2b. The shape of inner and outer flanges is not changed, because these parts are not influenced by the defined morphing box. The higher stiffness of the optimised structure can be verified considering structural deformation before and after optimisation in Figure 11.3.

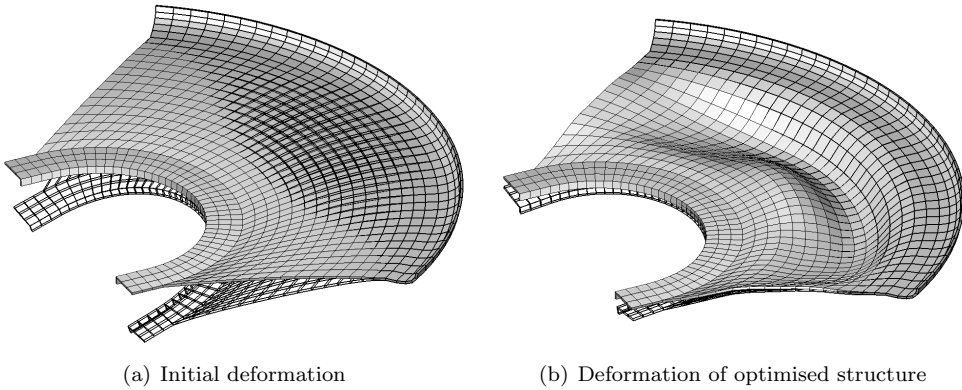


Figure 11.3: Reservoir bracket: deformation before and after optimisation

The highlight of the presented example is the morphing box, which is not a square block. In this case, the reverse computation of local finite element nodes positions corresponding to chapter 4, section 4.4.3 is slightly more time-consuming. Providently, this step is done once before optimisation starts.

11.2.2 3D hook

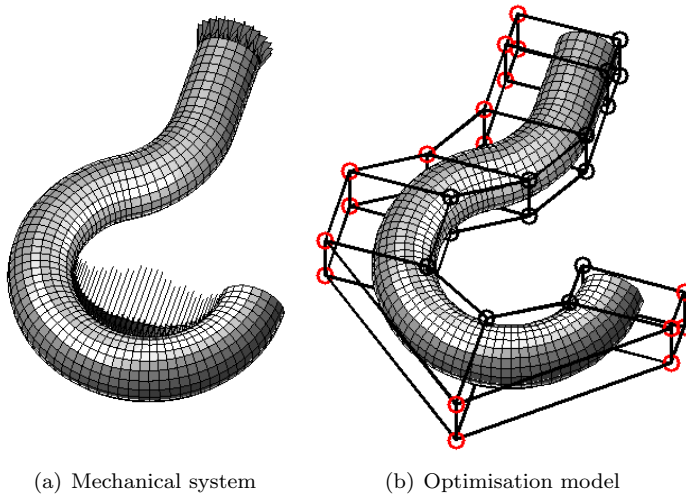


Figure 11.4: 3D hook: model problem

The considered solid shell elements can be used as pure solid elements. For this reason the ANS and the EAS enrichments must be deactivated. To give an example the 3D hook in Figure 11.4 is considered. The dimensions of the structure (height, width and depth) are $h = 38$, $w = 26$ and $d = 6$. The material properties are Young's modulus $E = 21000$ and Poisson's ratio $\nu = 0.3$. The load resultant is $Q = 0.024$. The applied boundary conditions are pictured in Figure 11.4a. The finite element mesh consists of 3510 elements and 4424 nodes with 13272 degrees of freedom. A morphing box is defined by 36 control points and is pictured in Figure 11.4b. All finite element nodes are controlled by this box. Positions of control points which are marked red are used as design variables. Some bounds for these positions are introduced to avoid self penetration of the FE-mesh.

Compliance minimisation. The compliance of the structure is minimised preserving a constant volume of the structure. The algorithm converges after 34 iterations. The corresponding iteration history for the objective is pictured in Figure 11.5a. The compliance is decreased to 60 % of its initial value. The optimised design is presented in Figure 11.5b.

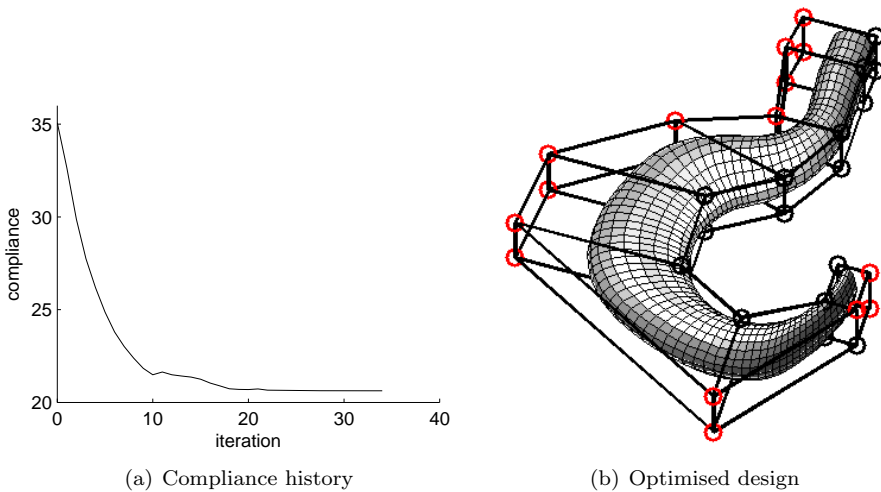


Figure 11.5: 3D hook: optimisation results for compliance minimisation

The depth of the structure is not changed as the control points were not allowed to be moved in the corresponding direction. A more detailed design can be reached employing morphing boxes with more control points. It is interesting to observe that also complex geometries can be easily parametrised by morphing boxes.

Volume minimisation. The volume of the 3D hook is minimised under stress constraints. The von Mises stress σ_v in all Gaussian points i is controlled with $\sigma_v^i \leq \bar{\sigma}$. For the considered example the stress limit is $\bar{\sigma} = 110$. Optimisation history for volume and maximum Von Mises stress are pictured in Figure 11.6.

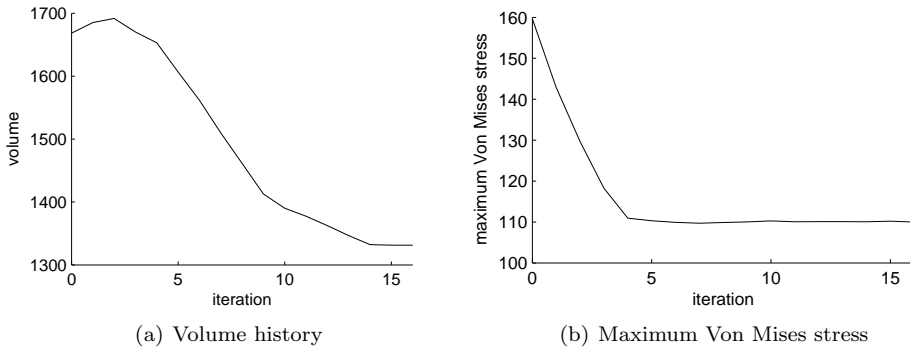


Figure 11.6: 3D hook: optimisation results for volume minimisation

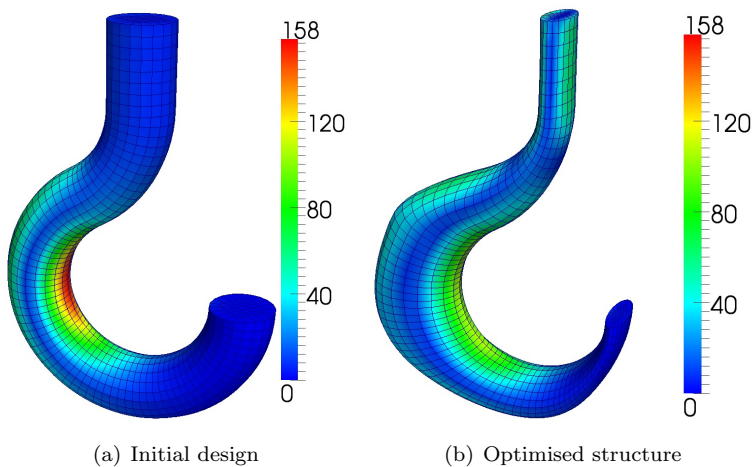


Figure 11.7: 3D hook: Von Mises stress

We note, that the optimisation started with an inadmissible initial design because some stress constraints were violated. This fact causes the small volume increase in the first two iterations as the algorithm attempted to decrease the maximum Von Mises stress. The Von Mises stress is pictured in Figure 11.7a for the initial design

and in Figure 11.7b for the optimised structure. A volume reduction of about 20% is reached. Smooth boundaries are obtained. Mesh distortions do not occur.

11.3 Generation of worst imperfections

In chapter 8 sensitivity based imperfections for buckling analysis are proposed. They are based on singular value decomposition of the pseudo load matrix, which is computed at the first critical point of the perfect structure. To give an example on this topic, a PET tube is considered.

11.3.1 PET tube: model problem

We consider the mechanical model, which is pictured in Figure 11.8. The structure is a PET tube under compression. The finite element mesh consists of 1600 elements and 3280 nodes with 6560 degrees of freedom. The finite element nodes on the right side of the tube are fixed in all three directions. The finite element nodes on the left side of the tube are fixed in directions normal to the tube axis to enforce buckling of surfaces and to exclude buckling of edges.

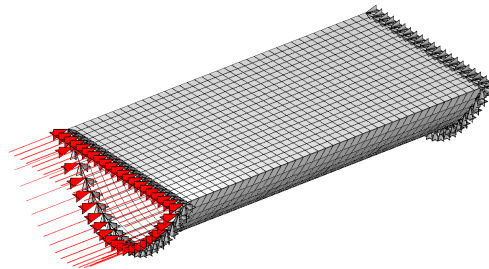


Figure 11.8: PET tube: mechanical model

The edges on the left side of the tube are loaded with a line load. The critical load λ_c is the load resultant and is to be detected for perfect and imperfect designs. The dimensions of the structure (height, width and length) are $h = 45$, $w = 100$ and $l = 200$. The shell thickness is $t = 0.3$. The bottom shell is an extruded parabola. The material properties are Young's modulus $E = 3500$ and Poisson's ratio $\nu = 0.4$.

11.3.2 PET tube: buckling analysis

Considering the perfect structure, which is pictured in Figure 11.8 the load parameter λ is gradually increased and the first instability point $\lambda_c^p = 15$ is calculated. The eigenvalue decomposition of the reduced tangent stiffness matrix at load level λ_c^p

provides a zero eigenvalue and the corresponding eigenvector, which is the buckling mode. This first buckling mode of the perfect structure is pictured in Figure 11.9a.

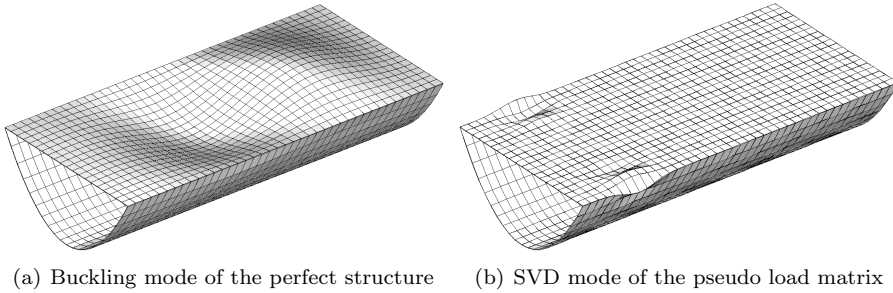


Figure 11.9: PET tube: different shapes of imperfection

This buckling mode mainly describes the buckling of the plane top shell. Following the classical buckling analysis procedure the perfect structure is disturbed corresponding to this mode. For this reason the buckling mode is scaled by an amplitude $a = l/200 = 1$ and is added to the finite element nodes coordinates. Such imperfect structure is analysed again and the first instability point is computed with $\lambda_c^B = 50$. Here, the index B denotes buckling mode based imperfection. The corresponding buckled structure is pictured in Figure 11.10a. We note, that the first instability point of the imperfect structure is at higher load level than that of the perfect one. Nevertheless, the structure could fail before the first instability point is reached if, for example, the maximum stress is exceeded. This fact is not considered within this example.

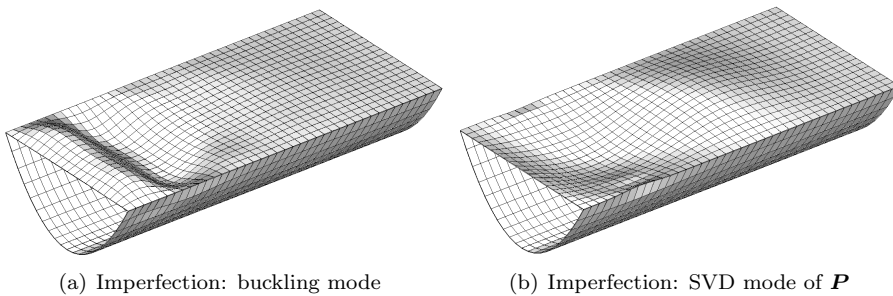


Figure 11.10: PET tube: buckling modes of imperfect structure

Next, the pseudo load matrix of the perfect structure is computed at the load level λ_c^p and is decomposed by the singular value decomposition. The first right singular vector, which is pictured in Figure 11.9b is utilised to create an alternative imperfection of the structure pictured in Figure 11.8. The amplitude of imperfection is again

$a = 1$. The computation of the first instability point of the now imperfect structure delivers the critical load $\lambda_c^P = 12.5$. Here, the index P denotes the imperfection, which is based on SVD of pseudo load matrix. The corresponding buckled structure is pictured in Figure 11.10b. We note that the imperfect structure buckles at a lower load level than the perfect one. The results of the performed buckling analysis are summarised in Table 11.1.

Table 11.1: PET tube: results of buckling analysis

type of imperfection	imperfection amplitude a	buckling load λ_c
Perfect structure		15
Buckling mode	1	50
SVD of \mathbf{P} mode	1	12.5

11.4 SVD based model reduction

In chapter 9 a modified shape optimisation procedure is presented. Singular value decomposition is utilised to generate shape modes. A subset of these shape modes is selected to perform model reduction. Singular values or weighting factors presented in section 9.3.1 can be used to identify shape modes, which have an extraordinary impact on mechanical behaviour of the structure. Within this section both selection criteria are compared.

11.4.1 Ceiling surface

The compliance of the structure, which is pictured in Figure 11.11 is minimised taking into account a constant volume constraint.

Model problem. The dimensions of the structure (height, width and length) are $h = 0.1$, $w = 3$ and $d = 4$. The material properties are Young's modulus $E = 30000$ and Poisson's ratio $\nu = 0.3$. The load $\bar{q} = 0.2$ is a surface load. The applied boundary conditions are pictured in Figure 11.11a. The finite element mesh consists of 3600 elements and 5084 nodes with 15252 degrees of freedom. A morphing box is defined by 384 control points and is pictured in Figure 11.11b. Vertical positions of 140 control points, which are marked red are used as design variables. Only the shape of the upper surface is optimised. The ANS and the EAS enrichments are deactivated to use pure solid element properties.

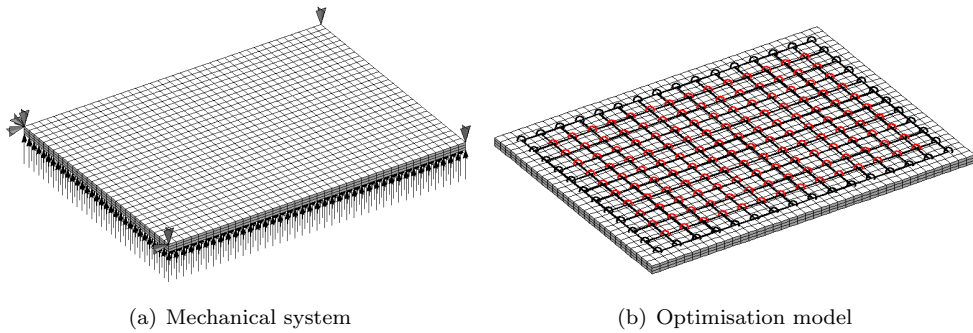


Figure 11.11: Ceiling surface: model problem

Optimisation results. The SVD based optimisation procedure presented in 9.6 is utilised to minimise the compliance of the structure pictured in Figure 11.11.

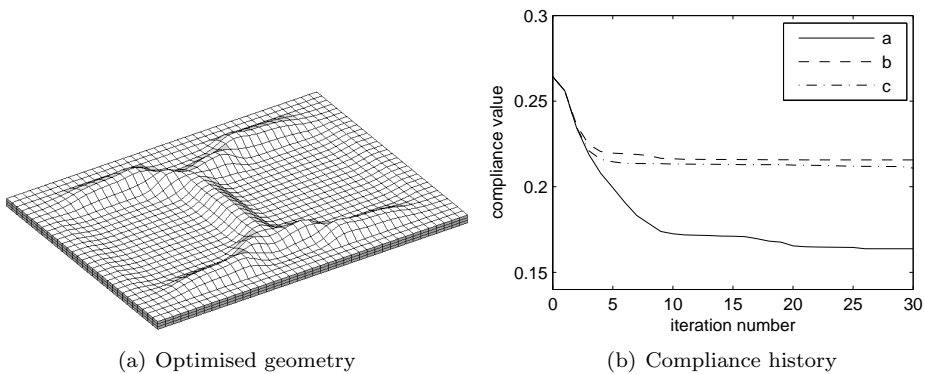


Figure 11.12: Ceiling surface: optimisation results

SVD of the sensitivity matrix is performed in every 5th iteration to generate shape modes. Shape optimisation based on all 140 available shape modes leads to the optimised geometry pictured in Figure 11.12a. In this case, only a coordinate transformation takes place and the results are the same as utilising the standard optimisation procedure. The compliance is minimised from its initial value $C_0 = 0.2643$ to $C = 0.1637$. The solid line in Figure 11.12b represents the corresponding compliance history. About 30 iterations are necessary to obtain convergence.

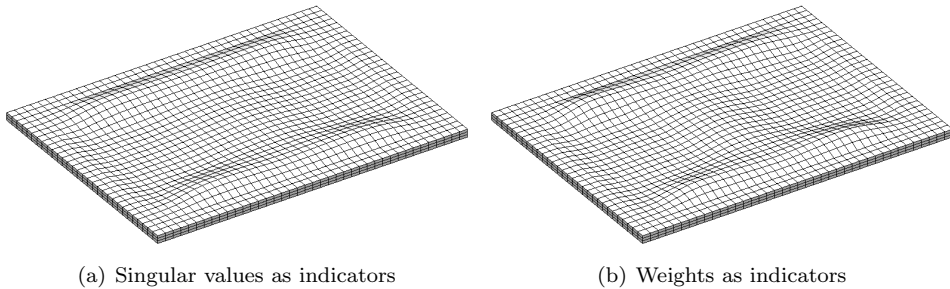


Figure 11.13: Ceiling surface: optimised geometries

Model reduction is performed utilising only shape modes, which correspond to the 30 largest singular values of sensitivity matrix. The optimised geometry for this case is pictured in Figure 11.13a and the dashed line in Figure 11.12b represent the corresponding compliance history. Only 30 iterations are performed to obtain comparable results. We note that the proposed model reduction is not very efficient for the considered example. Nevertheless, useful design is obtained based on only about 20 % of all possible shape modes.

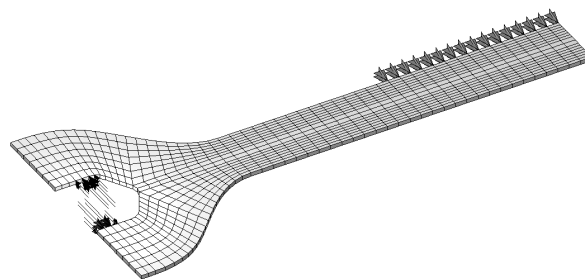
Next up, the influence of indicators for shape modes selection on optimisation results is investigated. For this reason, the weighting factors presented in section 9.3.1 are utilised to select 30 shape modes. The optimised geometry is pictured in Figure 11.13b, and the dashed dotted line in Figure 11.12b represent the corresponding compliance history. We note that in this case the optimisation results are not significant better than using singular values as indicators. One should use singular values as indicators to reduce the numerical effort of the proposed algorithm, as only the first 30 shape modes should be computed. This is only true in case of compliance as objective function. The criteria presented in section 9.3.1 are mainly heuristics but seem to be useful for the proposed model reduction.

11.4.2 Spanner

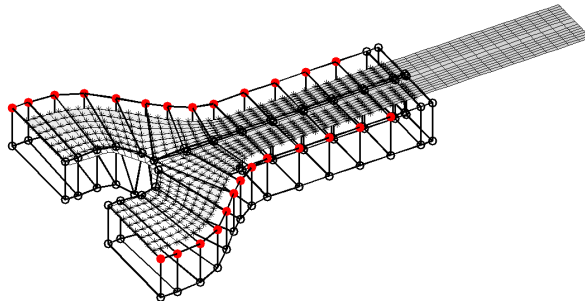
Structures considered before are subjected to bending stress. In this section an example on membrane stiffness optimisation is presented. Solid shell elements are used to model a 2D structure. In context of volume minimisation under stress constraints, SVD based model reduction is demonstrated.

Model problem. The spanner pictured in Figure 11.14 is considered. The dimensions of the structure (height, length and thickness) are $h = 59$, $l = 130$ and $t = 1$. The material properties are Young's modulus $E = 210000$ and Poisson's ratio $\nu = 0.3$.

Two opposite surface loads are applied to model momentum claim. Each load resultant is $Q = 250$. The applied boundary conditions are pictured in Figure 11.14a. The finite element mesh consists of 792 elements and 1744 nodes with 5232 degrees of freedom. Two symmetrical morphing boxes are defined and are pictured in Figure 11.14b. Each box consists of 60 control points. Finite element nodes, which are marked by a star are controlled by this boxes. Positions of control points which are marked red are used as design variables. Some bounds for these positions are introduced to avoid self penetration of the FE-mesh.



(a) Mechanical system



(b) Optimisation model

Figure 11.14: Spanner: model problem

Volume minimisation under stress constraints. The volume of the structure pictured in Figure 11.14 is minimised taking stress constraints into account. The Von Mises stress σ_v in all Gaussian points i is controlled with $\sigma_v^i \leq \bar{\sigma}$. For the considered example the stress limit is $\bar{\sigma} = 170$. Non symmetrical mechanical model is considered. Nevertheless, the optimised structure has to be symmetric due to the purpose of a spanner. Additional symmetry constraints are applied to the positions of control points, which are used as design variables. The optimisation model consists of 26 design variables and 13 symmetry constraints. The Von Mises stress is pictured in Figure 11.15a for the initial design and in Figure 11.15b for the optimised structure.

About 40 iterations are needed to obtain convergence. A volume reduction of about 25% is reached. Smooth boundaries are obtained. Mesh distortions do not occur.

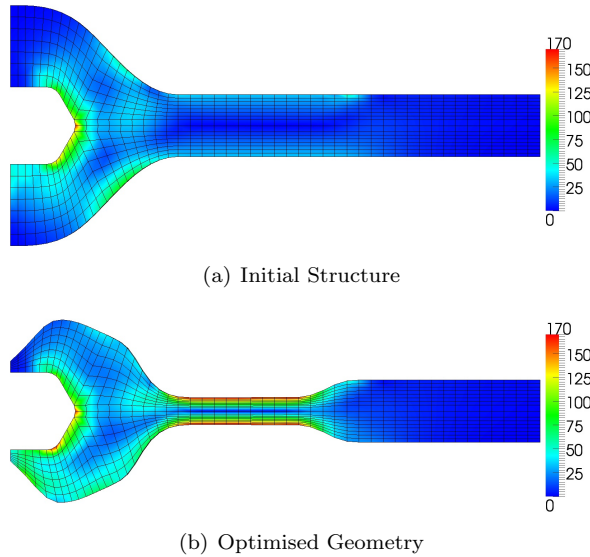


Figure 11.15: Spanner: Von Mises Stress

SVD based model reduction. Model reduction based on SVD of the sensitivity matrix is performed. Singular values are used as indicators to select shape modes. The optimised structures are presented in Figure 11.16. Optimisation with 6 and 13 modes of 26 is performed. Only 40 iterations are carried out to obtain comparable results. Reasonable shapes are obtained and all optimisation results are summarised in Table 11.2.

Table 11.2: Spanner: volume after the 40th iteration

number of modes (\cdot)/26	volume V	volume decrease V_{diff}	relative error %
6	2094	660	0.03
13	2084	670	0.02
26	2071	683	0

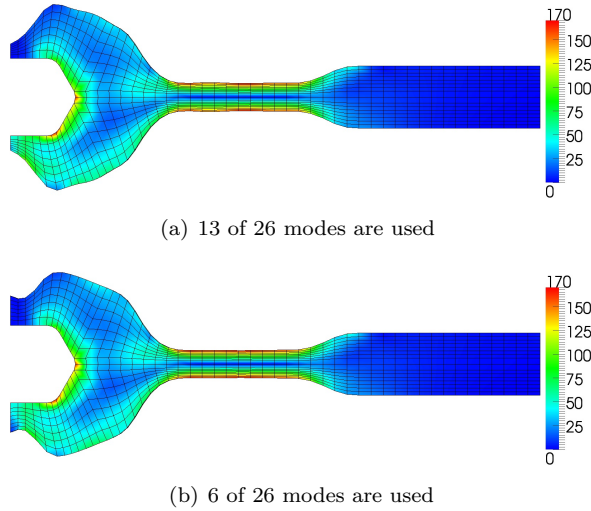


Figure 11.16: Spanner: SVD based model reduction; Von Mises Stress

11.5 Summary and concluding remarks

Morphing based shape optimisation of solid and shell structures is demonstrated. Some examples are based on morphing boxes, which have complex initial shape. In this case, the inverse computation of local coordinates of FE-nodes is performed utilising the proposed Newton's method based algorithm.

Several compliance minimisation problems are solved and structures with high global stiffness are obtained. Treatment of stress constraints is demonstrated minimising the volume of the structure and controlling the Von Mises Stress at Gaussian points.

Furthermore, the computation of SVD based imperfections for nonlinear buckling analysis is illustrated. This example demonstrates the applicability of sensitivity information to structural analysis.

In addition, model reduction is carried out utilising SVD of sensitivity matrix. These examples exhibit the information content of SVD based sensitivities.

To sum up, the properties and capabilities of the presented sensitivity analysis are demonstrated and applications of SVD based sensitivity information to structural analysis and optimisation are presented. All computations are performed using SOP.

12 Conclusion

This chapter gives a concluding summary of the presented research. The main aspects and results of the work are highlighted once more and an outlook on possible further investigations is given.

12.1 Summary

In the present work sensitivity analysis of a nonlinear solid shell was presented. The corresponding variational relations were derived and discretised to be used in context of structural optimisation, utilising the finite element method. Especially, material residual vector, the pseudo load matrix and the sensitivity matrix were derived. Objectives and constraints in structural optimisation usually depend on the structural response. The computation of their gradients requires the calculation of pseudo load and sensitivity matrices. Sensitivity relations for structural stresses were derived to give an example on this topic.

The main intention of this work was to analyse the inner structure of sensitivities considering their singular value decompositions and to show that they contain additional valuable information which is not used either in theory or in practical applications of structural optimisation yet. These expectations have been confirmed during the presented research. Special techniques have been utilised within this thesis to qualitatively and quantitatively analyse the pseudo load and sensitivity matrices. They are well known in the scope of statistics as well as of applied sciences and are especially based on *principal component analysis*, *factor analysis* and the computation of *variance* and *correlation*. To sum up, overall three applications of the discovered SVD based sensitivity information have been developed in context of structural analysis and optimisation:

- computation of sensitivity based imperfections for nonlinear buckling analysis,
- model reduction based on SVD of sensitivity information,
- SVD based design exploration.

These applications demonstrate the informational content of pseudo load and sensitivity matrices and provide new insights in the exploration of structural design. Overall, an enhanced analysis of sensitivities has been emphasised and unused substantial capabilities have been pointed to. The impact of the chosen models on the computed optimal designs, especially the influence of the chosen shape parametrisation, was analysed. This knowledge enables the design engineer to understand and improve the models systematically, which are usually set up entirely by engineering experience and intuition. The features and capabilities of the presented algorithms and techniques were demonstrated on several numerical examples of morphing based shape optimisation. Here, the corresponding design velocity fields matrices were derived analytically to suit variational design sensitivity analysis.

All derived relations and proposed algorithms have been implemented and tested in the *MATLAB* based *structural optimisation program* (SOP).

12.2 Future work

Within this thesis only shape modifications are considered as design changes. However, the proposed techniques are also valid for other types of variables like topological quantities, material properties or support and load positions. Hence, investigations in context of *material optimisation*, *robustness*, *uncertainty* and *reliability analysis*, where sensitivity of structural response with respect to some model parameters is analysed, are desirable.

Due to the linear approximation nature of first derivatives, all decisions and predictions based on observations of an optimisation time point are only valid for moderate changes in design. The iteration history of gradients, pseudo load and sensitivity matrices could provide additional valuable information which could be used within structural optimisation procedures. Within this thesis, techniques from *linear principal component analysis* (LPCA or short PCA) are utilised. Only rotation of a Cartesian coordinate system is performed in context of PCA. Linear and linearised relations are recognised by PCA. In further investigations, nonlinear PCA (NLPCA), see [122] and [121], could be used to take iteration history into account. Curvilinear coordinate systems and nonlinear relations within given data can be identified by NLPCA.

Future work might also address the application of the proposed techniques to large systems and real structural optimisation problems. More complex elastic and inelastic material laws might be considered. In this context it would be interesting to study the numerical effort for the proposed SVD based applications and possibilities of its reduction. Some hints on this topic were already given in this thesis but rigorous investigations are desired.

Bibliography

- [1] ANSA. www.ansa-usa.com/products/ansa/morphing.
- [2] ANSYS. www.ansys.com.
- [3] ARPACK. www.caam.rice.edu/software/ARPACK.
- [4] AVL. www.avl.com/ast.
- [5] BOEING Design Explorer. www.boeing.com.
- [6] GNU scientific library (GSL). www.gnu.org/software/gsl.
- [7] HYPERMORPH. www.altairhyperworks.com.
- [8] LAPACK. www.netlib.org/lapack.
- [9] MATLAB R2012b. www.mathworks.de.
- [10] OptiSlang. www.dynardo.de/software/optislang.html.
- [11] ParaView. www.paraview.org.
- [12] SCILAB. <http://www.scilab.org/>.
- [13] SVDPACK. www.netlib.org/svdpack.
- [14] Encyclopedia of Computational Mechanics. Online library, John Wiley and Sons, 2004. <http://onlinelibrary.wiley.com/book/10.1002/0470091355>.
- [15] E. Anderson, Z. Bai, C. Bischof, S. Blackford, J. Demmel, J. Dongarra, J. Du Croz, A. Greenbaum, S. Hammarling, A. McKenney, and D. Sorensen. *LAPACK Users' Guide*. PA: Society for Industrial and Applied Mathematics, Philadelphia, 1999.
- [16] A. C. Antoulas and D. C. Sorensen. Approximation of large-scale dynamical systems: An overview. *International Journal of Applied Mathematics and Computer Science*, 11(5):1093–1121, 2001.
- [17] J. Arbocz and J. H. Starnes(Jr). Future directions and challenges in shell stability analysis. *Thin-Walled Structures*, 40(9):729 – 754, 2002.
- [18] S. Arnout, M. Firl, and K.-U. Bletzinger. Parameter free shape and thickness optimisation considering stress response. *Structural and Multidisciplinary Optimization*, 45(6):801–814, 2012.

- [19] C. Audet. A survey on direct search methods for blackbox optimization and their applications. Technical report, Les Cahiers du GERAD, 2012.
- [20] Z. Bai, J. Demmel, J. Dongarra, A. Ruhe, and H. Van der Vorst. *Templates for the solution of algebraic eigenvalue problems: A practical guide*. Philadelphia, PA: Society for Industrial and Applied Mathematics, 2000.
- [21] H. Baier, C. Seibelberg, and B. Specht. *Optimierung in der Strukturmechanik*. Vieweg & Sohn Verlagsgesellschaft mbH, Braunschweig/Wiesbaden, 1994.
- [22] J. F. M. Barthelemy and R. T. Haftka. Approximation concepts for optimum structural design - a review. *Structural Optimisation*, 5:129–144, 1993.
- [23] F.-J. Barthold. *Zur Kontinuumsmechanik inverser Geometrieprobleme*. Habilitation, Braunschweiger Schriften zur Mechanik 44-2002, TU Braunschweig, 2002.
- [24] F.-J. Barthold. Remarks on variational shape sensitivity analysis based on local coordinates. *Engineering Analysis with Boundary Elements*, 32:971–985, 2008.
- [25] K. J. Bathe. *Finite Element Procedures*. Prentice-Hall, Inc., 1996.
- [26] A. Becker. *Strukturoptimierung stabilitätsgefährdeter Systeme mittels analytischer Gradientenermittlung*. PhD thesis, Hannover University, 1992.
- [27] M. P. Bendsøe. *Optimization of Structural Topology, Shape, and Material*. Springer-Verlag Berlin Heidelberg, 1995.
- [28] M. P. Bendsøe and N. Kikuchi. Generating optimal topologies in optimal design using a homogenization method. *Computer Methods in Applied Mechanics and Engineering*, 71:197–224, 1988.
- [29] M. P. Bendsøe and O. Sigmund. *Topology Optimization*. Springer Verlag Berlin Heidelberg New York, 2003.
- [30] M. Bischoff, K.-U. Bletzinger, W. A. Wall, and E. Ramm. *Models and Finite Elements for Thin-Walled Structures*. John Wiley & Sons, Ltd, 2004.
- [31] K.-U. Bletzinger, M. Firl, and F. Daoud. Approximation of derivatives in semi-analytical structural optimization. *Computers & Structures*, 86:1404 – 1416, 2008.
- [32] K.-U. Bletzinger, M. Firl, J. Linhard, and R. Wüchner. Optimal shapes of mechanically motivated surfaces. *Comput. Methods in Appl. Mech. and Engrg.*, 199(5-8):324 – 333, 2010.
- [33] P. T. Boggs and J. W. Tolle. Sequential quadratic programming. *Acta Numerica*, 4:1–51, 1996.

-
- [34] T. Borrvall. Topology optimization of elastic continua using restriction. *Archives of Computational Methods in Engineering*, 8(4):351–385, 2001.
- [35] V. Braibant and C. Fleury. Shape optimal design using B-splines. *Computer Methods in Applied Mechanics and Engineering*, 44:247–267, 1984.
- [36] C. G. Broyden. The convergence of a class of double-rank minimization algorithms 1. General considerations. *IMA Journal of Applied Mathematics*, 6(1):76–90, 1970.
- [37] C. Bucher and T. Most. A comparison of approximate response functions in structural reliability analysis. *Probabilistic Engineering Mechanics*, 23:154 – 163, 2008.
- [38] K. Carlberg and C. Farhat. A compact proper orthogonal decomposition basis for optimization-oriented reduced-order models. In *Proceedings of the 12th AIAA/ISSMO Multidisciplinary Analysis and Optimization Conference*, 2008.
- [39] D. Chenais. Shape optimization in shell theory: Design sensitivity of the continuous problem. *Engineering Optimization*, 11(3-4):289–303, 1987.
- [40] L. Chibani. *Optimum Design of Structures*. Springer-Verlag Berlin, Heidelberg, 1989.
- [41] D. Child. *The Essentials of Factor Analysis*. Continuum International Publishing Group, New York, London, 3 edition, 2006.
- [42] B. Choi, Y. H. Park, and K. K. Choi. Shape design optimization of joining mechanism using doubly curved shell. *Computers and Structures*, 77(5):495 – 507, 2000.
- [43] K. K. Choi and N.-H. Kim. *Structural sensitivity analysis and optimisation 1 - Linear systems*. Mechanical Engineering Series. Springer, 2005.
- [44] K. K. Choi and N.-H. Kim. *Structural sensitivity analysis and optimization 2 - Nonlinear systems and applications*. Mechanical Engineering Series. Springer, 2005.
- [45] P. W. Christensen and A. Klabring. *An Introduction to Structural Optimisation*. Springer Science and Business Media B. V., 2009.
- [46] B. Christian. Robustness analysis in structural optimization. *Structure and Infrastructure Engineering*, 5(4):287–293, 2009.
- [47] H. W. Coleman and W. G. Steele. *Experimentation, Validation, and Uncertainty Analysis for Engineers*. John Wiley & Sons, 2009.
- [48] H. de Boer and F. van Keulen. Refined semi-analytical design sensitivities. *International Journal of Solids and Structures*, 37:6961 – 6980, 2000.

- [49] C. de Boor. *A practical guide to splines*. Springer-Verlag, 1978.
- [50] M. Deml and W. Wunderlich. Direct evaluation of the 'worst' imperfection shape in shell buckling. *Computer Methods in Applied Mechanics and Engineering*, 149:201 – 222, 1997. Containing papers presented at the Symposium on Advances in Computational Mechanics.
- [51] H. Edelsbrunner. *Geometry and topology for mesh generation*. Cambridge University Press, 2001.
- [52] B. L. O. Edlund. Buckling of metallic shells: Buckling and postbuckling behaviour of isotropic shells, especially cylinders. *Structural Control and Health Monitoring*, 14(4):693–713, 2007.
- [53] EN 1993-1-6. Strength and stability of shell structures. *Eurocode 3: Design of steel structures*, 1.6, 2007.
- [54] EN 1993-1-6/NA. Strength and stability of shell structures. *National Annex - Nationally determined parameters - Eurocode 3: Design of steel structures*, 1.6, 2007.
- [55] H. Ersoy. Optimum laminate design by using singular value decomposition. *Composites Part B: Engineering*, 52:144 – 154, 2013.
- [56] H. Ersoy and A. Mugan. Design sensitivity analysis of structures based upon the singular value decomposition. *Computer methods in applied mechanics and engineering*, 191:3459–3476, 2002.
- [57] G. Farin. *Curves and surfaces for CAD: a practical guide*. Morgan Kaufmann Publishers Inc., San Francisco, CA, USA, 2002.
- [58] F. Flager, A. Adya, J. Haymaker, and M. Fischer. A bi-level hierarchical method for shape and member sizing optimization of steel truss structures. *Computers & Structures*, 131:1 – 11, 2014.
- [59] R. Fletcher. A new approach to variable metric algorithms. *The Computer Journal*, 13(3):317–322, 1970.
- [60] P. J. Frey and P. L. George. *Mesh generation: application to finite elements*. Hermes Science, 2000.
- [61] J. M. L. Gagne, M. Andersen, and L. K. Norford. An interactive expert system for daylighting design exploration. *Building and Environment*, 46(11):2351–2364, 2011.
- [62] S. Gaile, G. Leugering, and M. Stingl. Free material optimization with multidisciplinary optimization constraints for plates and shells. Technical Report PU-R-7-2008, Department of Mathematics, University of Erlangen-Nürnberg, 2009.

-
- [63] N. Gerzen and F.-J. Barthold. Enhanced analysis of design sensitivities in topology optimization. *Structural and Multidisciplinary Optimization*, 46:585–595, 2012.
- [64] N. Gerzen and F.-J. Barthold. Variational design sensitivity analysis of a nonlinear solid shell with applications to buckling analysis. *In Proc. of the 10th WCSMO*, 2013.
- [65] N. Gerzen, F.-J. Barthold, S. Klinkel, W. Wagner, and D. Materna. Variational sensitivity analysis of a nonlinear solid shell element. *International Journal for Numerical Methods in Engineering*, 96(1):29–42, 2013.
- [66] N. Gerzen, D. Materna, and F.-J. Barthold. The inner structure of sensitivities in nodal based shape optimisation. *Computational Mechanics*, 49:379–396, 2012.
- [67] A. Ghosh and S. Dehuri. Evolutionary algorithms for multi-criterion optimization: a survey. *International Journal of Computing & Information Sciences*, 2(1):38–57, 2004.
- [68] D. Goldfarb. A family of variable-metric methods derived by variational means. *Mathematics of Computation*, 24(1):23–26, 1970.
- [69] G. H. Golub and H. A. Van der Vorst. Eigenvalue computation in the 20th century. *Comp. Appl. Math.*, 123:35–65, 2000.
- [70] G. H. Golub and C. F. Van Loan. *Matrix computations*. Baltimore: John Hopkins University Press, 1996.
- [71] N. I. M. Gould, D. Orban, and P. L. Toint. Numerical methods for large-scale nonlinear optimization. *Acta Numerica*, 14:299–361, 2005.
- [72] R. T. Haftka and H. M. Adelman. Recent developments in structural sensitivity analysis. *Structural Optimisation*, 1:137–151, 1989.
- [73] R. T. Haftka and R.V. Grandhi. Structural shape optimization—a survey. *Computer Methods in Applied Mechanics and Engineering*, 57:91–106, 1986.
- [74] S. Hammerling. The singular value decomposition in multivariate statistics. *ACM SIGNUM Newsl.*, 20(3):2–25, 1985.
- [75] L. Harzheim. *Strukturoptimierung, Grundlagen und Anwendungen*. Wissenschaftlicher Verlag Harri Deutsch GmbH, 2008.
- [76] J. Haslinger, M. Kocvara, G. Leugering, and M. Stingl. Multidisciplinary free material optimization. *SIAM Journal on Applied Mathematics*, 70(7):2709–2728, 2010.
- [77] J. Haslinger and R. A. E. Mäkinen. *Introduction to shape optimization*. Society for Industrial and Applied Mathematics, 2003.

- [78] E. J. Haug, K. K. Choi, and V. Komkov. *Design Sensitivity Analysis of Structural Systems*. Academic Press, Orlando, 1986.
- [79] D. Ho. Buckling load of non-linear systems with multiple eigenvalues. *International Journal of Solids and Structures*, 10(11):1315 – 1330, 1974.
- [80] M. E. Hochstenbach. A Jacobi - Davidson type method for the generalized singular value problem. *Linear Algebra and its Applications*, 431(3-4):471 – 487, 2009. (Special Issue in honor of Henk van der Vorst).
- [81] W. Jin, B. H. Dennis, and B. P. Wang. Improved sensitivity analysis using a complex variable semi-analytical method. *Structural and Multidisciplinary Optimization*, 41(3):433–439, 2010.
- [82] I. T. Jolliffe. *Principal Component Analysis*. Springer, Heidelberg, 1986.
- [83] D. R. Jones. A taxonomy of global optimization methods based on response surfaces. *Journal of Global Optimization*, 21(4):345–383, 2001.
- [84] E. Kang, E. Jackson, and W. Shulte. An approach for effective design space exploration. In *FOCS'10 Proceedings of the 16th Monterey conference of foundations of computer software*, 2011.
- [85] M. Keller, E. Parent, and A. Pisanisi. On the role of decision theory in uncertainty analysis. Technical report, 2010.
- [86] A. Kilian. *Design Exploration through Bidirectional Modeling of Constraints*. PhD thesis, Massachusetts Institute of Technology, 2006.
- [87] N.-H. Kim, K. K. Choi, J.-S. Chen, and M. E. Botkin. Meshfree analysis and design sensitivity analysis for shell structures. *International Journal for Numerical Methods in Engineering*, 53(9):2087–2116, 2002.
- [88] U. Kirsch. *Structural Optimization*. Springer-Verlag Berlin Heidelberg, 1993.
- [89] S. Klinkel, F. Gruttmann, and W. Wagner. A robust non-linear solid shell element based on a mixed variational formulation. *Computer Methods in Applied Mechanics and Engineering*, 195:179 – 201, 2006.
- [90] S. Klinkel, F. Gruttmann, and W. Wagner. A mixed shell formulation accounting for thickness strains and finite strain 3d material models. *International Journal for Numerical Methods in Engineering*, 74(6):945–970, 2008.
- [91] S. Klinkel and W. Wagner. A piezoelectric solid shell element based on a mixed variational formulation for geometrically linear and nonlinear applications. *Computers and Structures*, 86:38 – 46, 2008.
- [92] W. T. Koiter. *On the Stability of Elastic Equilibrium*. H.J. Paris Publishers: Amsterdam, 1945 English translation Report No. AFFDL-TR-70-25, Air Force Flight Dynamics Laboratory, Wright Patterson AFB, Ohio, 1970.

-
- [93] C. Le, T. Bruns, and D. Tortorelli. A gradient-based, parameter-free approach to shape optimization. *Computer Methods in Applied Mechanics and Engineering*, 200(9-12):985 – 996, 2011.
- [94] A. Lenzen and H. Waller. Deterministische und stochastische Systemidentifikation mit Methoden der linearen Algebra zur Formulierung von mathematischen Modellen im Lebensdauerzyklus von Bauwerken. In K. Gürlebeck, L. Hempel, and C. Könke, editors, *Proceedings 16th International Conference on the Applications of Computer Science and Mathematics in Architecture and Civil Engineering*. IKM 2003, Weimar, 2003.
- [95] J. J. Lima Jr. and A. S. de Oliveira. Placement optimization of piezoelectric actuators in a simply supported beam, through svd analysis and shape function critic point. In *6th World Congress on Structural and Multidisciplinary Optimization*, 2005.
- [96] E. Lund and N. Olhoff. Shape design sensitivity analysis of eigenvalues using exact numerical differentiation of finite element matrices. *Structural optimization*, 8(1):52–59, 1994.
- [97] J. G. Martin. Subproblem optimisation by gene correlation with singular value decomposition. *GECCO 05: Proceedings of the 2005 conference on genetic and evolutionary computation*, pages 1507–1514, 2005.
- [98] D. Materna. *Structural and Sensitivity Analysis for the Primal and Dual Problems in the Physical and Material Spaces*. Shaker Verlag, 2010.
- [99] D. Materna and F.-J. Barthold. Variational design sensitivity analysis in the context of structural optimization and configurational mechanics. *Int. J. Fract.*, 147(1-4):133–155, 2007.
- [100] D. Materna and F.-J. Barthold. Goal-oriented r-adaptivity based on variational arguments in the physical and material spaces. *Comput. Methods Appl. Mech. Engrg.*, 198(41-44):3335–3351, 2009.
- [101] C. A. Mattson, A. A. Mullur, and A. Messac. Case studies in concept exploration and selection with s-Pareto frontiers. *International Journal of Product Development, Special Issue on Space Exploration and Design Optimization*, 9:32–59, 2009.
- [102] J. S. Moita, J. I. Barbosa, C. M. M. Soares, and C. A. M. Soares. Sensitivity analysis and optimal design of geometrically non-linear laminated plates and shells. *Computers and Structures*, 76:407 – 420, 2000.
- [103] N. Müller, L. Magaia, and B. M. Herbst. Singular value decomposition, eigenfaces, and 3d reconstructions. *SIAM Review*, 46(3):518–545, 2004.

- [104] T. T. Nguyen, S. Yang, and J. Branke. Evolutionary dynamic optimization: A survey of the state of the art. *Swarm and Evolutionary Computation*, 6:1 – 24, 2012.
- [105] J. Nocedal and S. Wright. *Numerical optimization*. Springer Science and Business Media, 2006.
- [106] M. Nunez. *Design Exploration for Engineering Design Optimisation (An Aircraft Conceptual Perspective)*. PhD thesis, School of Engineering Department of Aircraft Engineering, Cranfield University, 2011.
- [107] S. Obayashi, S. Jeong, and K. Chiba. Multi-objective design exploration for aerodynamic configurations. In *In proceedings of the 35 th AIAA Fluid Dynamics Conference and Exhibition*, 2005.
- [108] S. J. Owen and M. L. Staten. A comparison of mesh morphing methods for shape optimization. In WilliamRoshan Quadros, editor, *19th International Meshing Roundtable*, pages 293–311. Springer Berlin Heidelberg, 2010.
- [109] G.-J. Park, T.-H. Lee, K. H. Lee, and K.-H. Hwang. Robust design: An overview. *AIAA Journal*, 44(1):181–191, 2006.
- [110] E. Perry, R. Balling, and M. Landon. A new morphing method for shape optimization. *American Institute of Aeronautics and Astronautics, Inc.*, 4907:1510–1519, 1998.
- [111] J. E. V. Peter and R. P. Dwight. Numerical sensitivity analysis for aerodynamic optimization: A survey of approaches. *Computers & Fluids*, 39(3):373 – 391, 2010.
- [112] L. Piegl and W. Tiller. *The NURBS book*. Springer, 1997.
- [113] Z. P. Qiu, R. Huang, X. J. Wang, and W. C. Qi. Structural reliability analysis and reliability-based design optimization: Recent advances. *Science China Physics, Mechanics and Astronomy*, 56(9):1611–1618, 2013.
- [114] Abhiram G. R., Srikanth S. M., and Satyen K. A variation on svd based image compression. *Image Vision Comput.*, 25(6):771–777, 2007.
- [115] P. A. Ramachandran. Method of fundamental solutions: singular value decomposition. *Communications in Numerical Methods in Engineering*, 18(11):789–801, 2002.
- [116] R. Reitinger and E. Ramm. Buckling and imperfection sensitivity in the optimization of shell structures. *Thin-Walled Structures*, 23:159 – 177, 1995.
- [117] E. Riks. *Buckling. Encyclopedia of Computational Mechanics*. John Wiley & Sons, Ltd, 2004.

-
- [118] J. Sacks, W. J. Welch, T. J. Mitchell, and H. P. Wynn. Design and analysis of computer experiments. *Statistical Science*, 4:409–435, 1989.
- [119] M. Scherer, R. Denzer, and P. Steinmann. A fictitious energy approach for shape optimization. *International Journal for Numerical Methods in Engineering*, 82:269–302, 2010.
- [120] W. Schneider, I. Timmel, and K. Höhn. The conception of quasi-collapse-affine imperfections: A new approach to unfavourable imperfections of thin-walled shell structures. *Thin-Walled Structures*, 43(8):1202 – 1224, 2005.
- [121] M. Scholz. Validation of nonlinear pca. *Neural Processing Letters*, 36(1):21–30, 2012.
- [122] M. Scholz, M. Fraunholz, and J. Selbig. Nonlinear principal component analysis: Neural network models and applications. In A. N. Gorban, B. Kégl, D. C. Wunsch, and A. Zinovyev, editors, *Principal Manifolds for Data Visualization and Dimension Reduction*, volume 58 of *Lecture Notes in Computational Science and Enginnee*, pages 44–67. Springer Berlin Heidelberg, 2008.
- [123] A. Schumacher. *Optimierung mechanischer Strukturen*. Springer-Verlag Berlin Heidelberg, 2005.
- [124] D. F. Shanno. Conditioning of quasi-newton methods for function minimization. *Mathematics of Computation*, 24(1):647–656, 1970.
- [125] D. Sieger, S. Menzel, and M. Botsch. High quality mesh morphing usind triharmonic basis functions.
- [126] O. Sigmund. Morphology-based black and white filters for topology optimization. *Structural and Multidisciplinary Optimization*, 33:401–424, 2007.
- [127] O. Sigmund and J. Petersen. Numerical instabilities in topology optimization: A survey on procedures dealing with checkerboards, mesh-dependencies and local minima. *Structural Optimization*, 16:68–75, 1998.
- [128] T. W. Simpson, T. M. Mauery, J. J. Korte, and F. Mistree. Comparison of response surface and kriging models for multidisciplinary design optimization. Technical Report AIAA Paper 98-2421, American Institute of Aeronautics and Astronautics, 1998.
- [129] T. W. Simpson, J. D. Poplinski, P. N. Koch, and J. K. Allen. Metamodels for computer-based engineering design: Survey and recommendations. *Engineering with Computers*, 17(2):129–150, 2001.
- [130] P. Sompagdee. Survey of morphing. Department of Computer Science Thammasat University, 2000.

- [131] M. L. Staten, S. J. Owen, S. M. Shontz, A. G. Salinger, and T. S. Coffey. A comparison of mesh morphing methods for 3d shape optimization. In WilliamRoshan Quadros, editor, *Proceedings of the 20th International Meshing Roundtable*, pages 293–311. Springer Berlin Heidelberg, 2012.
- [132] C. J. Stull, C. J. Earls, and W. Aquino. A posteriori initial imperfection identification in shell buckling problems. *Computer Methods in Applied Mechanics and Engineering*, 198(2):260 – 268, 2008.
- [133] R. Su, L. Gui, and Z. Fan. Topology and sizing optimization of truss structures using adaptive genetic algorithm with node matrix encoding. *ICNC 09. Fifth International Conference*, 4:485–491, 2009.
- [134] J. M. T. Thompson. Optimization as a generator of structural instability. *Int. J. Mech. Sci.*, 14:627–629, 1972.
- [135] J. M. T. Thompson and G. W. Hunt. Dangers of structural optimization. *Engineering Optimization*, 1:99–110, 1974.
- [136] D. A. Tortorelli and P. Michaleris. Design sensitivity analysis: Overview and review. *Inverse Problems in Engineering*, 1(1):71–105, 1994.
- [137] N. Triantafyllidis and R. Peek. On stability and the worst imperfection shape in solids with nearly simultaneous eigenmodes. *International Journal of Solids and Structures*, 29(18):2281–2299, 1992.
- [138] K.-L. Tsui. An overview of taguchi method and newly developed statistical methods for robust design. *IIE Transactions*, 24(5):44–57, 1992.
- [139] A. Turan and A. Mugan. Structural and sensitivity reanalyses based on singular value decomposition. *Structural and Multidisciplinary Optimization*, 48(2):327–337, 2013.
- [140] M. A. Valdebenito and G. Schueller. A survey on approaches for reliability-based optimization. *Structural and Multidisciplinary Optimization*, 42(5):645–663, 2010.
- [141] H. A. Van der Vorst. Computational methods for large eigenvalue problems. *Ciarlet, P.G.(Hrsg.); Lions, J.L.(Hrsg.): Handbook of numerical analysis*, 3:3–179, 2002.
- [142] F. van Keulen, R. T. Haftka, and N.-H. Kim. Review of options for structural design sensitivity analysis. part 1: Linear systems. *Computer Methods in Applied Mechanics and Engineering*, 194:3213 – 3243, 2005.
- [143] G. Wang and S. Shan. Review of metamodeling techniques in support of engineering design optimization. *Journal of Mechanical Design*, 129(4):370–380, 2006.

- [144] L. Wei, T. Tang, X. Xie, and W. Shen. Truss optimization on shape and sizing with frequency constraints based on parallel genetic algorithm. *Structural and Multidisciplinary Optimization*, 43(5):665–682, 2011.
- [145] K. Wiechmann. *Theorie und Numerik zur Berechnung und Optimierung von Strukturen mit elastoplastischen Deformationen*. PhD thesis, Institut für Baumechanik und Numerische Mechanik, Universität Hannover, 2000.
- [146] G. Wolberg. Recent advances in image morphing. In *Proceedings of the Conference on Computer Graphics International*, 1996.
- [147] G. Wolberg. Image morphing: a survey. *The Visual Computer*, 14:360–372, 1998.
- [148] W. Wunderlich and U. Albertin. Analysis and load carrying behaviour of imperfection sensitive shells. *International Journal for Numerical Methods in Engineering*, 47(1-3):255–273, 2000.
- [149] S. Xu and G. Cheng. Optimum material design of minimum structural compliance under seepage constraint. *Structural and Multidisciplinary Optimization*, 41(4):575–587, 2010.
- [150] Y.-L. Yang, Y.-J. Yang, H. Pottmann, and N. J. Mitra. Shape space exploration of constrained meshes. *ACM Transactions on Graphics*, 30(6):to appear, 2011.
- [151] A. Zhou, B.-Y. Qu, H. L., S.-Z. Zhao, P. N. Suganthan, and Q. Zhang. Multi-objective evolutionary algorithms: A survey of the state of the art. *Swarm and Evolutionary Computation*, 1(1):32 – 49, 2011.
- [152] O. C. Zienkiewicz and R. L. Taylor. *The Finite Element Method for Solid and Structural Mechanics*. Butterworth-Heinemann Ltd, sixth edition, 2005.

Curriculum vitae

Person

Vorname: Nikolai
Name: Gerzen
Geburtsdatum: 12.01.1982
Geburtsort: Tokarewka (Kasachstan)
Staatsangehörigkeit: deutsch
Familienstand: verheiratet, ein Kind
Wohnort: Martener Straße 354, 44379 Dortmund

Ausbildung

08.2000-06.2003 Abitur, Marienschule Lippstadt, privates Gymnasium
10.2003-03.2008 Diplom, TU Dortmund, Studiengang Bauingenieurwesen,
Vertiefungsrichtung Konstruktiver Ingenieurbau

Tätigkeiten

04.2008-07.2008 Wissenschaftliche Hilfskraft, TU Dortmund,
Fakultät Architektur und Bauingenieurwesen,
Numerische Methoden und Informationsverarbeitung
Seit 08.2008 Wissenschaftlicher Mitarbeiter, TU Dortmund,
Fakultät Architektur und Bauingenieurwesen,
Numerische Methoden und Informationsverarbeitung